

**Titre:** Study of substrate integrated waveguide circulators for millimeter wave applications  
Title:

**Auteur:** William D'Orazio  
Author:

**Date:** 2004

**Type:** Mémoire ou thèse / Dissertation or Thesis

**Référence:** D'Orazio, W. (2004). Study of substrate integrated waveguide circulators for millimeter wave applications [Master's thesis, École Polytechnique de Montréal].  
Citation: PolyPublie. <https://publications.polymtl.ca/7471/>

 **Document en libre accès dans PolyPublie**  
Open Access document in PolyPublie

**URL de PolyPublie:** <https://publications.polymtl.ca/7471/>  
PolyPublie URL:

**Directeurs de recherche:** Ke Wu  
Advisors:

**Programme:** Unspecified  
Program:

# NOTE TO USERS

This reproduction is the best copy available.

**UMI<sup>®</sup>**





UNIVERSITÉ DE MONTRÉAL

STUDY OF SUBSTRATE INTEGRATED WAVEGUIDE CIRCULATORS FOR  
MILLIMETER WAVE APPLICATIONS

WILLIAM D'ORAZIO

DÉPARTEMENT DE GÉNIE ÉLECTRIQUE  
ÉCOLE POLYTECHNIQUE DE MONTRÉAL

MÉMOIRE PRÉSENTÉ EN VUE DE L'OBTENTION  
DU DIPLÔME DE MAÎTRE ÈS SCIENCES APPLIQUÉES (M.Sc.A)  
(GÉNIE ÉLECTRIQUE)

JUIN 2004



Library and  
Archives Canada

Bibliothèque et  
Archives Canada

Published Heritage  
Branch

Direction du  
Patrimoine de l'édition

395 Wellington Street  
Ottawa ON K1A 0N4  
Canada

395, rue Wellington  
Ottawa ON K1A 0N4  
Canada

*Your file    Votre référence*

*ISBN: 0-612-97938-5*

*Our file    Notre référence*

*ISBN: 0-612-97938-5*

#### NOTICE:

The author has granted a non-exclusive license allowing Library and Archives Canada to reproduce, publish, archive, preserve, conserve, communicate to the public by telecommunication or on the Internet, loan, distribute and sell theses worldwide, for commercial or non-commercial purposes, in microform, paper, electronic and/or any other formats.

The author retains copyright ownership and moral rights in this thesis. Neither the thesis nor substantial extracts from it may be printed or otherwise reproduced without the author's permission.

#### AVIS:

L'auteur a accordé une licence non exclusive permettant à la Bibliothèque et Archives Canada de reproduire, publier, archiver, sauvegarder, conserver, transmettre au public par télécommunication ou par l'Internet, prêter, distribuer et vendre des thèses partout dans le monde, à des fins commerciales ou autres, sur support microforme, papier, électronique et/ou autres formats.

L'auteur conserve la propriété du droit d'auteur et des droits moraux qui protègent cette thèse. Ni la thèse ni des extraits substantiels de celle-ci ne doivent être imprimés ou autrement reproduits sans son autorisation.

---

In compliance with the Canadian Privacy Act some supporting forms may have been removed from this thesis.

Conformément à la loi canadienne sur la protection de la vie privée, quelques formulaires secondaires ont été enlevés de cette thèse.

While these forms may be included in the document page count, their removal does not represent any loss of content from the thesis.

Bien que ces formulaires aient inclus dans la pagination, il n'y aura aucun contenu manquant.

UNIVERSITÉ DE MONTRÉAL

ÉCOLE POLYTECHNIQUE DE MONTRÉAL

Ce mémoire intitulé:

STUDY OF SUBSTRATE INTEGRATED WAVEGUIDE CIRCULATORS FOR  
MILLIMETER WAVE APPLICATIONS

présenté par: D'ORAZIO William

en vue de l'obtention du diplôme de: Maître ès sciences appliquées

a été dûment accepté par le jury d'examen constitué de:

M. BOSISIO Renato G., M.Sc.A., président

M. LAURIN Jean-Jacques, Ph.D., membre

M. WU Ke, Ph.D., membre et directeur de recherche

## DEDICATION

To my parents,

Thank you for your endless support.

## ACKNOWLEDGEMENTS

I would like to express my gratitude to my director, Dr. Ke WU, for his support, his patience and his suggestions during my time as a graduate student. A special thanks is also extended to Dr. Joe HELSZAJN for many helpful discussions.

I would also like to thank all the personnel at the Poly-GRAMES Research Center. In particular a special thanks is extended to Mr. Jules GAUTHIER, Mr. Roch BRASSARD, and Mr. Steve DUBÉ for their technical assistance and Mr. René ARCHAMBAULT for his administrative support.

I would also like to thank Filtronic, in particular Mr. Mark MCKAY, for their support in providing the ferrites.

A special thanks is also extended to Mr. Dominic DESLANDES for many helpful discussions and to all the researchers at Poly-GRAMES who have contributed directly or indirectly.

Finally I would like to extend my gratitude to my friends and girlfriend and to my parents for their endless love and moral and economic support.

## ABSTRACT

A current trend in connection with commercial telecommunication and sensor applications is the progression towards millimetre-wave and sub-millimetre-wave frequencies. Currently the design of millimetre wave components and systems span a wide range of planar processes including PCB, HTCC, LTCC, thin film, and MMIC. Although these processes offer low cost mass producible components, there still remains a significant problem: they are not suitable to the design of high quality filters, duplexers and couplers as well as other high-Q components. Waveguide technique is often used in the design of these high quality components and complex transition structures are required to integrate them with the planar ones, therefore requiring expensive post-fabrication assembly and tuning costs. This problem has in the past hindered the proliferation of these systems.

Recently a new platform in the design of high-Q components has emerged, this technique collectively known as Substrate Integrated Circuits (SIC's) consists of embedding classical bulky waveguides, such as rectangular and Non-Radiative Dielectric (NRD) waveguides, into the planar platforms previously mentioned. Two advantages of this technique is that the same process used for the planar circuits may now be used for the non-planar ones in the integrated waveguide, and the transitions between the planar and non-planar transmission mediums is significantly simplified, thus virtually removing the post fabrication assembly and tuning cost.

A number of SIC's have already been realized including numerous transitions, filters, couplers and power dividers. Although these are the key building blocks in the design of receiver front-end systems, ferrite devices are always needed for the design of tuneable and non-reciprocal components. Ferrite devices are ubiquitously used in phased array antennas and in isolators and circulators.

The purpose of this project is to demonstrate that substrate integrated waveguide ferrite circulators are realizable. Two design configurations are considered; one consists of a planar post resonator, with top and bottom electric walls and the other of a quarter-

wavelength with one face short circuited and the other open. These resonators have their own advantages and disadvantages, the post resonator is ideal for frequencies up to the K-band spectrum while the turnstile one may be more suitable at higher frequencies. A novel matching technique consisting of a substrate integrated ridge waveguide is utilized in the broadband matching problem.



## CONDENSÉ EN FRANÇAIS

Ce travail décrit un circulateur à guide d'onde en substrat intégré (GOSI) qui permet une intégration plus facile des composants actifs planaires avec des composants passifs à facteur de qualité élevé. Les résultats d'expériences pour un circulateur qui opère en bande-K de type jonction d'ordre-2 utilisant un résonateur de type *post*, sont présentés. Par ailleurs, on trouvera l'étude expérimentale du circuit équivalent à 1-port pour ce même type de jonction qui a servi à sa conception.

Dans la conception de systèmes complexes, il peut cependant être très avantageux d'utiliser un substrat épais car il a été démontré que les pertes de propagation sont inversement proportionnelles à la hauteur du substrat. Les *post* résonateurs à murs électriques sur les parois inférieure et supérieure ne sont pas convenables pour ce genre de substrat épais car les modes d'ordres supérieurs à grandes variations transversales seront excités. Une solution possible pouvant convenir à un diélectrique épais serait d'utiliser une jonction de type *turnstile re-entrant*. Bien que les résonateurs de types *turnstile* aient fait l'objet de nombreuses études dans la littérature, il s'agit de la première étude qui fait intervenir ce type de résonateur dans la conception de circulateurs GOSI de second ordre.

## INTRODUCTION

Un nouveau type de guide d'onde à trous métallisé de raccordement aussi appelé guide d'onde à substrat intégré (GOSI) a fait l'objet de récentes études pour rendre plus facile l'intégration de circuits actifs planaires avec des composantes passives à facteur de qualité élevé [21]. La Figure 1 présente la topologie typique de ce genre de circuit. Les plans de masse sur les parties supérieure et inférieure du substrat forment les parois horizontales du guide d'ondes alors qu'un réseau de trous métallisés de raccordement sert de parois verticales. Le réseau de trous métalliques sur les parties latérales peut être considéré comme des discontinuités non radiatives. Il est compris que les trous de

raccordements sur les parties latérales permettent une conduction complète des courants à orientation verticale issus du mode  $TE_{10}$ , empêchant ainsi toute radiation. Cette technique permet alors de concevoir des composants à base de guide d'ondes à l'aide du même procédé que pour les composants planaires.

Des composants intégrés tels que des filtres et des oscillateurs ont déjà été développés [25], [26]. Cependant, aucun composant à base de ferrites tels que des circulateurs ou isolateurs n'a fait l'objet de travaux expérimentaux jusqu'à présent. Le but de cette étude est donc de présenter de genre de circuits à base de ferrites. Le schéma typique du circulateur présenté à la Figure 2, se compose d'un résonateur planaire de type *post* ou *turnstile* aux raccordements des 3 branches du circulateur GOSI. La description du circuit de transition GOSI à ligne micro-ruban, utilisé à des fins de mesure, sera rapidement présentée. Une transition GOSI à guide d'onde rectangulaire, utilisée pour effectuer les mesures sur le circulateur de type *turnstile*, est aussi présentée.

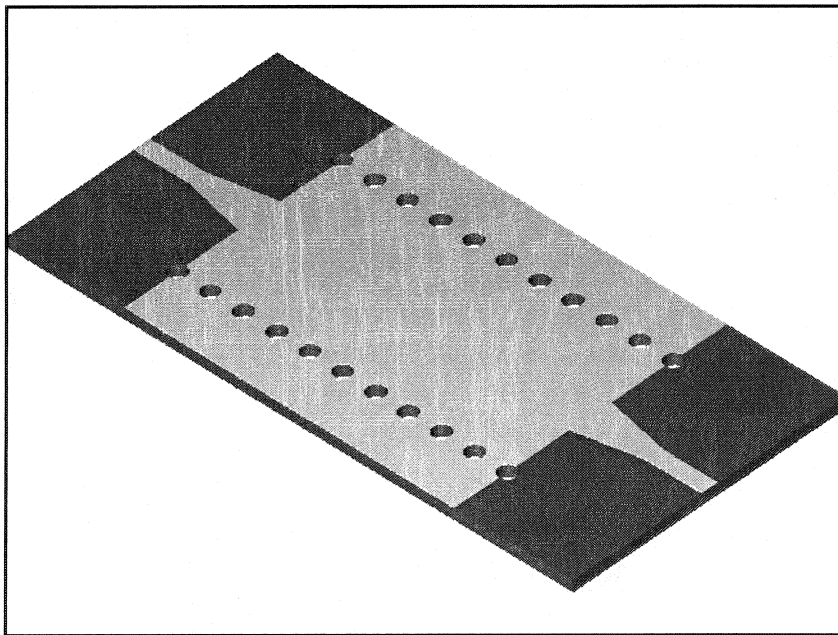


Figure 1: Transition entre guide d'onde en substrat intégré (GOSI) et ligne micro ruban

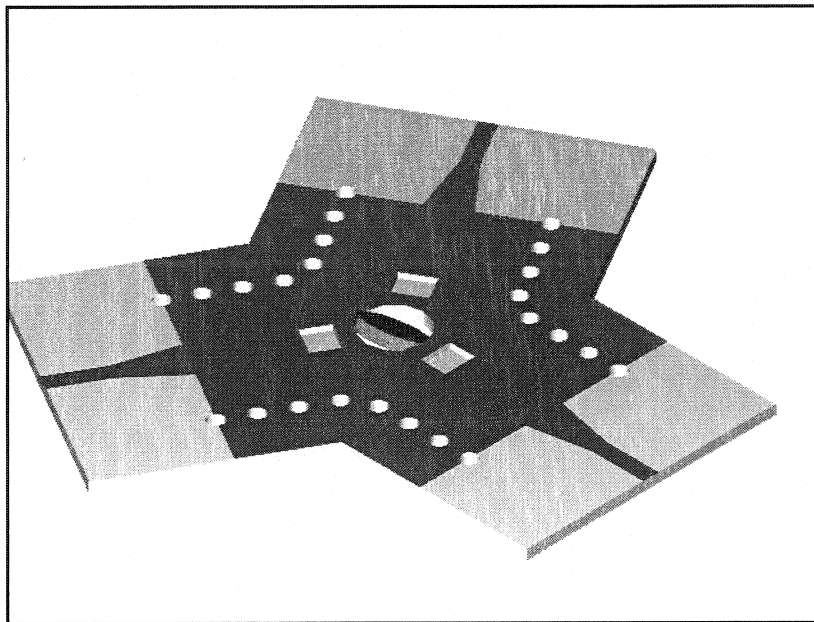


Figure 2: Circulateurs à guide d'onde en substrat intégré (GOSI)

## CIRCUITS DE TRANSITION

Bien que le circulateur soit conçu pour être adapté à l'impédance du guide d'onde, il n'existe pas de trousse de calibration en technologie GOSI. Afin d'effectuer les mesures il est nécessaire de concevoir un circuit de transition entre le circuit GOSI et une ligne classique quelconque. Même si la conception des transitions est en général spécifique à la topologie du circuit, on peut établir certaines règles générales de base à suivre. La conception de transition à large bande nécessite que les impédances caractéristiques des 2 médiums de transmission soient très voisines et que l'orientation des champs soit identique. L'excitation des modes d'ordre supérieur causée par la discontinuité entre des circuits de technologies différentes complique souvent la conception de ce type de circuit de transition. Ce qui fait qu'un simple circuit d'adaptation conçu à partir d'une transformation d'impédance à la fréquence centrale n'est en général pas suffisant. Nous proposons donc un système à éléments finis pour optimiser la performance du design avant la fabrication. En fait, cette manière de procéder réduit souvent le nombre d'itérations expérimentales à 1.

Une transition de GOSI à micro ruban a déjà été étudiée dans [21]. Le schéma explicatif est illustré à la Figure 1: elle se compose d'une section en biseau pour adapter la faible impédance caractéristique du GOSI à celle de la ligne micro ruban de référence. Le transformateur d'impédance est directement usiné sur la paroi supérieure du GOSI. Le champ électrique de la ligne est alors très proche de l'allure du champ du mode dominant du GOSI. Par conséquent, la transition devrait donner une adaptation à large bande. Les paramètres à optimiser sont la longueur de le transformateur d'impédance trapézoïdal (en forme de biseau,  $l_t$ ), la largeur du trapèze au niveau de la partie GOSI ( $w_i$ ) et l'impédance caractéristique de la ligne micro-ruban de référence ( $w$ ). Pour vérifier les résultats de simulation, un prototype a été conçu et testé. Les résultats expérimentaux obtenus comparés aux résultats de simulation sont présentés sur la Figure 3. Une perte d'insertion inférieure à 0.3 dB ainsi qu'une adaptation de 20dB ont été obtenues sur la bande passante complète du guide d'onde.

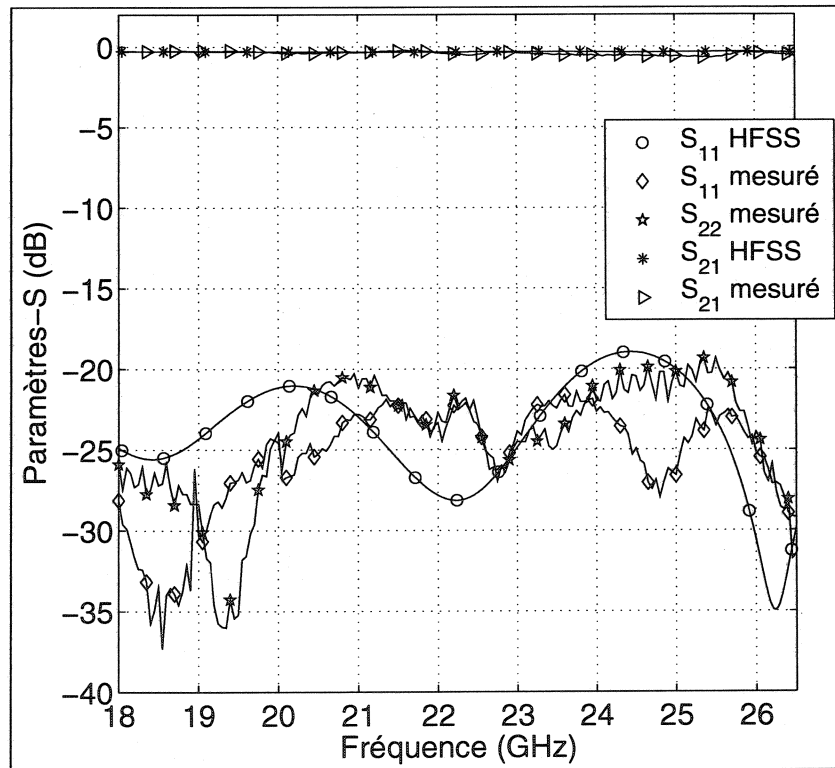


Figure 3: Résultats expérimentaux de transition entre GOSI et ligne micro ruban

Les lignes micro-rubans ne sont toutefois pas convenables pour les substrats épais étant donnée les pertes élevées dues au rayonnement. Une transition GOSI à guide d'onde co-planaire, bien que compatible avec des substrats épais, ne fournisse pas la bande passante élevée caractéristique des circulateurs. Par conséquent, une transition à guide d'onde rectangulaire a été choisie pour effectuer les mesures sur les circulateurs *turnstile*. La transition, illustrée sur la Figure 4, se compose d'un transformateur d'impédance à rainure incidente en escalier suivie d'un guide d'onde à rainure incidente partiellement rempli de diélectrique. Comme dans le cas de la transition micro-ruban, les champs de part et d'autre de la transition ont une orientation semblable de manière à obtenir une transition à large bande. Les résultats avec un transformateur avec un escalier à 3 niveaux sont décrits sur la Figure 5. On obtient une adaptation de 15 dB sur la bande complète du guide d'onde.

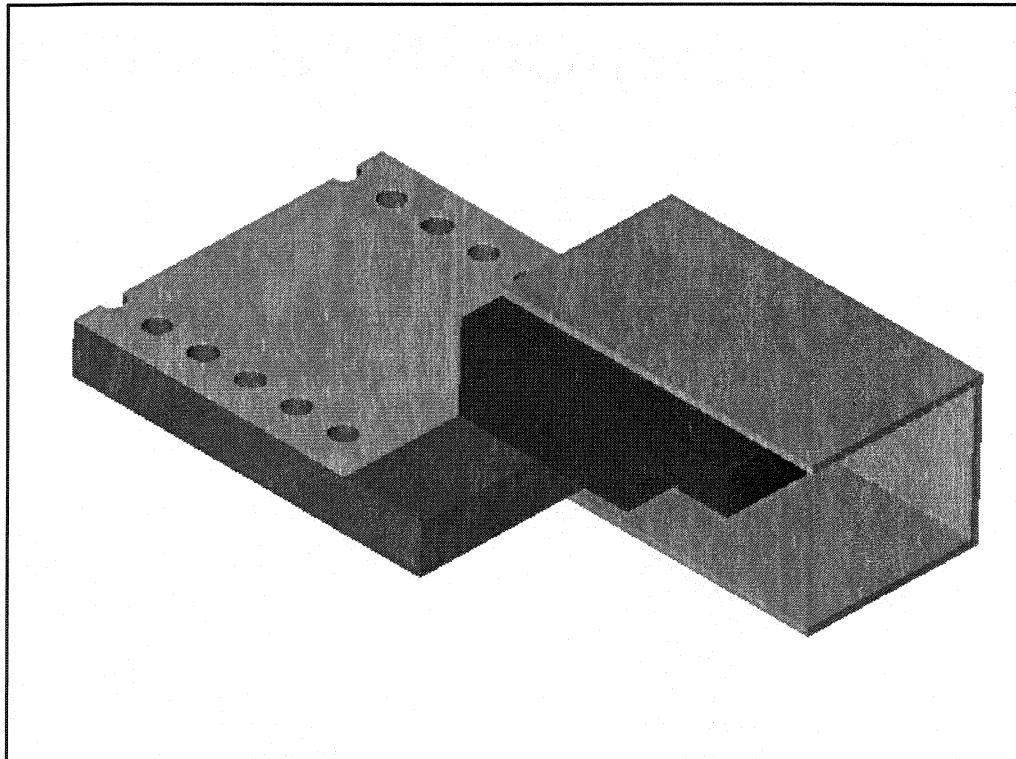


Figure 4: Transition entre GOSI et guide d'onde rectangulaire

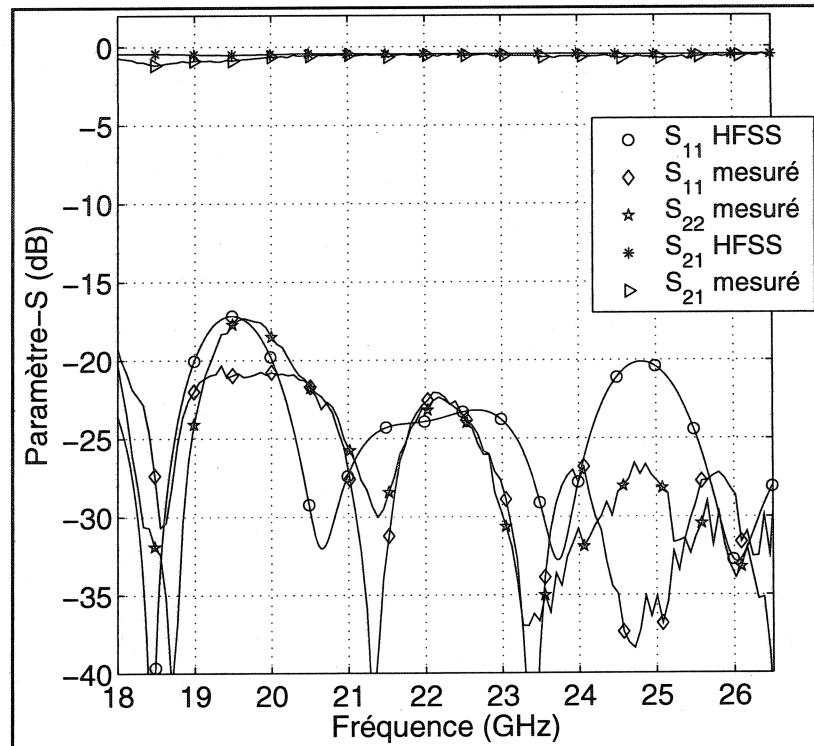


Figure 5: Résultats de transition entre GOSI et guide d'onde rectangulaire

## RÉSONATEUR GYROMAGNÉTIQUE

Un résonateur de type *post* au raccordement des 3 guides d'ondes rectangulaire est un problème très commun dans la littérature. Le fonctionnement de ce type de circulateurs repose sur la présence de trois distributions de champ: deux formées à polarisation circulaire mais à déphasages inverses produisent un mur magnétique à l'extrémité de la jonction, très semblable à la distribution d'un mode  $TM_{110}^m$ , et la troisième en phase impose au même endroit un mur électrique, équivalent à un mode  $TM_{010}^e$ . La fréquence de circulation se ramène donc à un problème d'extraction de valeurs propres traité en détails dans [48]. Le rayon du résonateur à ferrite correspondant à une certaine fréquence de résonance est intrinsèquement lié aux paramètres du résonateur et du GOSI. Le GOSI se caractérise par les dimensions géométrique du substrat, sa largeur  $a$  et sa hauteur  $b$ , le diamètre des trous de raccordements ( $\phi$ ), la distance qui les séparent ( $p$ ) et sa constante diélectrique ( $\epsilon_d$ ). La hauteur  $b$  vaut 0.508 mm et son rapport  $b/a$  vaut

0.07. La constante du diélectrique du substrat a une valeur de  $\epsilon_d=2.33$ . Les trous de raccordement sont espacés de  $p=1.524$  mm et leur diamètre est de  $\phi=0.8$  mm. La ferrite est faite de lithium avec une magnétisation de saturation de  $\mu_o M_s=0.4800$  T. Sa constante diélectrique relatif à une valeur de  $\epsilon_f=14.1$ . La fréquence d'étude est fixée à 22 GHz. La magnétisation de saturation normalisée vaut  $p=0.61$ . La perméabilité démagnétisée équivalente est  $\mu_d=0.86$ . Le rayon du résonateur est de  $R_f=1.45$  mm. Le nombre d'onde dominant correspondant à l'ensemble de ces paramètres est 2.61. Toutefois sa valeur expérimentale a été établie à 2.18. La différence vient du fait que le rapport du GOSI est relativement différent de celui d'un guide d'onde rectangulaire standard. Le choix d'un GOSI aussi fin permet de s'assurer que la longueur électrique de la ferrite ne coïncide pas avec un nombre entier de demi-longueur d'onde d'un quelconque mode hybride [49].

Pour les circulateur de type *turnstile*, on utilise un substrat de hauteur  $b=1.5748$  mm et de largeur satisfaisant le rapport  $b/a=0.2167$ . Vu le faible épaisseur du GOSI, un seul résonateur gyromagnétique d'un quart longueur d'onde de longueur avec une terminaison en court-circuit et l'autre en circuit ouvert est suffisant pour la conception du circulateur. Son mode de fonctionnement est similaire à celui du circulateur *post*, toutefois il repose sur les modes hybrides  $HE_{11\delta}$  du résonateur à ferrite [62].

## FRÉQUENCE D'OPÉRATION DE CIRCULATEUR

Comme cela a été mentionné précédemment, la fréquence d'opération (ou de circulation) se résume à un problème d'extraction de valeurs propres. La compréhension de son ajustement est aussi un problème de valeurs propres. Dans une jonction réciproque, la matrice  $S$  contient 3 valeurs propres. Une valeur propre en phase qui produit un court circuit indépendant de la fréquence aux terminaisons de la ferrite et 2 autres qui dans le cas idéal créent un mur magnétique. Cet agencement coïncide avec la première condition de circulation; choisissant le rayon de la ferrite pour un transfert maximum de puissance. La résolution de l'équation caractéristique d'un circulateur idéal

donne 3 valeurs qui sont régulièrement espacées sur le cercle unité. Les 2 valeurs en opposition de phase (counter-rotating) sont complexes conjuguées et ceci correspond à la deuxième condition de circulation qui consiste à ajuster la gyrotropie pour une isolation et adaptation maximale et une perte d'insertion minimale. La Figure 6 montre la fréquence de circulation par rapport au rayon de la ferrite pour le circulateur de type *post*. La deuxième condition de circulation est traitée en détail dans la prochaine section. Bien que la première condition de circulation ait été traitée jusqu'à un certain point, son étude expérimentale présente un intérêt particulier. La fréquence de circulation est obtenue lorsqu'on a un transfert maximum de puissance pour la jonction démagnétisée, et une isolation maximale pour la jonction soumise à un champ magnétique. Bien que dans le cas d'un circulateur idéal ces deux cas correspondent à des solutions dégénérées, ce n'est souvent pas le cas en pratique. Il est bon de noter qu'en pratique les valeurs propres ne sont pas complexes conjuguées (symétriquement écarté par rapport à l'axe des abscisses), ce qui fait que la circulation dépend de la gyrotropie.

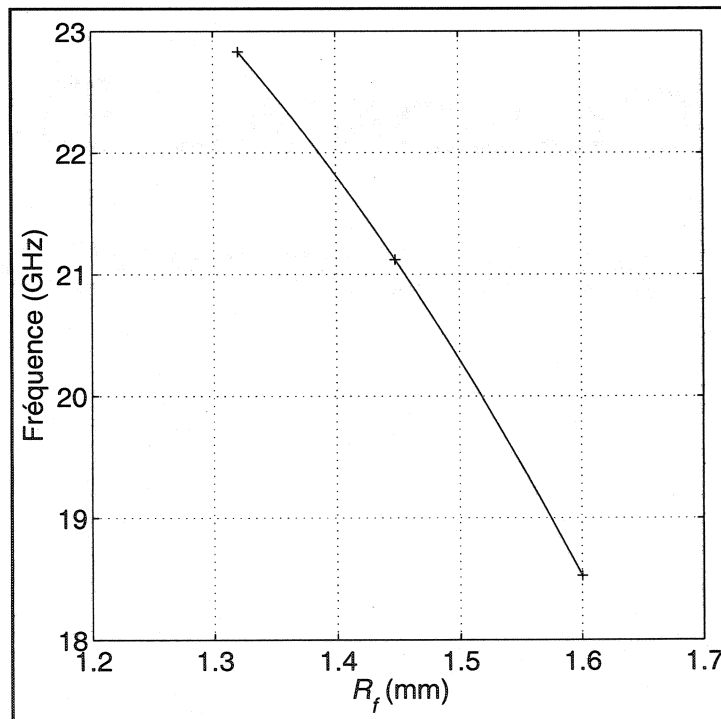


Figure 6: Fréquence d'opération par rapport au rayon de la ferrite



## CIRCUIT DE GYRATEUR COMPLEXE

La connaissance des propriétés de circuit gyrateur complexe est très utile pour la conception. Il se compose d'une conductance de  $g$  en parallèle avec un stub de quart de longueur d'onde terminé en court-circuit, caractérisé par son facteur de variation (ou pente) de la susceptance  $b$ . Pour une jonction de circulateur faiblement magnétisée, son facteur de qualité est fixé par les fréquences distinctes de résonance du résonateur gyromagnétique [5]

$$\frac{1}{Q} = \sqrt{3} \left( \frac{\omega_+ - \omega_-}{\omega_0} \right) \quad (1)$$

La pente de la susceptance est séparément déterminée par la géométrie du résonateur. Ces 2 grandeurs définissent la conductance du circuit gyrateur. La conductance du gyrateur normalisée est donnée par l'expression suivante [35]

$$g = \begin{cases} \sqrt{2r-1} & g \geq 1 \\ \sqrt{\frac{2-r}{r}} & g \leq 1 \end{cases} \quad (2)$$

Où  $r$  est le *TOS* (Taux d'Onde Stationnaire) à la fréquence d'opération. Ce circuit équivalent est important dans la conception des circulateurs à jonctions car il permet une synthèse exacte du circuit d'adaptation [38]. Il est à noter que la connaissance exacte des terminaisons de la jonction n'est pas nécessaire. Les Figure 7 et Figure 8 illustrent les résultats obtenus pour un résonateur de type *post*. Le circuit gyrateur complexe présente des paramètres  $g$  et  $b'$  d'une valeur respective de 2 et 4. Ces valeurs ne sont pas coïncidentes avec celles de composants ayant un coefficient d'adaptation de 20 dB. Un moyen efficace d'ajuster ces valeurs serait de diminuer l'épaisseur du substrat. La conductance du gyrateur et les fréquences de résonance à saturation ont été extraites avec un simulateur à éléments finis commercial et elles correspondent aux résultats expérimentaux.

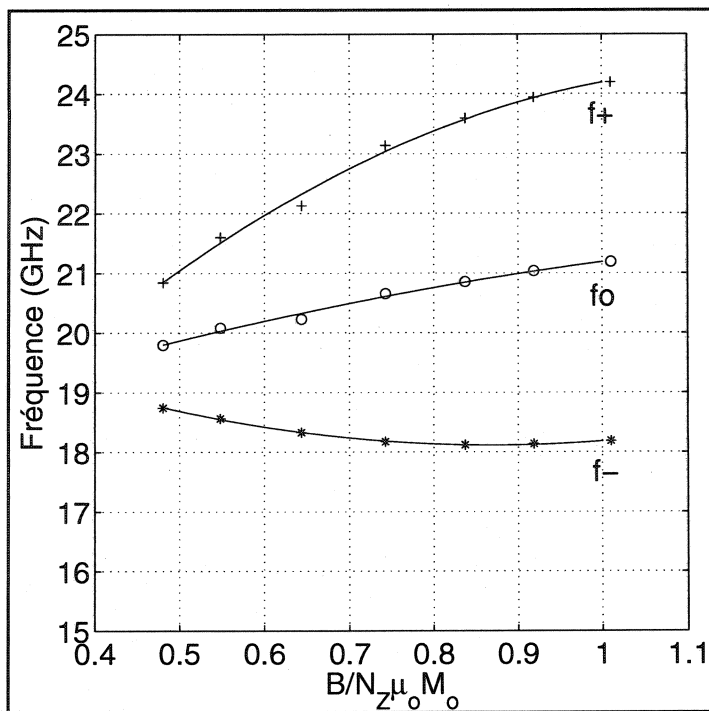


Figure 7: Fréquences distinctes de résonance ( $R_f=1.45$  mm)

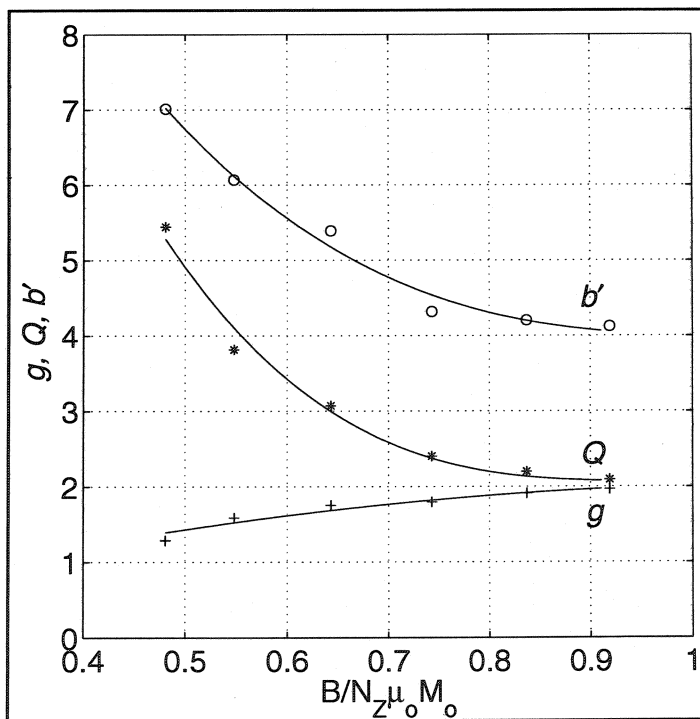


Figure 8: Paramètres de circuit gyrateur complexe ( $R_f=1.45$  mm)

## CIRCULATEUR DE DEGRÉS-2

Le circuit gyrateur complexe obtenu expérimentalement est compatible avec des dispositifs de degrés-2 qui possède une bande passante de 30% et d'un coefficient d'adaptation de 15 dB. Un moyen d'adapter cette jonction est d'utiliser un transformateur au quart d'onde aux terminaisons de la ferrite. Le problème que pose la présence d'un tel transformateur à cet endroit du résonateur est le mur électrique qu'il génère au niveau des terminaisons du circulateur. Un autre problème potentiel réside dans le fait que la paroi plate verticale du transformateur adjacent à la ferrite devient trop fragile pour être manipulé. Pour contourner ces difficultés, le transformateur a été arbitrairement déplacé de 20 degrés (0.635 mm) par rapport à la ferrite. La topologie de transformateur hybride conçu selon ce procédé a été calculée à l'aide d'un simulateur à éléments finis. Dans un premier temps, un résonateur magnétisé placé à l'intersection de 3 GOSI avec un quart de longueur d'onde à rainure incidente décalé de 20 degrés par rapport à la ferrite a été optimisé pour obtenir une réponse d'ordre 2. La transition micro ruban a ensuite été ajoutée dans la simulation et le processus d'optimisation réitéré. Le schéma du circuit complet est illustré à la Figure 2. Les grandeurs géométriques finalement obtenues sont les suivantes:  $s/a=0.21$ ,  $d/b=0.5$ ,  $l_r=1.27$  mm. La Figure 9 illustre la réponse d'ordre-1 et la Figure 10 la réponse d'ordre-2. L'isolation, omise ici pour raison de simplification, est du même ordre que le taux d'adaptation. Une bande passante de 18% à 15 dB avec une perte d'insertion inférieure à 1.3 dB a été obtenue. Ceci correspond à une ligne micro ruban de 10 mm, une longueur de guide d'onde de 20 mm et deux transitions. La différence entre les simulations et les résultats expérimentaux est explicable par le fait que le simulateur considère la ferrite comme étant uniformément saturée et par les imprécisions lors de l'ajustement de la profondeur du transformateur à rainure.

De même façon un circulateur de type *turnstile* a été conçu. Ces résultats sont illustrés à la Figure 11.

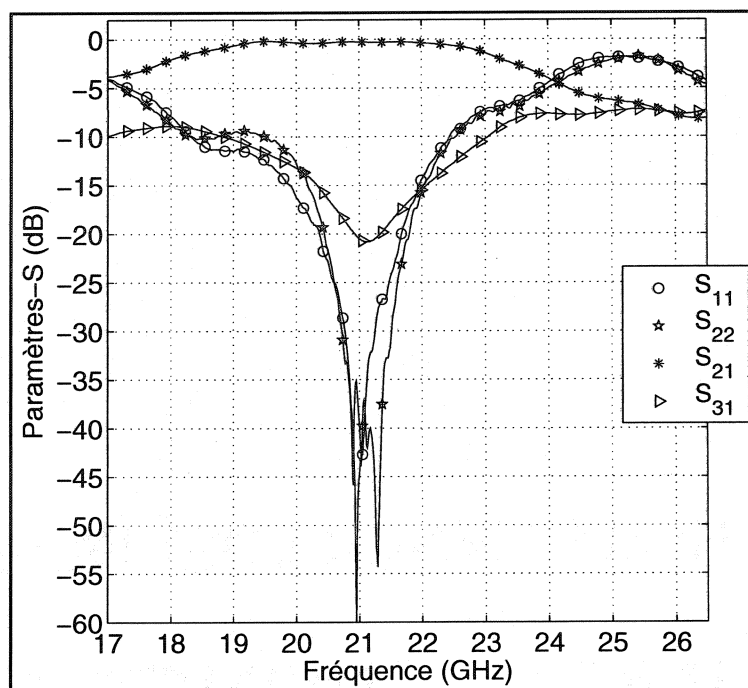


Figure 9: Réponse en fréquence de circulateur en guide d'onde en substrat intégré

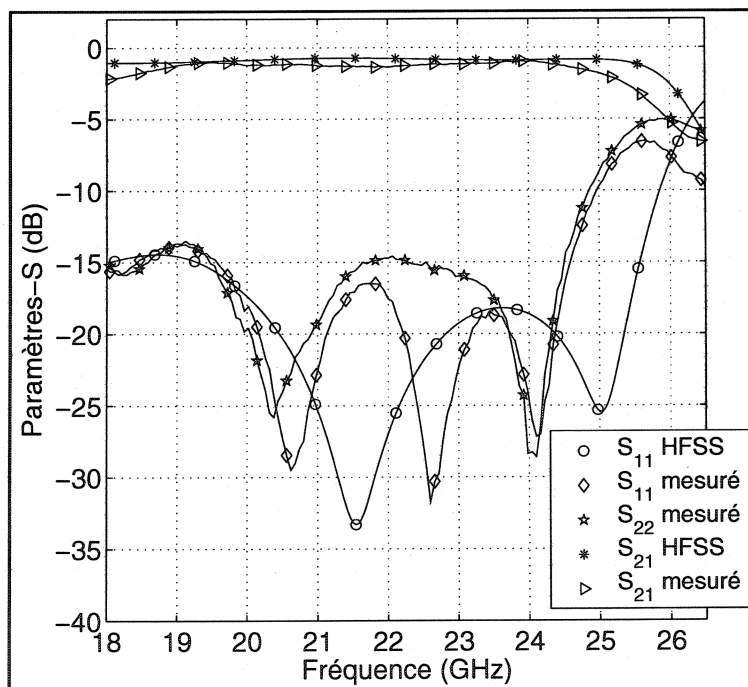


Figure 10: Résultats de circulateur en guide d'onde en substrat intégré d'ordre-2

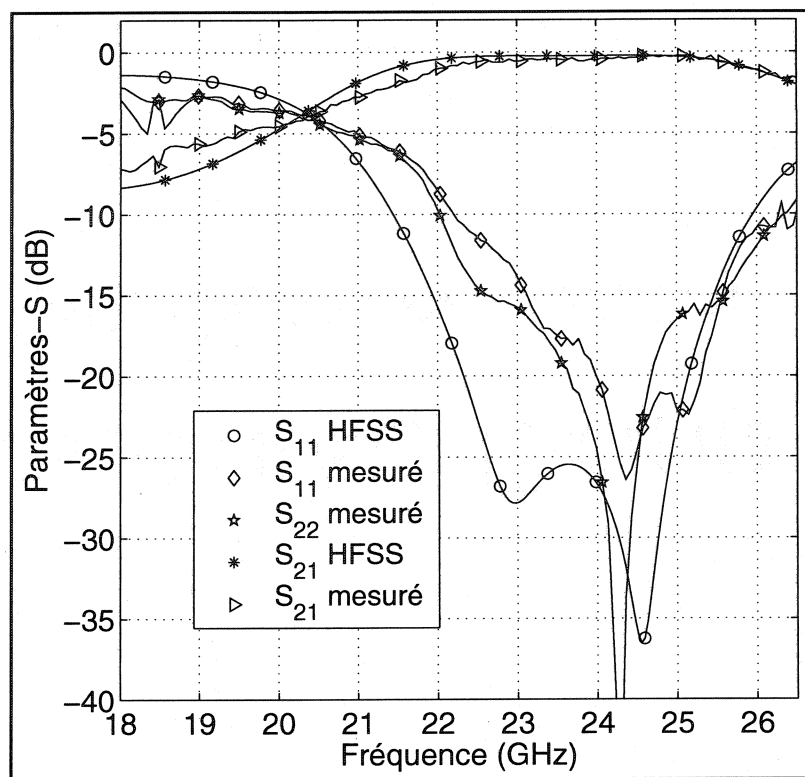


Figure 11: Résultats de circulateur de type *turnstile* d'ordre-2

## TABLE OF CONTENTS

DEDICATION .....	iv
ACKNOWLEDGEMENTS .....	v
ABSTRACT .....	vi
CONDENSÉ EN FRANÇAIS .....	viii
TABLE OF CONTENTS .....	xxi
LIST OF TABLES .....	xxiv
LIST OF FIGURES .....	xxv
INTRODUCTION .....	1
1 CHAPTER MAGNETIC PARAMETERS AND GYROTROPY SELECTION .....	6
1.1 Susceptibility Tensor .....	7
1.1.1 Linewidth of ferrites .....	10
1.1.2 Demagnetizing factors .....	10
1.2 Tensor Permeability .....	12
1.2.1 Normalized Parameters .....	13
1.2.2 Partially magnetized ferrites and low field loss .....	16
1.3 Selection of Ferrite Material and Operating Region .....	17
2 CHAPTER SUBSTRATE INTEGRATED WAVEGUIDE .....	20
2.1 Brief Historical Review .....	20
2.2 Design of Substrate Integrated Waveguide .....	22
2.2.1 Propagation constant .....	24
2.2.2 Characteristic impedance .....	24
2.2.3 Substrate selection and SIW dimensions .....	25
2.3 SIW Transitions .....	26
2.3.1 Transition from microstrip to 0.508 mm thick SIW .....	27
2.3.1.1 Transition design and optimization .....	28
2.3.1.2 Results of the transition .....	29
2.3.1.3 Sensitivity of the design .....	29

2.3.2	Transition from co-planar waveguide to 1.5748 mm thick SIW .....	31
2.3.2.1	Transition design and optimization.....	32
2.3.2.2	Results of the transition.....	33
2.3.2.3	Sensitivity of the design .....	33
2.3.3	Transition from rectangular waveguide to SIW .....	35
2.3.3.1	Transition design and optimization.....	35
2.3.3.2	Results of the transition.....	37
2.3.3.3	Sensitivity of the design .....	38
2.4	Transition Selection and Performance .....	40
3	CHAPTER CIRCUIT THEORY OF JUNCTION CIRCULATORS .....	43
3.1	Brief Historical Review.....	44
3.2	Matrix Description of the Junction Circulator .....	45
3.2.1	Scattering matrix description .....	45
3.2.2	Impedance and admittance matrices .....	49
3.3	Complex Gyrator Circuit.....	50
3.4	Impedance Matching.....	53
4	CHAPTER PLANAR SIW CIRCULATOR.....	56
4.1	Brief Historical Review.....	57
4.2	Degree-1 SIW Planar Post Circulator .....	57
4.2.1	Gyromagnetic resonator .....	58
4.2.2	Experimental procedure .....	59
4.2.3	Mode chart of SIW circulator .....	60
4.2.4	Complex gyrator circuit .....	62
4.3	Degree-2 Circulator.....	64
4.3.1	Quarter-wavelength coupled degree-2 solutions.....	68
4.3.2	Single ridge SIW quarter-wavelength coupled circulator.....	70
4.3.2.1	Ridge SIW cutoff space .....	70
4.3.2.2	Ridge SIW characteristic impedance .....	73
4.3.2.3	Single ridge SIW quarter-wavelength coupled design.....	74

4.3.2.4	Design sensitivity .....	77
4.3.2.5	Experimental results .....	79
4.3.3	Radial SIW quarter-wavelength coupled circulator .....	80
4.3.3.1	Radial SIW quarter-wavelength coupled design .....	81
4.3.3.2	Design sensitivity .....	83
4.3.3.3	Experimental results .....	85
5	CHAPTER TURNSTILE SIW CIRCULATOR .....	87
5.1	Brief Historical Review .....	87
5.2	Turnstile SIW Degree-1 Circulator .....	88
5.2.1	Gyromagnetic resonator .....	88
5.2.2	Inphase eigennetwork adjustment .....	92
5.2.3	Complex gyrator circuit .....	94
5.3	Experimental Procedure .....	94
5.4	Degree-2 Circulator .....	95
5.4.1	Topology using a $90^\circ$ unit element .....	96
5.4.1.1	Design of topology using a $90^\circ$ unit element .....	96
5.4.1.2	Design sensitivity .....	99
5.4.1.3	Experimental results .....	100
5.4.2	Topology using a $90^\circ$ and $180^\circ$ unit element .....	100
5.4.2.1	Design of topology using a $90^\circ$ and a $180^\circ$ unit element .....	102
5.4.2.2	Design sensitivity .....	104
5.4.2.3	Experimental results .....	105
	CONCLUSION AND FUTURE WORK .....	108
	REFERENCES .....	113



## LIST OF TABLES

Table 4.1: Network parameters of quaterwave coupled degree-2 circulators.....	69
Table 4.2: Calculation of single ridge SIW geometry.....	76
Table 5.1: Calculation of single ridge geometry.....	98
Table 5.2: Summary of SIW circulators experimental results .....	107

## LIST OF FIGURES

Figure 1.1: Magnetic moment precession in a typical gyromagnetic insulator .....	8
Figure 1.2: $\mu_{eff}$ as a function of $\sigma$ for parametric values of $p$ .....	14
Figure 1.3: External d.c. bias field for a typical above and below resonance junction....	15
Figure 1.4: $\mu_{eff}$ versus $B_o$ for a thin disk operating at 22GHz with $\mu_o Ms=0.48 T$ .....	16
Figure 1.5: $\kappa/\mu$ as a function of $\sigma$ for parametric values of $p$ .....	18
Figure 2.1: Substrate integrated waveguide .....	22
Figure 2.2: Design parameters of substrate integrated waveguide .....	23
Figure 2.3: SIW transmission characteristics .....	26
Figure 2.4: Microstrip to SIW transition.....	27
Figure 2.5: Schematic diagram of mirostrip to SIW transition.....	28
Figure 2.6: Simulation results of transition from microstrip to SIW .....	29
Figure 2.7: Sensitivity of the transition.....	30
Figure 2.8: GCPW to SIW transition .....	31
Figure 2.9: Schematic diagram of GCPW to SIW transition .....	32
Figure 2.10: Transition simulation results of GCPW to SIW .....	34
Figure 2.11: Sensitivity of transition from GCPW to SIW .....	34
Figure 2.12: Rectangular waveguide to SIW transition .....	35
Figure 2.13: Schematic diagram of mirostrip to SIW transition.....	36
Figure 2.14: Simulation results of degree-2 air filled waveguide to SIW transition .....	37
Figure 2.15: Simulation results of degree-3 air filled waveguide to SIW transition .....	38
Figure 2.16: Sensitivity of degree-2 air filled waveguide to SIW transition .....	39
Figure 2.17: Sensitivity of degree-3 air filled waveguide to SIW transition .....	39
Figure 2.18: Microstrip to SIW transition experimental results .....	41
Figure 2.19: SIW to rectangular waveguide transition experimental results .....	42
Figure 3.1: Eigenvalue diagram of demagnetized junction .....	46
Figure 3.2: Eigennetworks of a 3-port circulator .....	47

Figure 3.3: Eigenvalue diagram of an ideal circulator.....	48
Figure 3.4: Definition of input admittance.....	51
Figure 3.5: Matching of the junction circulator using $90^\circ$ UE's .....	54
Figure 3.6: Matching of the junction circulator using $90^\circ$ and $180^\circ$ UE's.....	55
Figure 4.1: SIW planar post circulator.....	59
Figure 4.2: Experimental setup for the characterization of the SIW circulator .....	61
Figure 4.3: Coaxial TRL calibration kit.....	61
Figure 4.4: Planar circulator test jig.....	62
Figure 4.5: Degree-1 SIW planar post circulator experimental results.....	63
Figure 4.6: Circulation frequency versus ferrite radius .....	63
Figure 4.7: Split frequencies versus normalized magnetization ( $R_f=1.32$ mm).....	65
Figure 4.8: Circuit parameters versus normalized magnetization ( $R_f=1.32$ mm) .....	65
Figure 4.9: Split frequencies versus normalized magnetization ( $R_f=1.45$ mm).....	66
Figure 4.10: Circuit parameters versus normalized magnetization ( $R_f=1.45$ mm) .....	66
Figure 4.11: Split frequencies versus normalized magnetization ( $R_f=1.6$ mm).....	67
Figure 4.12: Circuit parameters versus normalized magnetization ( $R_f=1.6$ mm) .....	67
Figure 4.13: Circuit parameters versus resonator thickness.....	68
Figure 4.14: Single ridge SIW .....	71
Figure 4.15: Cutoff space of quasi- $TE_{10}$ single ridge SIW mode .....	72
Figure 4.16: Cutoff space of quasi- $TE_{20}$ single ridge SIW mode .....	73
Figure 4.17: PV characteristic impedance versus $s/a$ for parametric values of $d/b$ .....	74
Figure 4.18: Ridge SIW quarter-wavelength coupled circulator simulation results.....	76
Figure 4.19: Ridge SIW quarter-wavelength coupled circulator without transition.....	77
Figure 4.20: Sensitivity of single ridge SIW quarter-wavelength coupled circulator .....	78
Figure 4.21: Sensitivity of single ridge SIW quarter-wavelength coupled circulator .....	78
Figure 4.22: Ridge SIW quarter-wavelength coupled circulator results: return loss.....	79
Figure 4.23: Ridge SIW quarter-wavelength coupled circulator results: isolation.....	80
Figure 4.24: Ridge SIW quarter-wavelength coupled circulator results: Wiltron .....	81
Figure 4.25: Ferrite radius versus dielectric constant of surrounding medium.....	82

Figure 4.26: Radial SIW quarter-wavelength coupled circulator simulation results .....	83
Figure 4.27: Sensitivity of radial SIW quarter-wavelength coupled circulator .....	84
Figure 4.28: Sensitivity of radial SIW quarter-wavelength coupled circulator .....	84
Figure 4.29: Radial SIW coupled circulator experimental results: return loss .....	85
Figure 4.30: Experimental results of radial SIW coupled circulator: isolation.....	86
Figure 5.1: Turnstile resonator configurations.....	89
Figure 5.2: Ferrite radius versus filling factor ( $k$ ) using an air spacer .....	91
Figure 5.3: Ferrite radius versus $k$ using a spacer of dielectric constant $\epsilon_d=2.33$ .....	91
Figure 5.4: Eigennetwork adjustment of turnstile resonator: ill adjusted diagram .....	93
Figure 5.5: Eigennetwork adjustment of turnstile resonator: adjusted diagram .....	93
Figure 5.6: Turnstile circulator test jig.....	95
Figure 5.7: Turnstile SIW circulator .....	96
Figure 5.8: Turnstile SIW circulator using a $90^\circ$ UE simulation results .....	98
Figure 5.9: Turnstile circulator using a $90^\circ$ UE sensitivity analysis: return loss.....	99
Figure 5.10: Turnstile SIW circulator using a $90^\circ$ UE sensitivity analysis: isolation ..	100
Figure 5.11: Turnstile circulator using a $90^\circ$ UE experimental results: return loss.....	101
Figure 5.12: Turnstile circulator using a $90^\circ$ UE experimental results: isolation.....	101
Figure 5.13: Frequency response at input and output terminals of $180^\circ$ UE .....	103
Figure 5.14: Turnstile SIW circulator using a $90^\circ$ followed by a $180^\circ$ one.....	103
Figure 5.15: Turnstile SIW circulator simulation results.....	104
Figure 5.16: Turnstile SIW circulator sensitivity analysis.....	105
Figure 5.17: Turnstile circulator using a $90^\circ$ and a $180^\circ$ UE results: return loss.....	106
Figure 5.18: Turnstile circulator using a $90^\circ$ and a $180^\circ$ UE results: isolation.....	106

## INTRODUCTION

The recent explosion of wireless communication systems such as cellular telephones and wireless internet as well as wireless sensor networks that has congested the VHF and UHF bands, coupled with the ever increasing trend toward higher bit rate applications, has forced the proliferation of microwave and millimetre wave systems. The ability of millimetre waves to provide broadband communication services has already been exploited in 28 GHz Local Multi-Point Distribution Systems (LMDS) and 24 GHz point-to-point radios. These systems, favoured for gaining market share in the last mile connectivity, have experienced great commercial success and it is expected that they will continue to do so in the future. The success of these systems is paving the way for more sophisticated ones including 60 GHz wireless Local Area Networks (LAN) and 77 GHz Car Collision Avoidance Radar (CCAR), to name a couple.

The commercial success of these systems depends on the particular technology that will implement various modules. Platforms that are capable of integrating active planar circuitry with high-Q passive components, are easy to manufacture and low cost, are highly desirable. Currently Monolithic Millimeter wave Integrated Circuits (MMIC) and waveguide are the technologies of choice for the active and passive components respectively. Although MMIC is an ideal technology for the low cost mass production of active planar devices its use in the development of high quality filters is limited by the low quality factor exhibited by such substrates. The increasingly stringent channel spacing requirement of modern communication systems requires filters with a high degree of selectivity while maintaining the lowest possible insertion loss. The specification of these filters cannot be met with such a millimetre wave technology. Lumped element filters also cannot be implemented in MMIC because of the low quality factor exhibited by the inductors. One other issue of concern with MMIC filters is crosstalk between transmit and receive channels. Because MMIC substrates are expensive it is not economically feasible to have a large separation between transmit and

receive filters. Often a diplexer is used for both receive and transmit channel separation and isolation, managing crosstalk on these filters becomes difficult.

One technology that solves all these issues and has experienced widespread commercial success is waveguide. Waveguide filters are ubiquitously used in current millimetre wave systems since they offer a very low loss transmission medium that virtually eliminates any crosstalk issues. Waveguide components are however expensive to manufacture. One other disadvantage of waveguide components is that they are difficult to integrate with other planar technologies such as MMIC. Although excellent transitions have been reported in the literature they are all elaborate structures that are difficult to assemble and therefore manufacture and mass-produce. The problem with these past transition schemes was that they tried to integrate a planar medium with a non-planar one.

It was not until recently that the idea of integrating the rectangular waveguide in a Printed Circuit Board (PCB) was introduced [17]. This novel waveguide has recently been referred to as Substrate Integrated Waveguide (SIW). The PCB's top and bottom ground planes form the broad walls of the waveguide and an array of metallized via holes form the narrow walls. The planar medium (microstrip or co-planar waveguide) is used for active components and some passive ones while the integrated waveguide is used in the design of high quality filters and other passive devices. Although the Q-factor obtainable with SIW is below that obtainable with standard rectangular waveguide, it is far superior to that available with MMIC and more importantly is sufficient for most millimetre wave applications. One other advantage with this technology is that it considerably reduces the complexity of the transition between the non-planar transmission medium and the planar one since they are both integrated in a common substrate. The process used to realize the planar components is therefore also used for the non-planar ones. It is therefore ideally suited to the integration of complete systems. To demonstrate the feasibility of the proposed substrate integrated waveguide a number of reciprocal components have been realized including numerous transitions, filters and directional couplers [21]-[25]. These are key building blocks required in any

transceiver design. However millimeter wave systems often require non-reciprocal components such as ferrite phase shifters and circulators. Phase shifters are extensively used in phased array antennas for beam steering and shaping. Circulators are often used to provide isolation between a transmitter and a receiver, and to protect an amplifier from antenna mismatch.

Presently millimetre-wave circulators are available in a rectangular waveguide or a microstrip drop in format. Waveguide millimetre-wave circulators exhibit very low insertion loss, however, just as with other waveguide components, require complex transition structures to interface them with other planar designs. They are therefore not suitable to the low cost mass production of complete integrated systems. Microstrip drop-in circulators, although compatible with other planar circuitry, have typically higher insertion loss than their waveguide counterparts. The purpose of this thesis is to propose and demonstrate and prove the benefit of an alternative configuration compatible with other SIW components.

The configuration, proposed here for the first time, consists of a gyromagnetic resonator at the junction of three substrate integrated waveguide branches. The selection of the appropriate gyromagnetic resonator is a function of the thickness of the substrate being used. A thin substrate is compatible with a microstrip technology and a planar post gyromagnetic resonator. This resonator has top and bottom electric walls and fields that do not vary along its axis. It is ideal for substrates with a thickness between 0.254 mm and 0.762 mm. However in system applications the loss per unit length associated with this thin SIW may be too high. A solution to this dilemma is to embed the SIW in a thicker substrate material. A thicker substrate is more compatible with co-planar waveguide and re-entrant turnstile gyromagnetic resonators. This resonator usually has one face short circuited and the other open and fields that vary along the symmetry axis of the junction. To demonstrate the feasibility of these circulators this thesis realizes two distinct designs in SIW. It is demonstrated that such circulators can compete with present commercial specifications.

The thesis is divided as follows. Chapter 1 serves to provide a brief review of some theoretical notions of propagation in gyromagnetic media and to derive the permeability tensor. One purpose of this chapter is to introduce the reader to the common terminology encountered in the design of ferrite devices. It is also the purpose of this chapter to demonstrate the selection of an appropriate ferrite material in the design of millimetre wave SIW circulators. This is done by examining some fundamental relationships between the circulator properties and the ferrite ones.

The second chapter is devoted to the study of the substrate integrated waveguide and to the different transition configurations between SIW and other planar technologies encountered in the literature. A method of broad-banding one SIW to co-planar waveguide configuration is demonstrated here for the first time. A doubling of the gain bandwidth product is realized with this technique. In addition an SIW to rectangular waveguide transition is also demonstrated here for the first time. This transition enables the characterization of re-entrant turnstile circulators in thick substrates where a wideband co-planar waveguide one is not currently available. Two transitions are realized and their experimental performances are given.

The third chapter returns to the study of circulators. It is the purpose of this chapter to familiarize the reader with the circuit theory of junction circulators. It is the authors opinion that a circuit description of the circulator is often more informative than a full wave electromagnetic one since insight into the circulators adjustment is embodied in this circuit description. The methods outlined in this chapter in conjunction with a commercial Finite Element (FE) package will be used to characterize the circulators in the next two chapters.

The fourth chapter is devoted to the study of planar SIW circulators compatible with thin substrates. This chapter uses a semi-experimental approach to characterize the SIW circulator. The complex gyrator circuit is experimentally extracted and a commercial FEM solver is used to optimize the design of two quarterwave coupled circulators with a filter response of order-2 (degree-2). The designs are manufactured and tested to verify the theoretical simulations.



The fifth chapter is devoted to the study of re-entrant turnstile SIW circulators compatible with thick substrates. A commercial FEM solver is used in this case to extract the circuit parameters via the eigenvalues of the junction. The designs of two distinct turnstile circulators are optimized with this FEM solver. Again the designs are manufactured and tested to verify the theoretical simulations. The results obtained are in fair agreement with the theory.

Finally the conclusion summarizes the contribution of this thesis to the advancement of the art. Also included in this section are suggestions to improve the performance of SIW circulators. Finally insight into possible future work is suggested.

# 1 CHAPTER

## MAGNETIC PARAMETERS AND GYROTROPY SELECTION

There are basically two classes of passive microwave devices: reciprocal and non-reciprocal. In a reciprocal device the transmission response between any two ports is not dependent on the direction of signal flow. In the scattering matrix representation this implies that  $S = S^T$ , where  $S^T$  is the transpose of  $S$ . Reciprocal devices are devices that contain isotropic mediums and they include filters and power dividers. Non-reciprocal devices are devices where the transmission response between any two ports may be dependent on the direction of signal flow. In this case,  $S \neq S^T$ , for  $S$  parameter representation. Non-reciprocal devices are devices that contain anisotropic mediums characterized by a permeability or permittivity tensor and they include such devices as circulators, isolators and phase shifters.

The most ubiquitous anisotropic materials for microwave applications include ferromagnetic compounds such as garnets and ferrites. These gyromagnetic materials are characterized by a permeability tensor of the form

$$\begin{bmatrix} \mu & -j\kappa & 0 \\ j\kappa & \mu & 0 \\ 0 & 0 & 1 \end{bmatrix}$$

Most of the macroscopic theory of microwave ferrite devices is derived from Maxwell's equations in conjunction with this permeability tensor and the boundary conditions of the problem region. The permeability tensor is derived from the equation of motion of the magnetization vector. A simple microscopic model of the atom associates magnetization in ferrites to current loops of the electron orbit around the nucleus and electron spin about its axis. In ferrite materials the latter is the predominant effect and is the only one usually taken into account in deriving the permeability tensor. In ferrite material specifications the Landé g-factor is a measure of the relative contributions of

the magnetizations due to orbital and spin moment. A g-factor of 2 implies that the magnetization is mainly due to the spin moment. A typical g-factor of a microwave garnet or ferrite material is 1.98 [1].

### 1.1 Susceptibility Tensor

In a magnetic material in the absence of an applied d.c. field the electron spins are randomly oriented so that the initial magnetization is small. The application of an external static d.c. field aligns the dipole moments to create a net magnetization  $\vec{M}_s = N\vec{\mu}$ , where  $M_s$  is the magnetization in A/m,  $\mu$  is the dipole moment due to a single electron and  $N$  is the number of unbalanced spins per unit volume. In the absence of an applied a.c. field the dipole moment naturally precesses about the applied d.c. field,  $\vec{H}_o$ , at an angular velocity  $\omega_o = \mu_o \gamma H_o$  and in the presence of loss it spirals inward until it is completely aligned with  $H_o$ . However the presence of a small, transversely polarized, microwave magnetic field will cause a forced precession of the magnetization about the  $\vec{H}_o$  field vector at an angle and angular velocity determined by the applied a.c. field as shown in Figure 1.1. In the presence of a microwave signal the total field acting on the magnetic dipole consists of a d.c. field ( $\vec{H}_o$ ) and a microwave field ( $\vec{h}$ ), for a total of  $\vec{H} = \vec{H}_o + \vec{h}$ . The equation of motion for the forced precession of the magnetization vector is then given by [1]

$$\frac{d\vec{M}}{dt} = -\mu_o \gamma (\vec{M} \times \vec{H}) \quad (1.1)$$

where  $\gamma$  is referred to as the gyromagnetic ratio and is numerically equal to  $1.759 \times 10^{11} \text{ C/kg}$ ,  $\vec{M} = \vec{M}_s + \vec{m}$ ,  $\vec{M}_s$  being the d.c. magnetization and  $\vec{m}$  the a.c. magnetization. The  $\vec{H}_o$  field vector is normally taken along one axis of the rectangular coordinate system, typically the z-axis, and produces a d.c. magnetization along the same coordinate axis. Introducing phasor notation and using a small signal

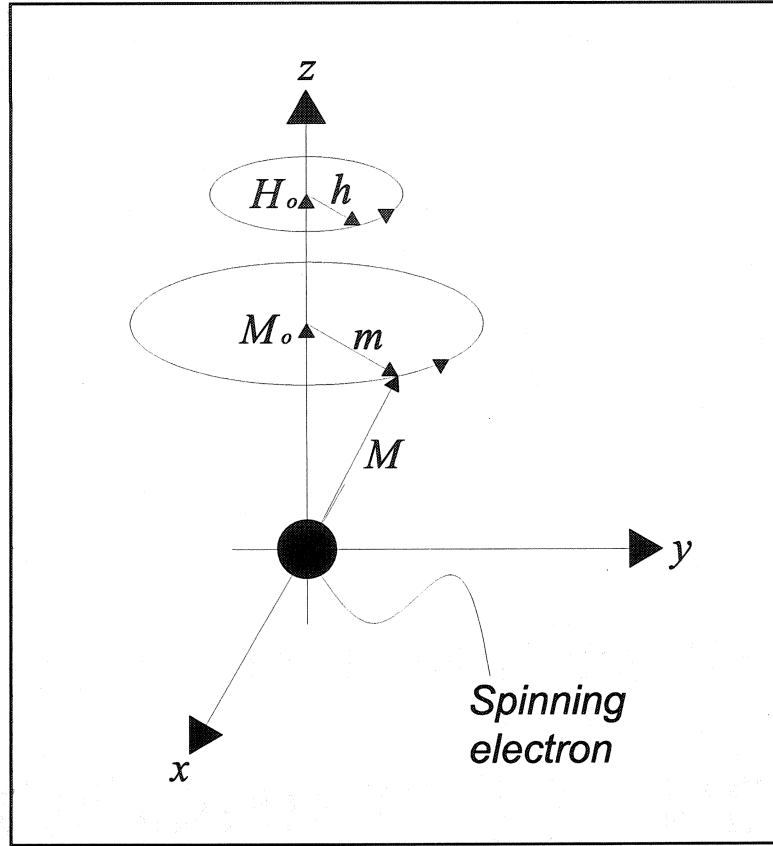


**Figure 1.1: Magnetic moment precession in a typical gyromagnetic insulator**

approximation whereby higher order terms of  $\vec{m}$  and  $\vec{h}$  are neglected, enables a susceptibility tensor to be defined that relates the r.f. steady state magnetization to the r.f. steady state field

$$\vec{m} = [\chi] \vec{h} = \begin{bmatrix} \chi_{xx} & \chi_{xy} & 0 \\ \chi_{yx} & \chi_{yy} & 0 \\ 0 & 0 & 0 \end{bmatrix} \vec{h}. \quad (1.2)$$

The components of the susceptibility tensor are given by

$$\begin{aligned} \chi_{xx} = \chi_{yy} &= \frac{\omega_m \omega_o}{\omega_o^2 - \omega^2} \\ \chi_{xy} = -\chi_{yx} &= \frac{j\omega_m \omega}{\omega_o^2 - \omega^2} = -j\kappa \end{aligned} \quad (1.3)$$

and

$$\begin{aligned}\omega_m &= \mu_o \gamma M_s \\ \omega_o &= \mu_o \gamma H_o\end{aligned}\tag{1.4}$$

To get a better understanding of the interaction of an a.c. signal with a ferrite sample, the eigenvectors of the susceptibility tensor will be determined. An eigenvector is an excitation of a system whereby the response is directly proportional to the excitation [2]. The equation to be solved is

$$([\chi] - \chi_s [I]) \vec{h} = 0\tag{1.5}$$

where  $\chi_s$  is a scalar susceptibility or eigenvalue of the system. This equation has non-trivial solutions provided that the determinant of the matrix vanishes. This gives the characteristic equation of the system, a third order equation in  $\chi_s$ . The roots of the characteristic equation are the eigenvalues:

$$\begin{aligned}\chi_+ &= \chi_{xx} + j\chi_{xy} = \frac{\omega_m}{\omega_o - \omega} \\ \chi_- &= \chi_{xx} - j\chi_{xy} = \frac{\omega_m}{\omega_o + \omega} \\ \chi_3 &= 0\end{aligned}\tag{1.6}$$

The eigenvectors are determined by substituting the eigenvalues back into (1.5). The eigenvalues correspond to right hand circularly polarized (RHCP) and left hand circularly polarized (LHCP) waves respectively. These two normal modes have different susceptibilities and therefore different propagation constants. The bias field therefore sets up a preferential precession direction that coincides with the direction of forced precession for a RHCP wave. This effect gives rise to the classic Faraday Rotation phenomena. Equation (1.6) also demonstrates that a singularity exists at  $\omega = \omega_o = \mu_o \gamma H_o$ , the Larmor precession frequency, for a RHCP excitation. This resonance is referred to as gyromagnetic resonance and occurs when the forced precession coincides in frequency and direction with the natural precession. It is similar to the response of a resonant circuit when the driving frequency is equal to the natural resonant frequency of the circuit. Like any other resonant system loss must be introduced to stabilize the motion of the magnetization vector at resonance. For a LHCP

excitation this resonance is not manifested since the precession direction is opposite to the natural precession direction in the absence of an a.c. excitation. This phenomenon is used in the design of ferrite isolators. The third eigenvector corresponds to the case where the r.f. magnetic field is parallel to the biasing field. To such a wave the medium does not exhibit any gyromagnetic properties, that is, the medium appears isotropic.

### 1.1.1 Linewidth of ferrites

To stabilize the motion of the magnetization vector at resonance loss must be introduced. A typical way that loss is accounted for is by making the resonant frequency complex  $\omega_o \rightarrow \omega_o + j\alpha\omega$ . Introducing this complex resonant frequency into equation (1.3) produces a loss component to the susceptibility tensor elements. One parameter often encountered in the specification of ferrite material is the ferrite line width. The line width of a ferrite is defined as the additional magnetic field required such that the imaginary part of the complex susceptibility tensor element  $\chi_{xx}''$  reduces to half its resonant value. It is analytically found by setting  $\chi_{xx}''(H, \omega_o) = 1/2 \chi_{xx}''(H_o, \omega_o)$  and is given by [2]

$$\alpha\omega = \frac{\mu_o \gamma \Delta H}{2}. \quad (1.7)$$

The ferrite line width is always specified in manufacturer datasheets, it typically ranges from 8000-50000 A/m and is often used as a measure of the loss of a ferrite.

### 1.1.2 Demagnetizing factors

In the preceding sections it was assumed that the ferrite medium was infinite in extent so that the applied field is the field in the ferrite medium. Gyromagnetic resonance is thus directly proportional to the applied field. In a finite sized ferrite sample the internal field is generally different from the external field due to the boundary conditions at the ferrite faces. One means of determining the internal field is through a full wave

electromagnetic solution. Another means is to correct the external field with a demagnetizing one. In general the internal field is given by

$$\vec{H}_{\text{int}} = \vec{H} + \vec{H}_{\text{dem}} \quad (1.8)$$

where  $\vec{H}_{\text{dem}} = -[N] \cdot \vec{M} / \mu_o$  and  $[N]$  are the demagnetizing factors in the x,y and z directions

$$[N] = \begin{bmatrix} N_x & 0 & 0 \\ 0 & N_y & 0 \\ 0 & 0 & N_z \end{bmatrix}. \quad (1.9)$$

Of particular interest to this work are the demagnetizing factors for a thin disk

$$N_z = 1 - \left( \frac{L}{2R} \right) \left[ 1 + \left( \frac{L}{2R} \right)^2 \right]^{-1/2} \quad (1.10)$$

$$N_x = N_y = \frac{1}{2}(1 - N_z)$$

of length  $L$  and radius  $R$  and those for a long cylinder

$$N_z = 1 - \left[ 1 + \left( \frac{2R}{L} \right)^2 \right]^{-1/2} \quad (1.11)$$

$$N_x = N_y = \frac{1}{2}(1 - N_z)$$

Substituting equation (1.8) into equation (1.1) enables a susceptibility tensor to be defined that relates the magnetization to the external r.f. fields in a similar manner as was done in the case of an infinite medium. It must however be noted that the permeability tensor to be used in conjunction with Maxwell's equations is that associated with the infinite medium with the applied d.c. field corrected with the appropriate demagnetizing field. It is not necessary to introduce the r.f. demagnetizing factors since they are intrinsically satisfied when the appropriate boundary conditions are enforced. As a result the external susceptibility tensor is only of academic interest and will not be displayed here. Nevertheless one useful result of this substitution is that

it demonstrates that the shape of the ferrite sample alters the gyromagnetic resonance frequency. It is expressed as a function of the demagnetizing factors as

$$\omega = \omega_r = \sqrt{\omega_x \omega_y} = \sqrt{(\omega_o - N_z \omega_m + N_x \omega_m)(\omega_o - N_z \omega_m + N_y \omega_m)} \quad (1.12)$$

and is usually referred to as Kittel's resonance formula [2].

## 1.2 Tensor Permeability

In solving Maxwell's equation the susceptibility tensor is usually written as a permeability tensor by using the constitutive relation between the magnetic flux density and magnetic field intensity

$$\vec{b} = \mu_o (\vec{h} + \vec{m}) \quad (1.13)$$

Substituting the r.f. susceptibility tensor into equation (1.13) defines the permeability tensor

$$[\mu_r] = \begin{bmatrix} \mu & -j\kappa & 0 \\ j\kappa & \mu & 0 \\ 0 & 0 & 1 \end{bmatrix} \quad (1.14)$$

where  $\mu = 1 + \chi_{xx}$  and  $\kappa = j\chi_{xy}$ . Loss may be introduced in a similar manner by making the resonant frequency complex. In addition the scalar permeability of the normal modes may be found in a manner similar to the scalar susceptibility, they are given by

$$\begin{aligned} \mu_+ &= \mu - \kappa \\ \mu_- &= \mu + \kappa \\ \mu_3 &= 1 \end{aligned} \quad (1.15)$$

In general the effective permeability seen by a plane  $\theta$  directed wave with the ferrite sample magnetized along the z-axis is given by [2]

$$\mu_{\pm}(\theta) = \frac{(\mu^2 - \kappa^2 - \mu) \sin^2(\theta) + 2\mu \mp \{(\mu^2 - \kappa^2 - \mu) \sin^4(\theta) + 4\kappa \cos^2(\theta)\}^{1/2}}{2\{1 + (\mu - 1) \sin^2(\theta)\}} \quad (1.16)$$



When  $\theta = 0$  the two permeabilities reduce to the previous scalar permeabilities where they now correspond to circularly polarized plane waves. When  $\theta = 90^\circ$ , the case encountered in the design of junction circulators, the two permeabilities are

$$\begin{aligned}\mu_e &= \frac{\mu^2 - \kappa^2}{\mu} \\ \mu_{ord} &= 1\end{aligned}\tag{1.17}$$

The extra-ordinary permeability, often referred to as the effective permeability  $\mu_{eff}$ , corresponds to the case where the magnetic field is perpendicular to the d.c bias field. To this wave the medium exhibits gyromagnetic properties. The ordinary wave corresponds to a wave that has its magnetic field in the same direction as the applied d.c. bias field, to this wave the medium exhibits no gyromagnetic properties [1]. These waves constitute linearly polarized ones.

### 1.2.1 Normalized Parameters

It is clear from equation (1.3) that the tensor susceptibility elements can be expressed in terms of a normalized saturation magnetization and a normalized internal magnetic field:

$$\begin{aligned}p &= \frac{\omega_m}{\omega} = \frac{\mu_o M_s}{\omega} \\ \sigma &= \frac{\omega_o - N_z \omega_m}{\omega} = \mu_o (H_o - N_z M_s) \frac{1}{\omega}\end{aligned}\tag{1.18}$$

where the external applied field has been explicitly shown. As previously stated it is the tensor elements in an infinite medium that appear in Maxwells equations and therefore in the final solution. The demagnetizing factors come into play only in modifying the d.c. applied bias field appropriately. The expressions for the tensor elements may be expressed in terms of these normalized parameters. They are given by

$$\begin{aligned}\mu &= 1 + \frac{p\sigma}{\sigma^2 - 1} \\ \kappa &= \frac{p}{\sigma^2 - 1}\end{aligned}\tag{1.19}$$

Gyromagnetic resonance is now given by  $\sigma = 1$ . In order to avoid high losses one must either operate the junction below or above ferromagnetic resonance [3], [4]. To obtain a better understanding of the different modes of operation the effective permeability is illustrated in Figure 1.2 versus the normalized internal magnetic field for parametric values of the normalized saturation magnetization [4]. The effective permeability must be positive to obtain a real propagation constant. The figure demonstrates that this is possible either below  $\sigma \leq 1$  or above  $\sigma \geq 1$  the main resonance. Two differences are immediately apparent from this figure. In the above resonance case the effective permeability is greater than one and the ferrite dimension is therefore smaller for the same circulation frequency compared to a below resonance one. At millimetre wave frequencies where the ferrite dimension is inherently very small this is a disadvantage. The figure also illustrates that the applied bias field is greater in an above resonance circulator. Figure 1.3 demonstrates the external field required for a disk junction operating above resonance in K-band with a saturation magnetization of  $\mu_o M_s = 0.48 \text{ T}$

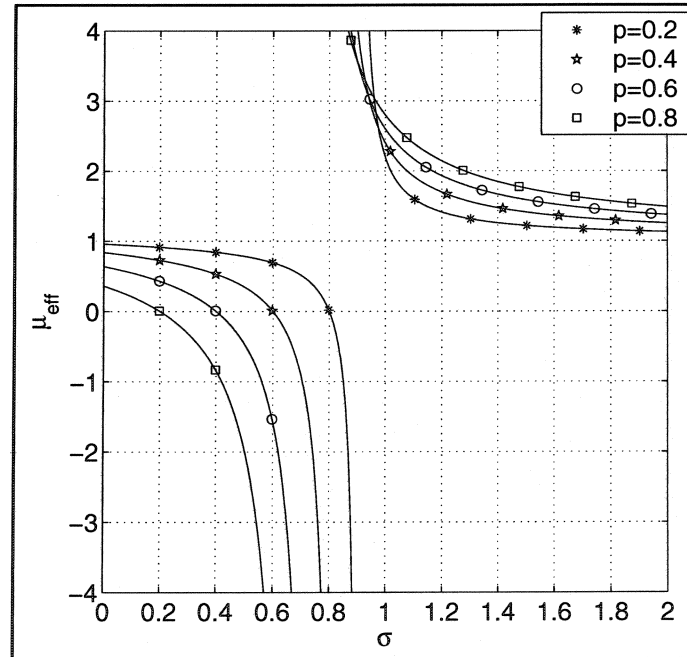
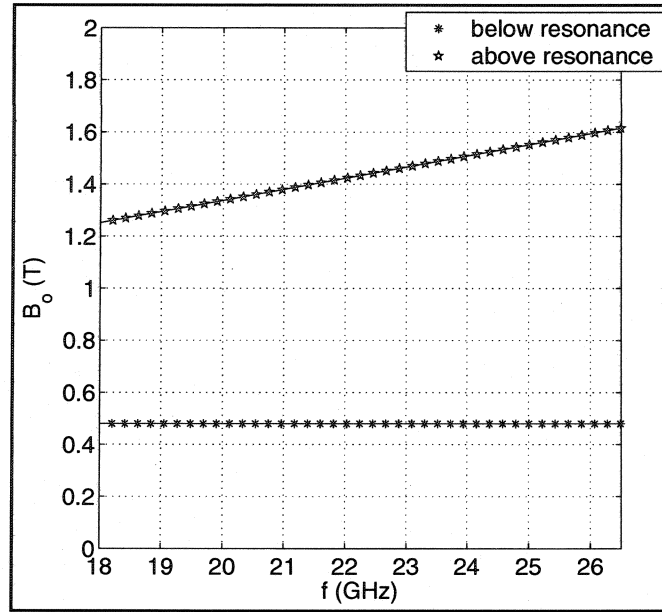


Figure 1.2:  $\mu_{eff}$  as a function of  $\sigma$  for parametric values of  $p$



**Figure 1.3: External d.c. bias field for a typical above and below resonance junction**

and  $\sigma = 1.2$ . Also illustrated in Figure 1.3 is the external field required for a disk junction operating below resonance in K-band with a saturation magnetization of  $\mu_o M_s = 0.48$  T and  $\sigma = 0$ . The d.c. bias field required for an above resonance circulator is approximately 3 times that required for a below resonance one. It is therefore not practical to operate a K-band circulator above resonance because of the constraint on the magnetic circuit. In the below resonance case, although the external field is independent of frequency, it is constrained to values such that the effective permeability tensor is real. These are analytically determined by setting  $\mu_e = 0$ , and are given by

$$\sigma = \frac{-p + \sqrt{p^2 - 4(p-1)}}{2} \quad (1.20)$$

Figure 1.4 illustrates the effective permeability as a function of the applied bias field for a below resonance thin disk arrangement operating at 22 GHz with  $\mu_o M_s = 0.48$  T. This arrangement is encountered in a later chapter. The figure illustrates the maximum applied bias field before resonance absorption losses begin to manifest themselves.

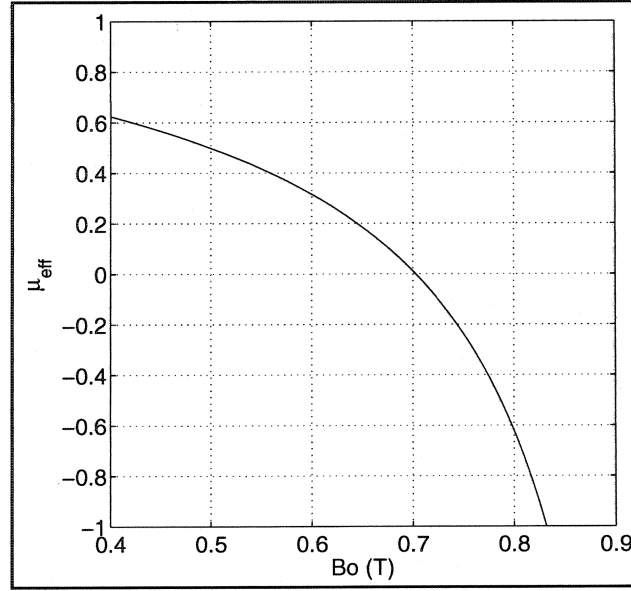


**Figure 1.4:**  $\mu_{eff}$  versus  $B_o$  for a thin disk operating at 22GHz with  $\mu_o M_s = 0.48$  T

### 1.2.2 Partially magnetized ferrites and low field loss

In the preceding sections it was always assumed that the applied external field is such that the junction is completely magnetized, saturated. Saturation is identified with  $\sigma = 0$ . At saturation all the magnetic dipoles are aligned with the result that the magnetization equals the saturation magnetization  $M_s$ . For junction circulators operating below ferrimagnetic resonance it was demonstrated that temperature stability is obtained at an applied bias field that does not fully saturate the junction [6]. More specifically temperature stability is obtained when the ratio of the magnetization to saturation magnetization is  $M/M_s = 0.7$ . In a partially magnetized ferrite medium the magnetization is such that the internal field is nearly zero

$$H_{in} = H_o - N_z M \cong 0 \quad (1.21)$$

so that

$$\frac{H_o}{M_s} \cong N_z \frac{M}{M_s} \cong N_z 0.7 \quad (1.22)$$

A number of papers have been devoted to the subject of the tensor permeability of partially magnetized ferrite samples, a number of representative examples are [7], [8], [9]. Green gave empirical relations on the real part of the tensor elements of a partially magnetized sample,

$$\begin{aligned}\mu' &= \mu_d + (1 - \mu_d) \left( \frac{M}{M_s} \right)^{3/2} \\ \mu_d &= \frac{2}{3} [1 - p^2]^{2/3} + \frac{1}{3} \\ \kappa' &= \zeta \kappa\end{aligned}\tag{1.23}$$

where  $\zeta$  is the ratio of the partial magnetization to saturation magnetization. In an unsaturated ferrite sample two resonance absorption peaks are observed at a particular frequency. One resonance is obtained at a field given by Kittle's equation and another when the ferrite is demagnetized. This second peak is referred to as low field loss. Since in a below resonance circulator the operating bias field is between these two limits care must be taken to avoid low field loss. Igarashi demonstrated that low field loss is eliminated when the normalized saturation magnetization  $p \leq \sqrt{5}/3$  at the lowest frequency of interest [8]. However, it must be noted, that the bandwidth of a circulator is related to the gyrotropy and hence normalized saturation magnetization as illustrated in Figure 1.5. Therefore a compromise must be made between avoiding low field loss and producing the maximum bandwidth for the circulator.

### 1.3 Selection of Ferrite Material and Operating Region

It was demonstrated that at millimeter wave frequencies the magnetic circuit required to bias the ferrite for above resonance operation was impractical. A below resonance operating region is therefore necessary. In a below resonance operation the magnetic field is constrained to a value below that which causes the effective permeability to become imaginary. This value is approximately determined from Figure 1.4 to be  $B/\mu M_s \leq 1.45$ .

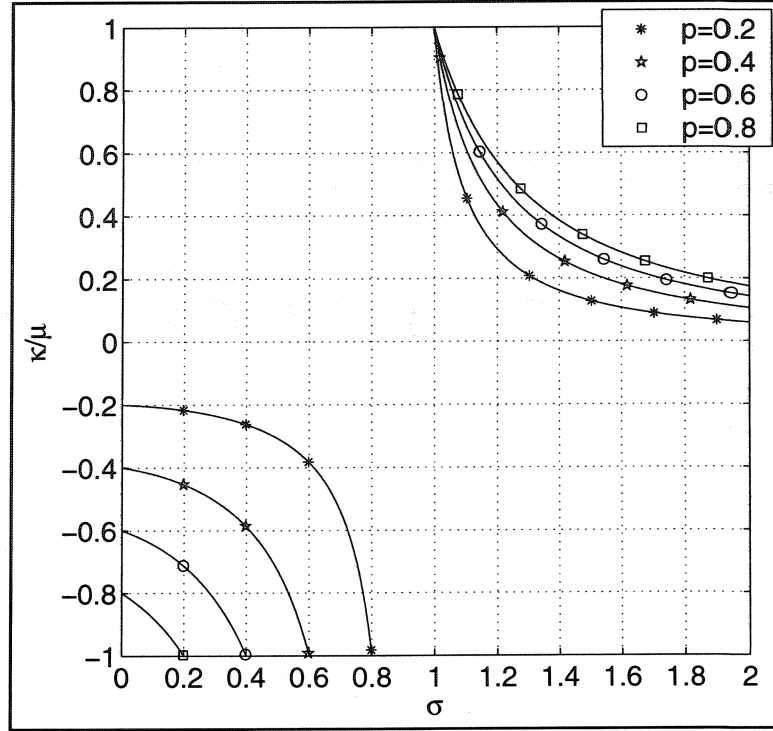


**Figure 1.5:**  $\kappa/\mu$  as a function of  $\sigma$  for parametric values of  $p$

However, for below resonance operation, increasing the magnetic field increases the splitting between the degenerate modes and therefore the operating bandwidth. In addition, in a partially magnetized sample, low field loss occurs when the normalized saturation magnetization increases above a critical value. Also related to the normalized saturation magnetization is the bandwidth of the circulator, a higher  $p$  implies a larger bandwidth. Even in the absence of low field loss a higher  $p$  implies a higher insertion loss. Riccardo gave a semi-empirical formula for the insertion loss of a waveguide circulator in the absence of low field loss [10]

$$IL = -10 \log \left( 1 - 2.85 \chi_e'' - 1.6 \tan(\delta) - 0.017 \right) \quad (1.24)$$

Using a Taylor series expansion for the logarithmic function and retaining only the first term in the expansion demonstrates that the insertion loss is directly proportional to the imaginary part of the tensor element

$$IL = -0.4343 \left( 2.85 \chi_e'' + 1.6 \tan(\delta) + 0.017 \right) \quad (1.25)$$

and hence normalized saturation magnetization. A compromise must therefore be made between the saturation magnetization of the ferrite sample, the circulator bandwidth and the insertion loss. A normalized saturation magnetization of  $p = 0.6$  was assumed to be a reasonable compromise between bandwidth and low field loss. This roughly corresponds to a saturation magnetization of  $\mu_o M_s = 0.48 \text{ T}$ . Such a value of  $\mu_o M_s$  can only be obtained with a ferrite material as opposed to a garnet one, which typically have maximum  $\mu_o M_s$  values of  $0.2 \text{ T}$ . Within the ferrite family of gyromagnetic materials a nickel or lithium ferrite would be required. A catalog of low power loss parameters has been published by Green to enable one to select a ferrite material for the appropriate application [11]. The experimental results indicate that nickel ferrites are in general very lossy. A lithium ferrite was therefore selected. In the lithium ferrite family only TT71-4800 and TT71-4100 have the required saturation magnetization. Due to monetary constraints only a TT71-4800 was utilized in this work.

## **2 CHAPTER**

### **SUBSTRATE INTEGRATED WAVEGUIDE**

With recent developments of millimetre wave systems, such as wireless Local Area Networks (LANs) (59-60 GHz), Car Collision Avoidance Radar (76.5-77.5 GHz), and Local Multi-Point Distribution Systems (LMDS), a transmission medium that is compatible with integrated circuitry, has low loss and is relatively inexpensive to manufacture is required. During the last 20 years numerous millimetre wave transmission mediums were envisioned [12], [13]. However to date rectangular waveguide appears to be the transmission platform of choice. Commercially available components in rectangular waveguide cover the frequency range up to 300GHz, however rectangular waveguides are not suited to a low cost transition to integrated circuitry [14]-[16]. Systems based on rectangular waveguides are bulky, costly and very expensive. They are not suitable to mass production.

The purpose of this chapter is to introduce the reader to substrate integrated waveguide (SIW), a transmission medium that is gaining in popularity. The chapter begins with a brief historical review of past work. Design aspects of SIW are then given. The chapter continues with a study of transitions between SIW and other planar and non-planar transmission mediums. It concludes with some experimental results on two transitions that are used in subsequent chapters.

#### **2.1 Brief Historical Review**

Recently the idea of integrating the rectangular waveguide in a printed circuit board (PCB) was introduced [17]. The ground planes of the PCB form the broad walls of the dielectric loaded synthetic rectangular waveguide and an array of metallic via holes form the narrow walls. The waveguide was proposed, however, no transmission characteristics were given. Hirokawa and al. used this waveguide as a feed structure to



an antenna array in the 40GHz range and provided some transmission characteristics of the embedded waveguide [18]. He also suggested the idea of an effective broad wall dimension. A laminated version of the embedded waveguide was proposed by Uchimura and al. [19]. The via hole array was replaced with a grid like structure to reduce radiation losses at discontinuities. Based on simulation it was suggested that minimal radiation loss occurs for a pitch spacing of  $p/\lambda \leq 0.25$ . Waveguide bends and T-junctions were studied intensively using a finite element package and reasonable results were obtained. The experimental setup consisted of a feeding pin transition spaced a quarter-wavelength from the waveguide edge. However no results of this transition were presented.

It was not until recently that the idea of integrating circuits into the embedded waveguide was appreciated. In 2001 Jain and al. presented the results of a microstrip to embedded waveguide transition [20]. His waveguide was composed of a continuous wall, and suggested that a via hole array may also be used. More importantly he suggested that integrated waveguide filters may be conceived with via holes as inductive or capacitive elements. An improved microstrip to SIW transition was recently proposed by Deslandes and al. [21]. A transition, suitable for thick dielectric substrates using a coplanar waveguide was also developed by the same authors [22]. Huong and al. proposed a transition from laminated waveguide to standard rectangular waveguide [23]. This idea of substrate integrated waveguide (SIW) circuits allows the possibility of using existing waveguide theory and practice. Cassivi and al. demonstrated the feasibility of H-plane and E-plane directional couplers [24]. Deslandes and al. realized integrated inductive post filters [25]. Injection locked microwave oscillators and resonators were also conceived and Q-factors of over 150 were achieved [26]. However to the author's knowledge no non-reciprocal devices have been realized to date. One attempt at integrating a ferrite phase shifter in SIW has been theoretically formulated by Che and al., however, no experimental results were presented [27].

## 2.2 Design of Substrate Integrated Waveguide

A three dimensional view of the SIW is illustrated in Figure 2.1. The PCB's ground planes form the broad walls of the SIW and a linear array of metallized via holes is used for the narrow walls. Since only vertically oriented currents can flow on the via hole wall, this structure is capable of containing mode patterns with only vertical components of the electric field vector. Mode patterns with horizontal components of the electric field vector will have horizontal components of the current distribution on the via hole wall and will radiate. The SIW is thus ideally suited for containing the dominant mode pattern in rectangular waveguide. The substrate integrated waveguide is completely characterized by the diameter of the via holes ( $\phi$ ), the spacing or pitch between via holes ( $p$ ) and the distance between the two rows ( $a$ ). The details are illustrated in Figure 2.2.

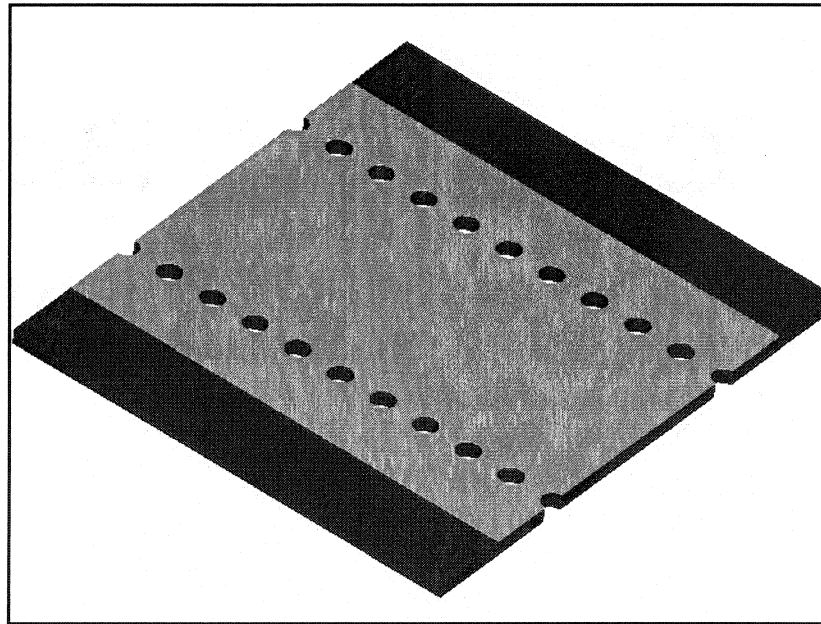


**Figure 2.1: Substrate integrated waveguide**

In some earlier work it was demonstrated that the loss of the SIW decreased as the diameter of the via holes increased and the spacing between them decreased [25]. Some design rules were also presented to ensure a low loss waveguide:

$$\begin{aligned}
 \phi &< \frac{\lambda_g}{5} \\
 p &\leq 2\phi \\
 \frac{\phi}{a} &\leq 0.4
 \end{aligned}
 \tag{2.1}$$

In addition to these design rules a method for calculating the effective propagation constant was proposed. This included the measurement of the phase difference between two equivalent SIW's of different lengths. A formula for the effective width of the waveguide was later presented by Cassivi and al. [28]:

$$a_{eff} = a - \frac{\phi^2}{0.95p} \tag{2.2}$$

The SIW is thus equivalent to a standard rectangular waveguide with a distance between narrow walls of  $a_{eff}$ . This effective width is schematically illustrated in Figure 2.2. From the effective width the propagation constant and characteristic impedance of the guide can be ascertained. For completeness these expressions are provided in the following sections.

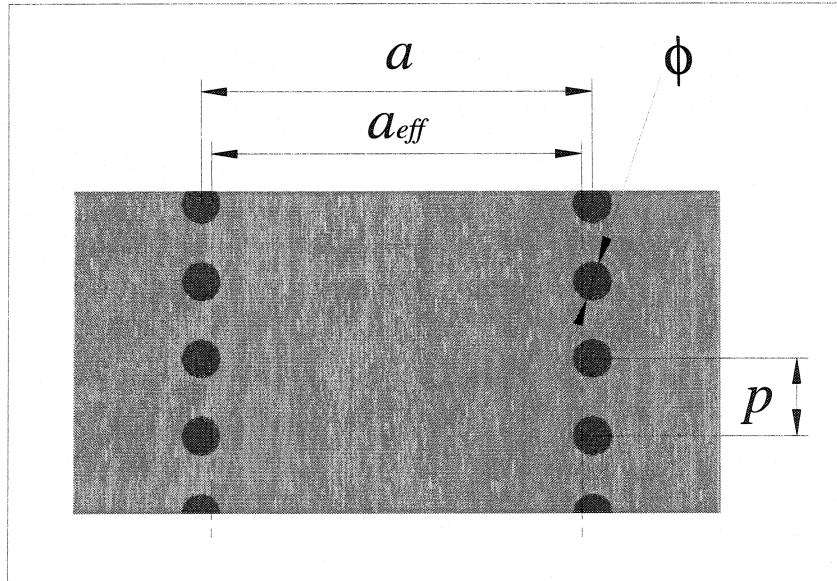


**Figure 2.2: Design parameters of substrate integrated waveguide**

### 2.2.1 Propagation constant

The propagation constant is needed in the design of any matching circuit to determine the electrical length of the line and its characteristic impedance. The propagation constant is determined from the cutoff wave number. It is given by

$$\beta = \sqrt{k^2 - k_c^2} \quad (2.3)$$

where

$$k_c = \sqrt{\left(\frac{m\pi}{a_{eff}}\right)^2 + \left(\frac{n\pi}{b}\right)^2}. \quad (2.4)$$

### 2.2.2 Characteristic impedance

One definition of impedance in a rectangular waveguide is the wave impedance. This impedance, however, does not take into account the geometry of the transmission line. Another impedance more often employed in the design of matching networks is the characteristic impedance. The characteristic impedance in a transmission line supporting a TEM wave can be defined in one of three following ways:

$$\begin{aligned} Z_{PV} &= \frac{VV^*}{2P_t} \\ Z_{PI} &= \frac{2P_t}{II^*} \\ Z_{VI} &= \frac{V}{I} \end{aligned} \quad (2.5)$$

In a rectangular waveguide however the choice of voltage and current is not unique and these definitions do not produce the same results. The choice of which definition is more suitable depends on the problem. The three definitions of characteristic impedance in an SIW are given by

$$\begin{aligned}
Z_{PV} &= \frac{2b}{a_{eff}} Z_{TE} \\
Z_{PI} &= \frac{\pi^2 b}{8a_{eff}} Z_{TE} \\
Z_{PV} &= \frac{\pi b}{2a_{eff}} Z_{TE}
\end{aligned} \tag{2.6}$$

where  $Z_{TE}$  is the wave impedance of the TE mode.

### 2.2.3 Substrate selection and SIW dimensions

Simulations carried out on HFSS indicate that selecting a substrate with a higher dielectric constant, as opposed to one with a dielectric constant in the vicinity of 1, produces equivalent circuit parameters that are not compatible with respectable network specifications. More on these parameters will be said in subsequent chapters. In the present work a Rogers RT-Duroid 5870 high frequency laminate was used. The dielectric constant of the substrate is  $\epsilon_r=2.33$ . Once the substrate electrical characteristics are known the design of the SIW proceeds as follows. A K-band equivalent waveguide is desired, with an operating bandwidth between 18 GHz and 26 GHz. An initial starting point is to scale an air filled rectangular waveguide to the required dielectric constant. An optimum choice may then be found with a finite element method (FEM) package [29]. In the present work the distance between via holes is  $a=7.68$  mm, the pitch spacing is  $p=1.524$  mm and the diameter of the via holes is  $\phi=0.800$  mm. All dimensions respect the design rules mentioned previously.

Simulation results of the SIW are illustrated in Figure 2.3. An extra piece of waveguide with the equivalent dimension was added to each port to have a proper definition of the port. The figure also demonstrates that a return loss of better than 30dB is achievable.

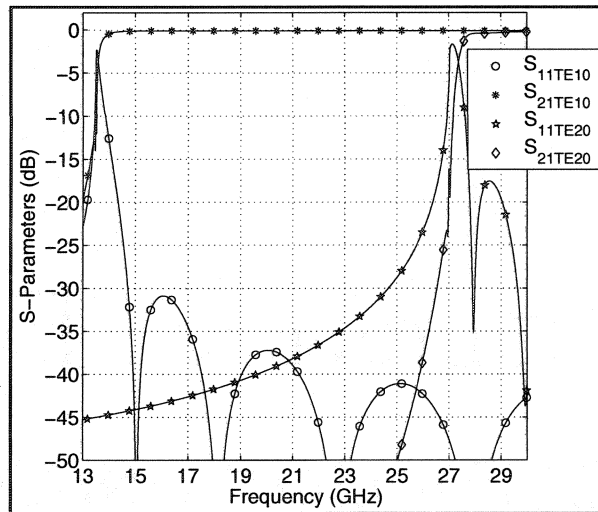


**Figure 2.3: SIW transmission characteristics**

### 2.3 SIW Transitions

Transitions from SIW to microstrip or coplanar waveguide are necessary to couple high-Q waveguide components to active planar ones. In addition these transitions are necessary to be able to experimentally characterize the SIW components. These transitions should have the following properties, broadband, low loss and minimum VSWR. Several articles have been already devoted to the subject, and many more are sure to come. This section provides design details of 3 transitions. The first consists of a transition from SIW to microstrip and is suitable for thin substrates. The next two are intended for thicker substrates. A transition from air filled rectangular waveguide to SIW is presented in this section. This transition, being presented for the first time, is suitable for the measurement of wideband components in thick dielectric substrates, where a wideband planar transition is not readily available. Although the design of transitions is specific to a particular geometry, some basic general guidelines can be appreciated. The design of broadband transitions, in general, requires that the level of the characteristic impedances be similar, and that the field distributions of the coupling structure be similarly oriented. The design of transitions between two dissimilar structures is complicated by the excitation of higher order modes at the discontinuity.

As such a simple calculation of the matching transformer based on the characteristic impedances of the reference lines, is usually not sufficient. In order to reduce the number of experimental iterations required to produce an optimum design a commercial software package is used to fix the optimum dimensions. In fact this method often reduces the experimental iterations to 1. In this work a FEM package is used to optimize the performance of the designs prior to fabrication [29].

### 2.3.1 Transition from microstrip to 0.508 mm thick SIW

The first transition to be designed was first introduced by Deslandes and al. [21]. A 3-dimensional view of the transition is illustrated in Figure 2.4. It consists of a tapered section of transmission line to match the low characteristic impedance of the substrate integrated waveguide to the reference microstrip line. The transformer is milled directly into the broadwall of the SIW. The electric field pattern of the microstrip transition is very similar to the dominant mode field pattern of the SIW and therefore it is expected that this transition will produce a broadband response. The parameters to be optimized are the length of the tapered transformer ( $l_t$ ), the width of the taper at the SIW face ( $w_t$ ) and the width of the reference line ( $w$ ). These parameters are schematically illustrated in Figure 2.5.

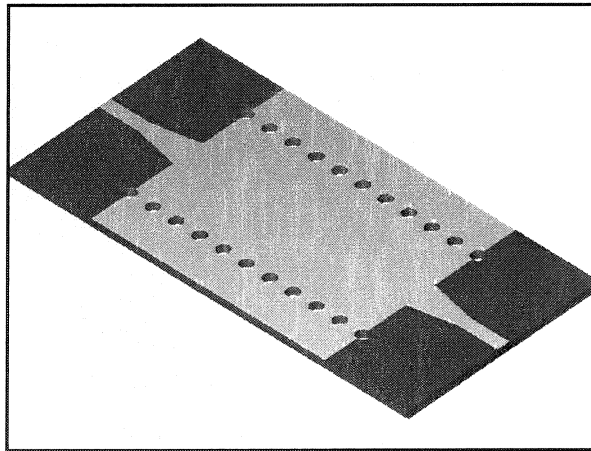


**Figure 2.4: Microstrip to SIW transition**

### 2.3.1.1 Transition design and optimization

With the help of a commercial finite element method package the transition is optimized. The goal of the optimization is to obtain a transition with the minimum return loss over the widest band possible. In addition minimum insertion loss is also desirable. A good starting point is always required to reduce the number of iterations to an optimum solution. Referring to Figure 2.5 the transition length is initially fixed to be a quarter-wavelength at the desired center frequency, 22 GHz in this case. The width of the transformer at the SIW face is initially chosen to be equal to the characteristic impedance of the SIW using a power voltage definition. The SIW has a characteristic impedance of  $Z_{TEPV}=43.48 \Omega$ . This corresponds to a microstrip width of  $w_t=1.8796$  mm. The initial length at 22 GHz is  $l_t=2.3876$  mm. The reference microstrip impedance was chosen as  $75 \Omega$ , corresponding to a width of  $w=0.762$  mm. The transformer is optimized with the use of the Smith chart. A tight loop around the center of the smith chart is the desired response. The dimensions of the following iteration are determined based on the location of the loop of the previous one. The final dimensions after optimization were found to be  $l_t=3.048$  mm,  $w_t=1.8796$  mm and  $w=0.762$  mm. These are in fair agreement with those calculated theoretically.

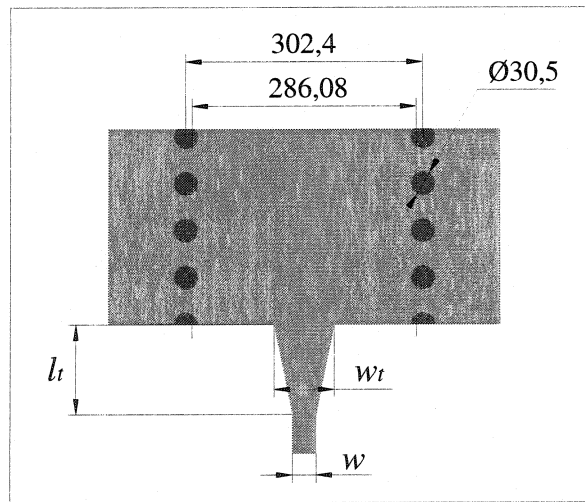


**Figure 2.5: Schematic diagram of microstrip to SIW transition**



### 2.3.1.2 Results of the transition

Figure 2.6 illustrates the results of the transition. A return loss of 19dB and an insertion loss better than 0.3 dB were obtained over the full waveguide band, from 18 GHz to 26.5 GHz. The simulation results correspond to a single transition from microstrip to SIW.

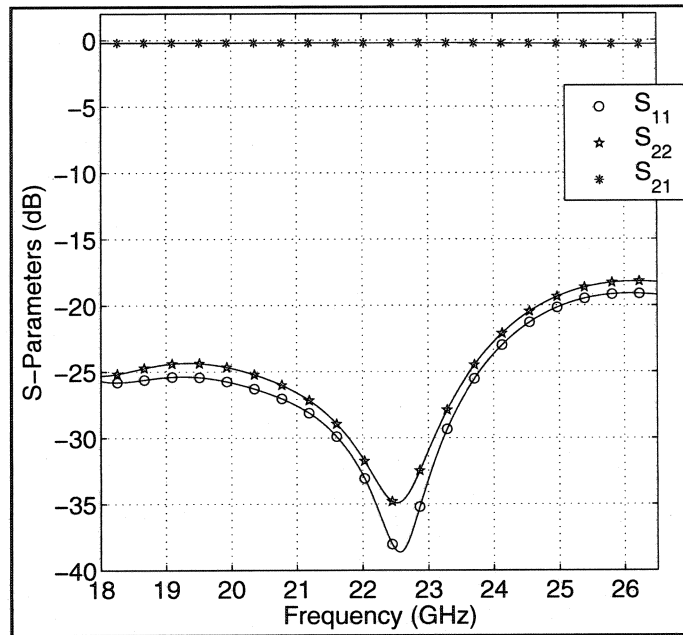
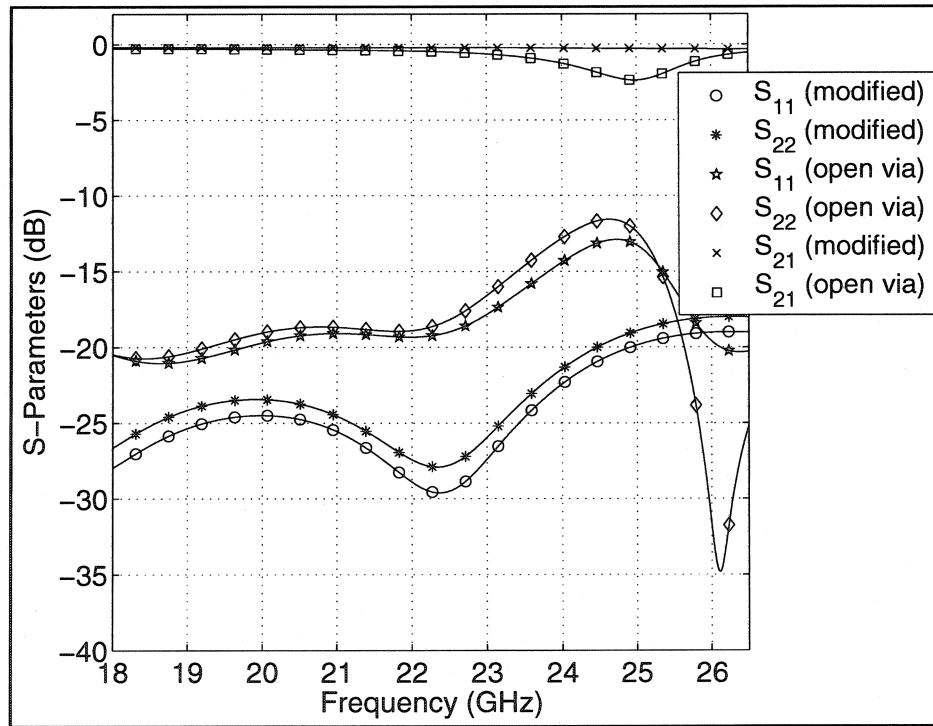


Figure 2.6: Simulation results of transition from microstrip to SIW

### 2.3.1.3 Sensitivity of the design

Mechanical tolerances in the construction of any circuit impede the performance of the design. It is therefore imperative to obtain a qualitative measure of this sensitivity prior to construction. One method that this can be done is to resort to simulation. The response of the circuit under slight modifications of the transition geometry is studied in an attempt to quantify the sensitivity of the design. The modifications are a function of the capabilities of the manufacturing tolerance in the Laboratory. A ProtoMat C60 is used in this work to manufacture the circuits. With this machine it is possible to position a via hole to within 0.0254 mm of the desired location and it is also possible to obtain a

precision of 0.0254 mm on the milling depth. The circuit has been re-simulated with the broad wall dimension of the SIW enlarged by 0.0508 mm, the diameter of the via holes reduced by 0.0254 mm and the transition width also reduced by the same amount. The simulated results are illustrated in Figure 2.7 under the label modified. The design is not sensitive to manufacturing tolerance since no major changes in the response are observed. Apart from manufacturing tolerance, one other factor that may degrade the response of the transition is the improper grounding of the via holes. The via holes are formed by electrolytically plating the PCB after the holes have been drilled. It is therefore probable to assume that a via may not be properly grounded to the broad wall of the SIW. Included in Figure 2.7 is the response of the transition when a single via is not properly grounded. The characteristics have been altered significantly. The return loss has increased to  $-13\text{dB}$  and the insertion loss to  $2\text{dB}$ . This simulation illustrates that it is imperative to obtain a proper grounding of the vias to the broad walls of the SIW.



**Figure 2.7: Sensitivity of the transition**

### 2.3.2 Transition from co-planar waveguide to 1.5748 mm thick SIW

An integrated transition from grounded co-planar waveguide (GCPW) to SIW was recently proposed by Deslandes here at the Poly-GRAMES Research Center. This transition uses a single post to establish the magnetic field pattern in the SIW. The transformer is milled directly into the broadwall of the SIW. The parameters to be optimized are the diameter of the post, the impedance of the feed GCPW, the location of the inductive post from the back wall of the SIW and the length of the open circuit GCPW used to tune the transition. Although this transition is very simple to design a modification was implemented to increase its gain bandwidth product. A  $\lambda/2$  filter was embedded in the transition to provide a filter response of order-2. A 3-D view of the transition is illustrated in Figure 2.8. The parameters to be optimized in this transition are the diameter of the post ( $\phi$ ), the width ( $w_m$ ) and length ( $l_l + l_m$ ) of the  $\lambda/2$  transformer, the width of the reference line ( $w$ ), the location of the inductive post with reference to the back wall of the SIW ( $l_l$ ), the length of the open circuit GCPW after the inductive post ( $l_o$ ) and the length of the transition to the reference line ( $l_t$ ). All the gap widths were fixed to the minimum width that is practically achievable in the laboratory. These parameters are illustrated in Figure 2.9.

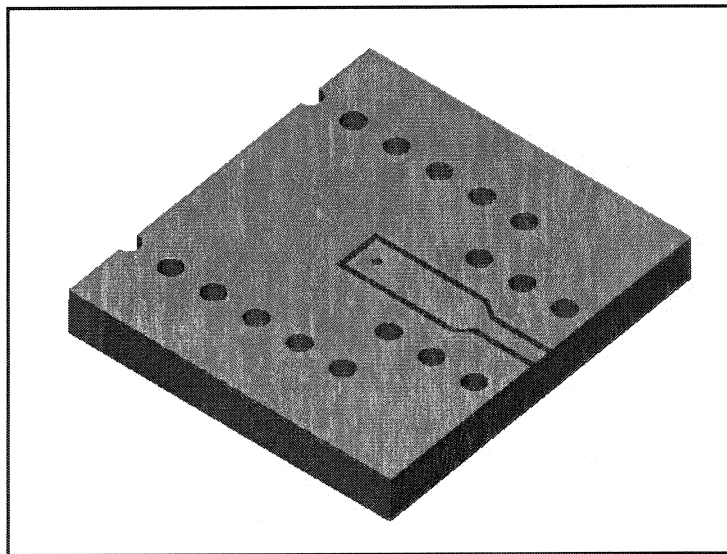


**Figure 2.8: GCPW to SIW transition**

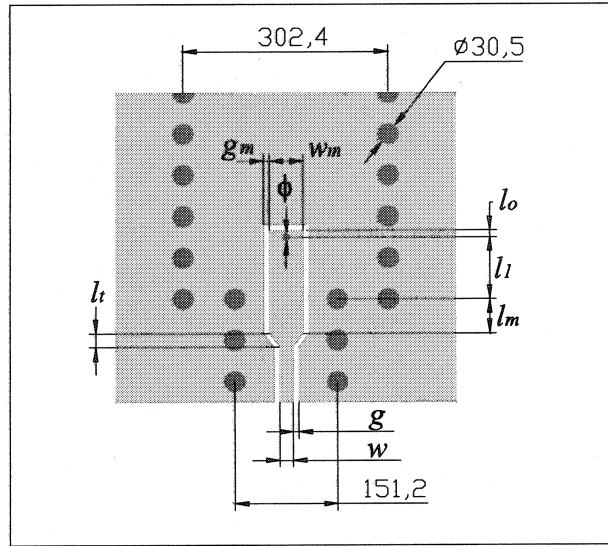


**Figure 2.9: Schematic diagram of GCPW to SIW transition**

### 2.3.2.1 Transition design and optimization

As in the previous case, HFSS was used to optimize the design prior to fabrication. To reduce the simulation time required for an iteration the SIW via wall is replaced with an equivalent continuous wall. An equivalent circuit of this transition without the  $\lambda/2$  transformer section was proposed by Deslandes. Neglecting the fringing effects of the open GCPW and assuming an inductive post position of exactly  $\lambda/4$  reduces the equivalent circuit to a series resonator. One method of broadbanding this circuit is to introduce a suitable  $180^\circ$  unit element (UE) to produce a bandpass filter response of order 2.

The design of this transition proceeds as follows. Initially Deslandes's configuration is optimized to produce a filter response of order 1. The initial position of the via hole is fixed at a  $\lambda/4$  wavelength at the desired center frequency and the open circuited stub is removed. The initial via diameter is arbitrarily chosen to be 0.800 mm, a standard diameter used in the laboratory. Since this transition is dependent on magnetic field coupling, a power current definition of the characteristic impedance is used in the following calculations. The design proceeds by matching the characteristic impedance

of the SIW and feed GCPW and optimizing the via diameter to obtain the maximum gain bandwidth product. The initial dimension of the feed GCPW are  $w=0.635$  mm and  $g=0.2032$  mm. A return loss of 20dB and an insertion loss better than 0.5dB were obtained over an 8% bandwidth from 23.6 to 26.2GHz. A  $\lambda/2$  unit element at a design frequency of 24GHz is now embedded in the broad wall of the SIW. The length of the tapered section was arbitrarily chosen as 0.508 mm. The width of all gaps is fixed at 0.2032 mm. The transition was optimized and the final dimensions are provided for completeness:  $w=0.508$  mm,  $l_t=0.508$  mm,  $w_m=1.27$  mm,  $l_m=1.27$  mm,  $l_f=2.642$  mm,  $l_o=0.356$  mm and  $\phi=0.102$  mm.

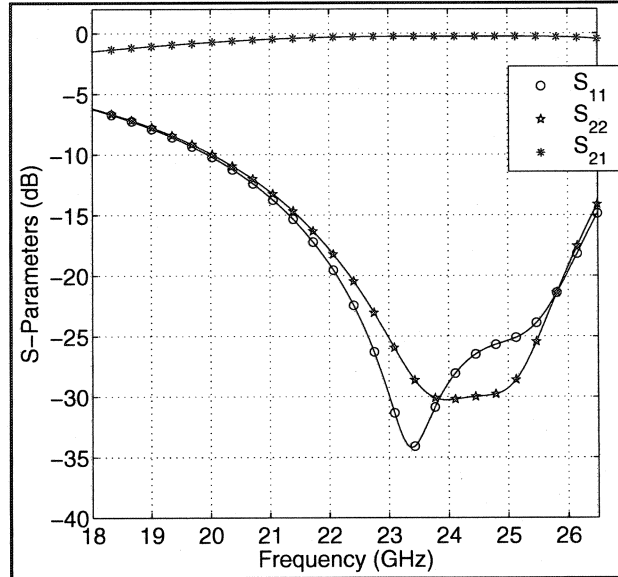
#### 2.3.2.2 Results of the transition

Figure 2.10 illustrates the results of the transition. A return loss of 20dB and an insertion loss better than 0.4 dB were obtained over a 16% bandwidth from 22.3 to 26 GHz. The simulation results correspond to a single transition from GCPW to SIW. The introduction of the 180° UE approximately doubled the gain bandwidth product of the transition. It is expected that this may also be used in thinner substrates to produce full band transitions using GCPW.

#### 2.3.2.3 Sensitivity of the design

The response of the circuit under slight modifications of the transition geometry was studied in an attempt to quantify the sensitivity of the design. The modifications are a function of the capabilities of the manufacturing tolerance in the laboratory as previously underlined. The critical dimension of this transition was determined to be the diameter of the single post. A 0.0254 mm tolerance on the radius of the via was simulated. Figure 2.11 illustrates the frequency response of this modified transition. The change in frequency response is substantial, a decrease in the radius of the via reduced the bandwidth of the transition at the 20dB return loss points to 10%. An increase in its radius, although significantly decreased the midband return loss,

somewhat increased the operating bandwidth. It is however noted that the tolerance on the diameter of the via holes may be kept within 0.0254 mm and it is therefore expected that with careful adjustment this transition will produce satisfactory results.



**Figure 2.10: Transition simulation results of GCPW to SIW**

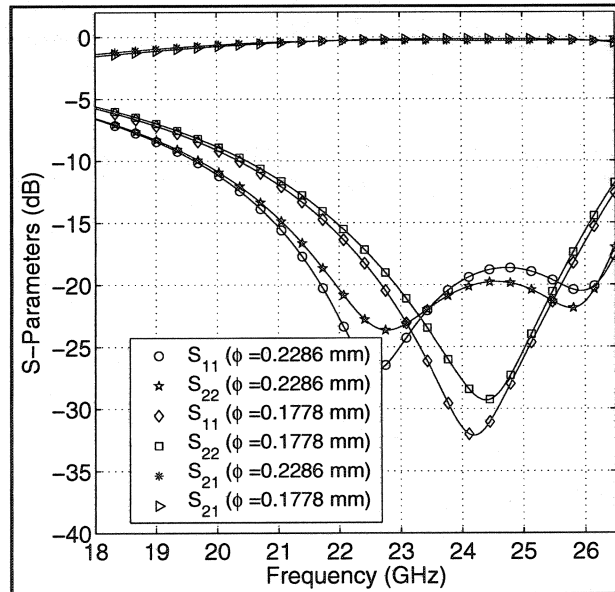


**Figure 2.11: Sensitivity of transition from GCPW to SIW**

### 2.3.3 Transition from rectangular waveguide to SIW

A transition from standard rectangular waveguide to a laminated waveguide was proposed by Huang and al. [23]. In this configuration the rectangular waveguide was coupled via a slot in the broad wall of the SIW. A new configuration where the rectangular waveguide is inline with the SIW is proposed in this work. The transition is illustrated in Figure 2.12. It consists of a multi-step ridge impedance transformer followed by a dielectric filled ridge waveguide with fields that are oriented similar to a microstrip line. Just like the microstrip to SIW transition it is expected that this transition will produce a broadband response since the fields of the transition and SIW are similarly oriented. The parameters to be optimized in this transition are the aspect ratios and lengths of the ridges, namely:  $l_m$ ,  $s_{r1}/a$ ,  $d_{r1}/b$ ,  $l_{r1}$ ,  $s_{r2}/a$ ,  $d_{r2}/b$  and  $l_{r2}$ . These parameters are identified in Figure 2.13.

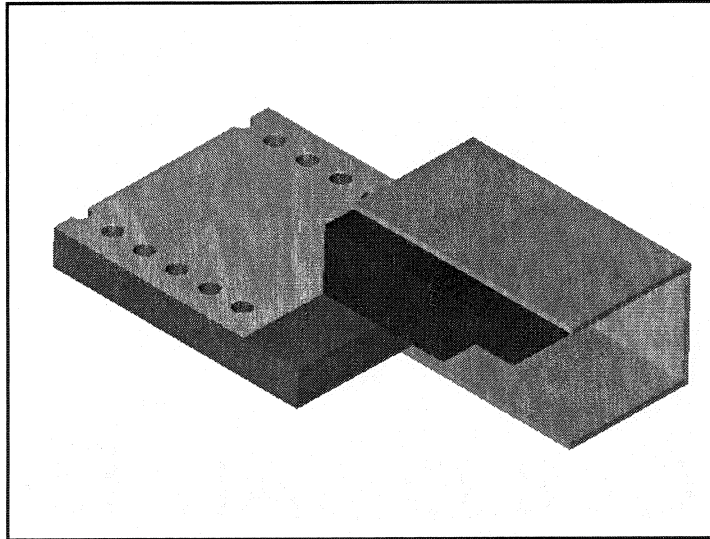


**Figure 2.12: Rectangular waveguide to SIW transition**

#### 2.3.3.1 Transition design and optimization

The detail design of multi-step impedance matching transformers with a prescribed frequency response is well established [1]. One means of obtaining suitable impedance steps to match the low characteristic impedance of the SIW is to have recourse to a ridge

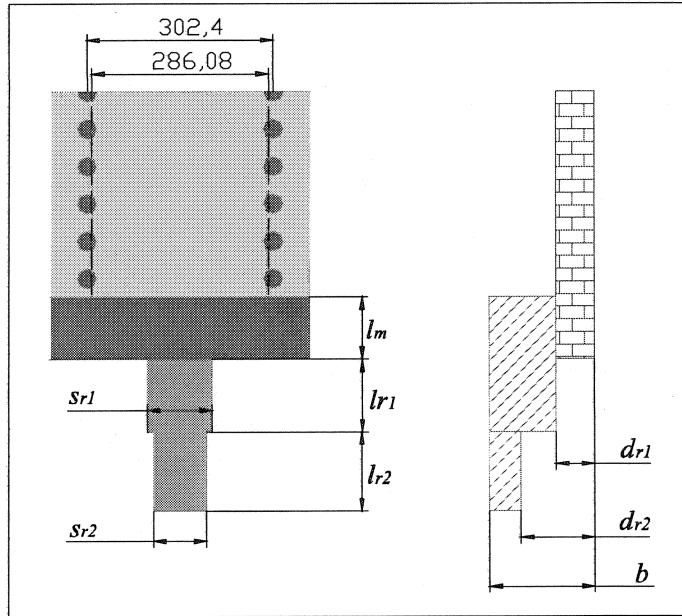


**Figure 2.13: Schematic diagram of microstrip to SIW transition**

waveguide. The ridge waveguide has the characteristic that the impedance of the guide decreases as the ridge steps increase. A design from WR-42 to SIW is contemplated. The initial dimensions were ascertained as follows. The ratio of the characteristic impedance of the air filled waveguide to SIW is approximately 2.9. With a two section matching transformer the required characteristic impedances are approximately  $Z_{r1}=108\Omega$  and  $Z_{r2}=177\Omega$ . The  $d/b$  ratio of the first impedance matching section is fixed to coincide with the thickness of the substrate. The required  $s/a$  ratio to obtain the necessary characteristic impedance is subsequently determined by solving the transcendental equation. For simplicity this  $s/a$  ratio is maintained for the second impedance matching transformer and its  $d/b$  ratio is calculated to satisfy its required characteristic impedance. The length of all sections are originally chosen to be equal to a  $\lambda/4$  wavelength at the desired center frequency of 22 GHz. A  $\lambda/4$  wavelength section of dielectric filled ridge waveguide was empirically determined necessary to increase the bandwidth of the transition. The transition was optimized with HFSS. The final dimensions after optimization were found to be  $l_m=2.54$  mm,  $s_{r1}/a=0.25$ ,  $d_{r1}/b=0.365$ ,



$l_{r1}=2.9718$  mm,  $s_{r2}/a=0.25$ ,  $d_{r2}/b=0.7$  and  $l_{r2}=3.2258$  mm. A matching transformer with three steps was similarly designed. Its dimensions are noted for completeness  $l_m=2.032$  mm,  $s_{r1}/a=0.238$ ,  $d_{r1}/b=0.365$ ,  $l_{r1}=3.3528$  mm,  $s_{r2}/a=0.238$ ,  $d_{r2}/b=0.6$  and  $l_{r2}=3.429$  mm,  $s_{r3}/a=0.238$ ,  $d_{r3}/b=0.853$  and  $l_{r3}=3.937$  mm.

### 2.3.3.2 Results of the transition

Figure 2.14 illustrates the results of the 2-step transition. A 20 dB return loss with an insertion loss better than 0.4dB is possible over the full waveguide band, however, it was decided to center the response about a midband frequency of 24GHz. This transition is useful in characterizing wideband components in thick substrates where a wideband planar transition is not available. The simulation results correspond to a single transition from air filled rectangular waveguide to SIW. The results of the 3-step design are separately illustrated in Figure 2.15.

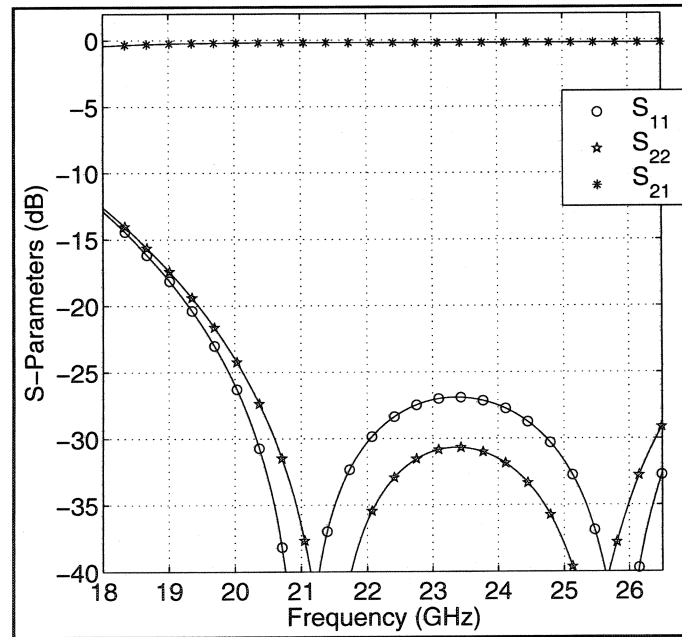
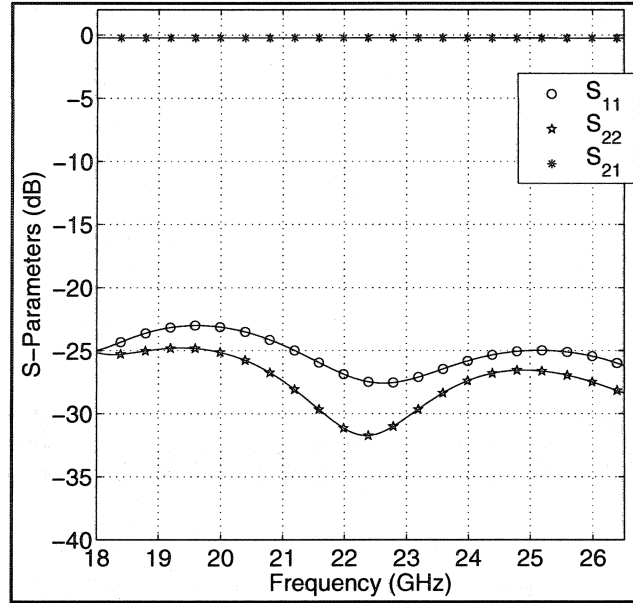


Figure 2.14: Simulation results of degree-2 air filled waveguide to SIW transition



**Figure 2.15: Simulation results of degree-3 air filled waveguide to SIW transition**

### 2.3.3.3 Sensitivity of the design

The modifications in this design were determined based on the ability to properly align the ridge transformer on the SIW. To determine the sensitivity to inaccuracies in cutting the ends of the PCB, one modification consisted of varying  $l_m$  by 0.254mm. To determine the sensitivity of the design to milling errors, the milling depth was increased by 0.127 mm. It must be noted that although the design is also sensitive to changes in the ridge dimensions, the tolerance on these values is within 0.0254mm. These changes were applied to both the degree-2-and degree-3 transformers. The results of the degree-2 transition are illustrated in Figure 2.16. The midband return loss and operating bandwidth have been somewhat degraded. It must be noted that, with careful adjustment, a precision on the order of 0.0254 mm is possible on the milling depth. The degree-3 results are separately illustrated in Figure 2.17. Again no significant modification is observed. It is however less sensitive than its degree-2 counterpart.

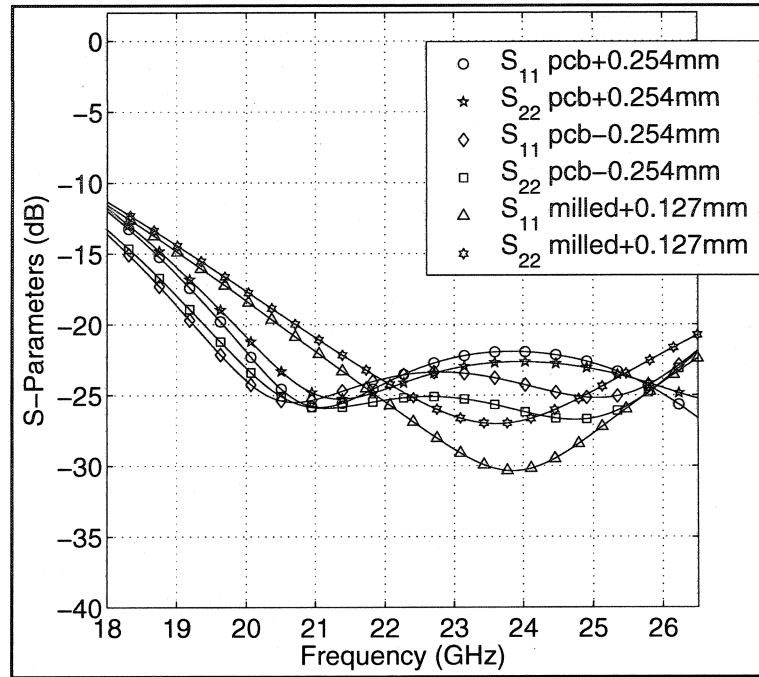


Figure 2.16: Sensitivity of degree-2 air filled waveguide to SIW transition

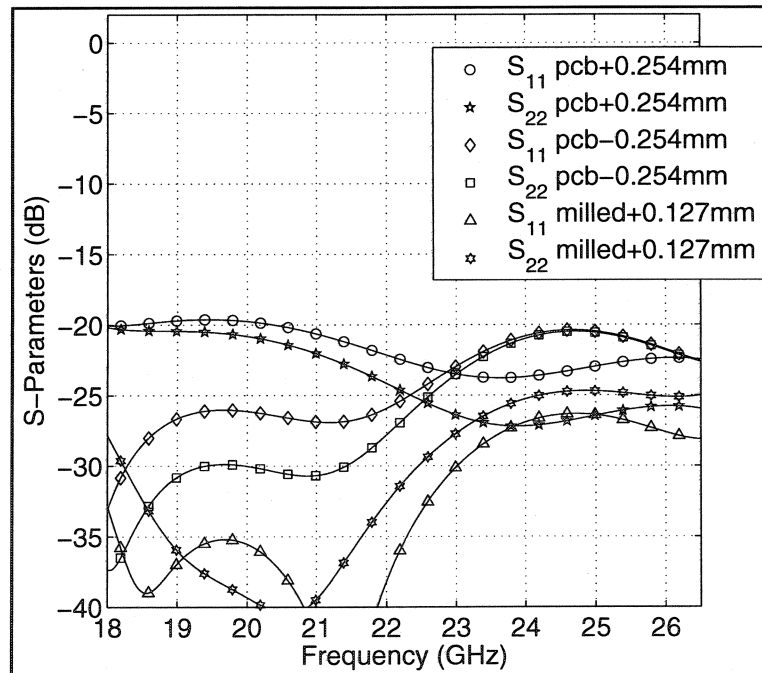
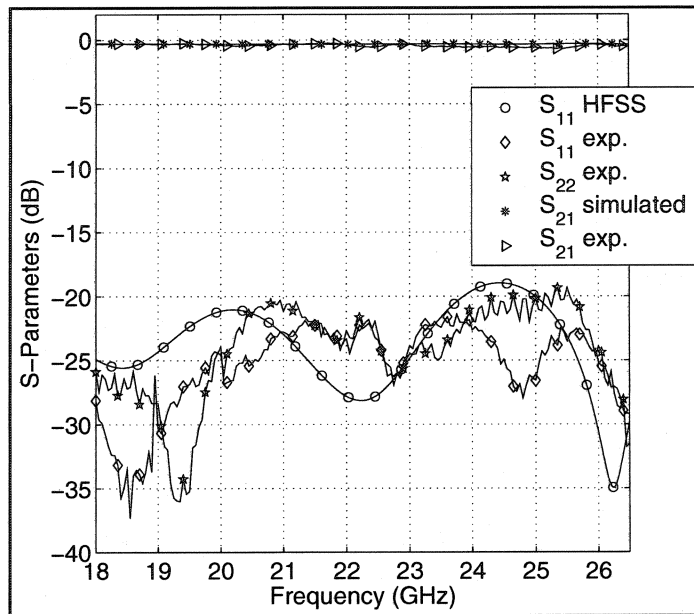


Figure 2.17: Sensitivity of degree-3 air filled waveguide to SIW transition

## 2.4 Transition Selection and Performance

A transition suitable to characterize SIW components must have a low return loss, a reasonable bandwidth and must also be insensitive to small errors in the manufacturing process. The microstrip to SIW transition possesses all these characteristics. It is very stable, displaying minimal variation in its characteristics with changes in its dimensions. As a result this transition was used to characterize the planar circulator in a 0.508mm thick substrate. In order to verify the theoretical simulations a microstrip to SIW transition was manufactured and experimentally verified. The circuit consists of a microstrip to SIW transition, followed by a piece of SIW to sufficiently attenuate higher order modes excited by the transition, followed by another SIW to microstrip transition. The substrate used was a glass microfiber reinforced PTFE composite with a dielectric constant of 2.33. The effective dimensions of the SIW are  $a_{eff}=7.2664$  mm and  $b=0.508$  mm. The SIW therefore has an aspect ratio of 0.07. The transition's dimensions are repeated for convenience  $l_t=3.048$  mm,  $w_t=1.8796$  mm and  $w=0.762$  mm. The reference line impedance was selected to be  $75\ \Omega$  to ensure that no higher order microstrip modes were propagating. The fabrication of the transition is simple. A C60 ProtoMat machine is used to drill the via holes and mill the transitions. Vias are then manually positioned and soldered to the broad walls of the SIW. In a current process the substrate is electrolytically plated with copper and the transitions are subsequently milled. This process avoids the need to manually insert every via hole. The measurements were carried out with a Wiltron test fixture, model CS5226, and a TRL calibration kit was used to remove any discontinuities that are not part of the transition. The measurement results are compared to the simulated ones in Figure 2.18. A good agreement between simulation and experiment is observed. The experimental insertion loss was less than 0.3dB per transition.

In system applications a thick substrate material may be necessary to reduce the conductor loss in the SIW. A transition from microstrip to SIW may not be suitable in this case due to high radiation loss in the microstrip section. Although this may somewhat be alleviated with a thick microstrip width, higher order microstrip modes



**Figure 2.18: Microstrip to SIW transition experimental results**

prohibits this practice. A more suitable transition is one based on GCPW or rectangular waveguide. The GCPW transition is relatively narrow band and is somewhat sensitive to the pin diameter. The rectangular waveguide one has a very large band and is insensitive to errors in the manufacturing of the transition. Since the sole purpose of this transition is to characterize a SIW circulator, the rectangular waveguide one was selected. The 3-step impedance matching transformer was used since it was somewhat less sensitive to manufacturing tolerance. The substrate used was a glass micro-fiber reinforced PTFE composite with a dielectric constant of 2.33. The effective dimensions of the SIW are  $a_{eff}=7.2664$  mm and  $b=1.5748$  mm. The SIW therefore has an aspect ratio of 0.2167. The transition's dimensions are repeated for convenience  $l_m=2.032$  mm,  $s_{r1}/a=0.238$ ,  $d_{r1}/b=0.365$ ,  $l_{r1}=3.3528$  mm,  $s_{r2}/a=0.238$ ,  $d_{r2}/b=0.6$  and  $l_{r2}=3.429$  mm,  $s_{r3}/a=0.238$ ,  $d_{r3}/b=0.853$  and  $l_{r3}=3.937$  mm. The experimental results are illustrated in Figure 2.19. A 20dB return loss with an insertion loss better than 0.4dB per transition is achieved between 20 and 26.5 GHz. The results correspond to a back-to-back transition oriented  $120^\circ$  from each other with a joining section of curved SIW. The simulation results of the SIW bend are superimposed for comparison.

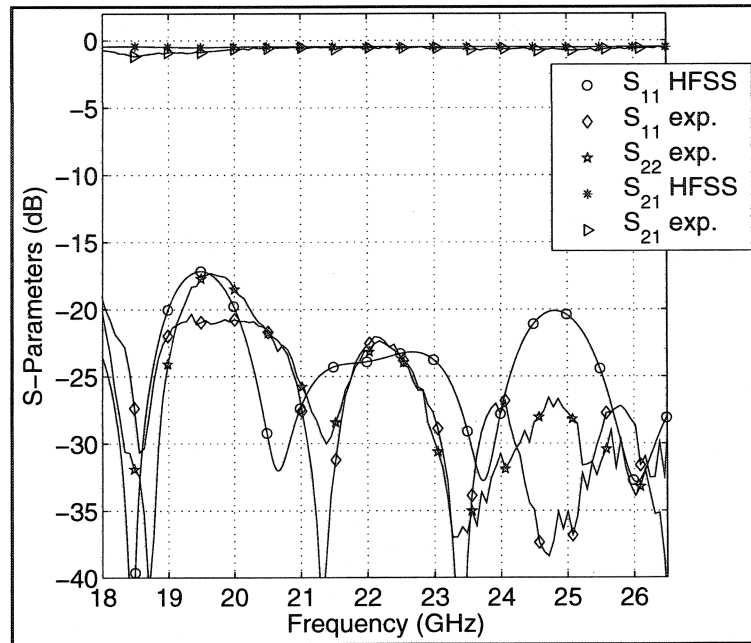


**Figure 2.19: SIW to rectangular waveguide transition experimental results**

### **3 CHAPTER**

## **CIRCUIT THEORY OF JUNCTION CIRCULATORS**

In this chapter an introduction to the theory of junction circulators will be presented. Given that the circulator was originally developed in the 1950's, its operation is now well known. Nevertheless the sheer volume of publications in the literature has, to some extent, buried the fundamentals for a novice in the field. This chapter is an attempt to recover these fundamentals. The principles reviewed herein will form the basis of the preceding chapters in the realization of SIW junction circulators. It is understood that although this chapter is sufficient for the present work, it is certainly not a complete review and the reader is referred to many publications on the topic. Although there are many numerical packages that are available for use in the design of circulators the fundamentals are important in the efficient use of these packages. The purpose of this chapter is therefore not to provide a detailed electromagnetic formulation of the circulator, which is often too complex; it is to provide a circuit description of its operation.

The chapter begins with a brief historical review of past work. It continues by introducing the matrix description of junction circulators. This naturally follows into the classic complex gyrator circuit, which is instrumental in the design of these devices. A method of experimentally characterizing the circulator is also presented. Finally the chapter ends with a brief introduction to broad banding of this device.

### 3.1 Brief Historical Review

The eigenvalues of the scattering matrix provides insight into the necessary adjustment of a symmetrical 3-port junction to achieve circulation. Auld demonstrated the usefulness of the scattering matrix eigenvalues in the synthesis of 3, 4 and 6 port circulators [30]. Separately the scattering matrix eigenvalues however do not provide any details on the required matching element to broadband the device. What is required is an equivalent circuit. One equivalent circuit formulated by Hagelin consisted of an ideal 3-port circulator with 2-port reactive networks connected to each arm to set the degree of matching [31]. The elements of the equivalent circuit are determined by accurately measuring the ratio of the isolation to the insertion loss of the circulator across the complete bias conditions and desired frequency range. The required complexity in characterizing the equivalent circuit restricts its usefulness in practical applications. One simple equivalent circuit for the input impedance of a circulator was proposed by Bosma [32] and Fay and al. [5]. It consists of a series connection of two shunt resonators and in the vicinity of band-center it was demonstrated to be equivalent to a single shunt resonator. Anderson demonstrated the usefulness of this circuit in broad-banding the response [33]. One method of experimentally extracting this circuit was suggested by Simon [34]. It consisted of placing a triple stub tuner at port-2 to effectively decouple port-3. Other, more convenient, experimental methods have also been suggested [35]. While the scattering matrix provides one means of characterizing a circulator, its admittance and impedance matrices provide yet another two for its characterization. By suitably relating the eigenvalues of these matrices many different properties of the circulator can be revealed [36], [37].

In the past many ways were introduced to match the junction to the reference lines. One method is to use a quarter-wavelength transformer at the terminals of the resonator where the junction displays a shunt LCR circuit there [5], [38]. Another is to resort to a half wave filter at the characteristic planes where the junction displays a series LCR one [39]. A combination of both of these resonators was used in the design of a high power



waveguide circulator [40]. The use of evanescent mode cutoff sections loaded with capacitive tuning stubs was also reported in the literature [41].

### 3.2 Matrix Description of the Junction Circulator

An understanding of the junction circulator is, strictly speaking, an eigenvalue problem. One description that reveals this adjustment is the scattering one. Other descriptions that do not readily reveal this adjustment however provide insight into its operation is the impedance and admittance ones. These matrices will now be described.

#### 3.2.1 Scattering matrix description

Since the center frequency of a circulator is in the vicinity of its demagnetized one, an understanding of the nature of both of these bias conditions is necessary to the understanding of the junction circulator. The scattering matrix ( $S$ ) of a reciprocal three-port junction with three-fold symmetry is

$$S = \begin{bmatrix} S_{11} & S_{21} & S_{21} \\ S_{21} & S_{11} & S_{21} \\ S_{21} & S_{21} & S_{11} \end{bmatrix} \quad (3.1)$$

The adjustment of the device is more readily understood through the eigensolutions of the  $S$  matrix. The eigenvalues of the scattering matrix are the 1-port reflection coefficients obtained by exciting the ports with the corresponding eigenvectors. The former are ascertained by solving the characteristic equation of the matrix. They are related to the  $S$  matrix through a linear combination of its entries

$$\begin{aligned} s^o &= S_{11} + 2S_{21} \\ s^+ &= s^- = S_{11} - S_{21} \end{aligned} \quad (3.2)$$

The entries of  $S$  are related to the eigenvalues in a similar fashion

$$\begin{aligned} S_{11} &= \frac{s^o + 2s^+}{3} \\ S_{21} &= \frac{s^o - s^+}{3} \end{aligned} \quad (3.3)$$

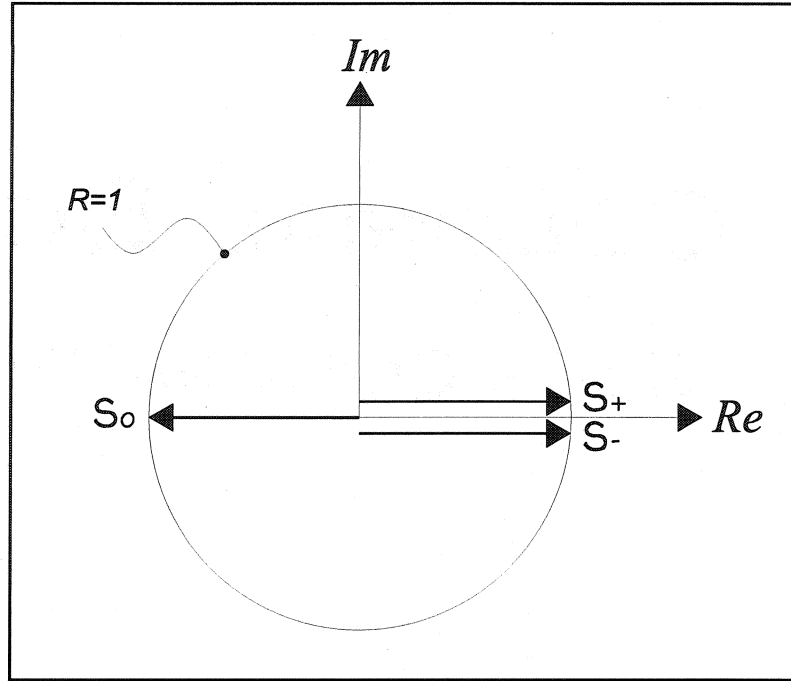


**Figure 3.1: Eigenvalue diagram of demagnetized junction**

The first circulation adjustment coincides with the maximum power transfer condition of the junction. This is obtained by setting  $s_o = -s_+$ . This adjustment also corresponds to the minimum return loss. One eigenvalue diagram that satisfies the first circulation adjustment is illustrated in Figure 3.1. Although this is not the only diagram, it is one that is often encountered in the literature. One set of eigennetworks that coincides with this eigenvalue diagram is illustrated in Figure 3.2 with  $\theta_o = \theta_l = \pi/2$  and  $\theta_+ = \theta_- = 0$ . These eigennetworks are the 1-port equivalent circuits obtained when the junction is separately excited by each eigenvector. If the inphase eigennetwork is approximated by a short circuit boundary condition at the terminals of the ferrite, adjusting the resonance frequency of the ferrite to coincide with the eigenvalue diagram is the only step required in satisfying the first circulation condition. The second circulation adjustment is embedded in the scattering matrix of a circulator. The scattering matrix of a general non-reciprocal junction with three-fold symmetry is given by

$$S = \begin{bmatrix} S_{11} & S_{21} & S_{31} \\ S_{31} & S_{11} & S_{21} \\ S_{21} & S_{31} & S_{11} \end{bmatrix} \quad (3.4)$$

The corresponding eigenvalues may be ascertained by first finding the eigenvectors of an ideal junction. The eigenvectors of the ideal circulator coincide with those of the non-ideal one since these are determined solely by the symmetry properties of the junction. The eigenvalues may be obtained directly from its definition by exciting the junction with the corresponding eigenvectors.

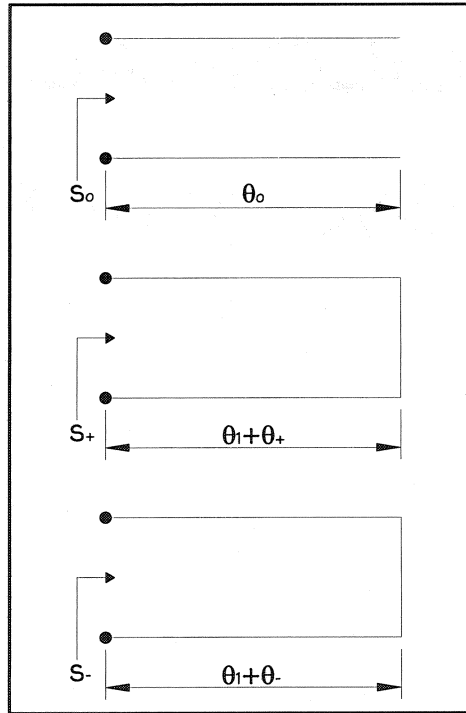


**Figure 3.2: Eigennetworks of a 3-port circulator**

The mathematical details may be found in standard texts and are omitted for brevity [41]. It can be shown that the eigenvalues are related to the entries of the scattering matrix by

$$\begin{aligned} s^o &= S_{11} + S_{21} + S_{31} \\ s^+ &= S_{11} + \alpha S_{21} + \alpha^2 S_{31} \\ s^- &= S_{11} + \alpha^2 S_{21} + \alpha S_{31} \end{aligned} \quad (3.5)$$

Similarly the entries of  $S$  are related to its eigenvalues by

$$\begin{aligned} S_{11} &= \frac{s^o + s^+ + s^-}{3} \\ S_{21} &= \frac{s^o + \alpha s^+ + \alpha^2 s^-}{3} \\ S_{31} &= \frac{s^o + \alpha^2 s^+ + \alpha s^-}{3} \end{aligned} \quad (3.6)$$

where  $\alpha = e^{-j\frac{\pi}{3}}$ . One eigenvalue diagram that satisfies the scattering matrix of an ideal circulator is illustrated in Figure 3.3. It may be obtained from the reciprocal junction by removing the degeneracy between the two split eigenvalues. This adjustment corresponds to the second circulation condition and completes the adjustment of the circulator. It coincides with the maximum isolation, and minimum return and insertion loss. A possible set of ideal eigennetworks is illustrated in Figure 3.2 with  $\theta_o = \theta_l = \pi/2$  and  $\theta_+ = -\theta_- = -\pi/6$ . One means of removing this degeneracy is by introducing a suitable

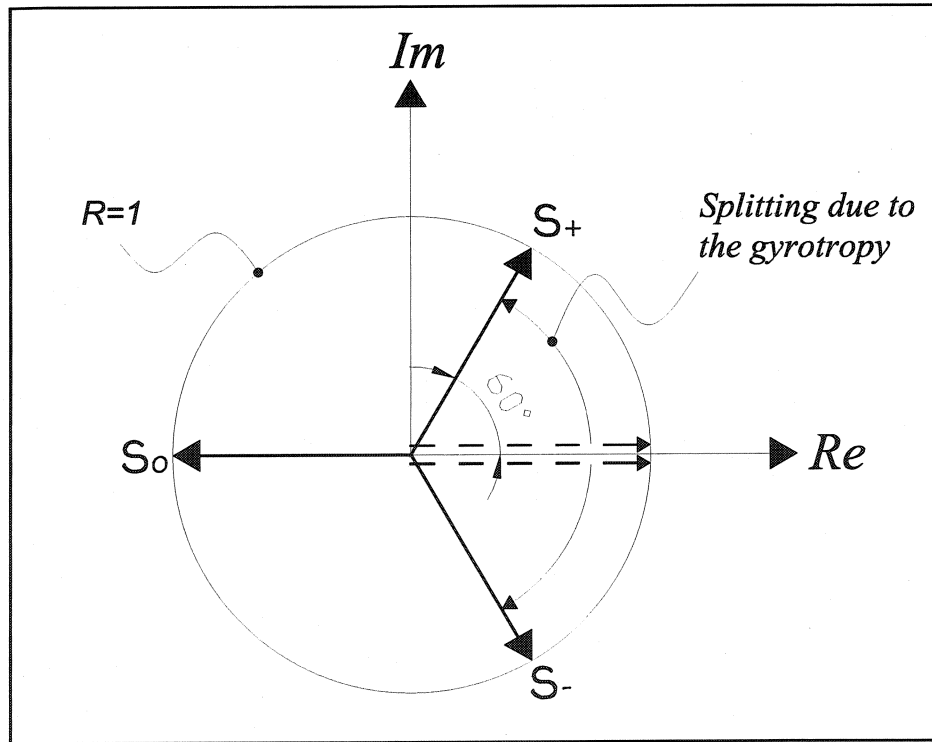


Figure 3.3: Eigenvalue diagram of an ideal circulator

gyromagnetic medium. The necessary splitting is then obtained by magnetizing the junction. An appreciation of this requires an appreciation of the eigenvectors. They are given by

$$\bar{V}^o = \frac{1}{\sqrt{3}} \begin{bmatrix} 1 \\ 1 \\ 1 \end{bmatrix}, \quad \bar{V}^+ = \frac{1}{\sqrt{3}} \begin{bmatrix} 1 \\ \alpha \\ \alpha^2 \end{bmatrix}, \quad \bar{V}^- = \frac{1}{\sqrt{3}} \begin{bmatrix} 1 \\ \alpha^2 \\ \alpha \end{bmatrix} \quad (3.7)$$

These eigenvectors are consistent with the eigennetworks in that the inphase eigenvector produces an electric field maximum or open circuit boundary condition on the axis of the ferrite and the counter rotating ones produce an electric field null on the same axis [41]. The counter rotating eigenvectors produce clockwise and counter clockwise fields on the axis of the ferrite which are suitably adjusted by a gyromagnetic medium as explained in Chapter 1.

### 3.2.2 Impedance and admittance matrices

Although the  $S$  matrix of the junction circulator provides insight into its adjustment it is seldom used in developing equivalent circuits. The impedance or admittance matrix is more appropriate for this purpose. The impedance matrix of a general non-reciprocal junction with three-fold symmetry is

$$Z = \begin{bmatrix} Z_{11} & Z_{21} & Z_{31} \\ Z_{31} & Z_{11} & Z_{21} \\ Z_{21} & Z_{31} & Z_{11} \end{bmatrix} \quad (3.8)$$

Its eigenvalues are related to its open circuit parameters in an analogous way as in the scattering matrix description

$$\begin{aligned} z^o &= Z_{11} + Z_{21} + Z_{31} \\ z^+ &= Z_{11} + \alpha Z_{21} + \alpha^2 Z_{31} \\ z^- &= Z_{11} + \alpha^2 Z_{21} + \alpha Z_{31} \end{aligned} \quad (3.9)$$

The open circuit parameters are related to the impedance eigenvalues as follows

$$\begin{aligned}
Z_{11} &= \frac{z^o + z^+ + z^-}{3} \\
Z_{21} &= \frac{z^o + \alpha z^+ + \alpha^2 z^-}{3} \\
Z_{31} &= \frac{z^o + \alpha^2 z^+ + \alpha z^-}{3}
\end{aligned} \tag{3.10}$$

The impedance eigenvalues may also be obtained from the scattering ones by the usual bilinear transformation between the two

$$z_i = Z_o \frac{1 + s_i}{1 - s_i} \tag{3.11}$$

The impedance eigenvalues of an ideal circulator are

$$\begin{aligned}
z^o &= 0 \\
z^+ &= -j Z_o / \sqrt{3} \\
z^- &= j Z_o / \sqrt{3}
\end{aligned} \tag{3.12}$$

The relationships in the admittance plane are similar to those obtained in the impedance plane and are omitted for brevity. The interested reader is referred to [41].

### 3.3 Complex Gyrator Circuit

Applying the unitary condition to a symmetrical matched three-port lossless junction it can be shown that such a junction must circulate. This has been exploited in the development of wideband circulators by introducing suitable matching networks at each port. One method of doing so is to decouple port-3 with a triple stub tuner at port-2 [34]. The input impedance may then be matched with an appropriate matching network. Analytically this corresponds to introducing appropriate boundary conditions at port-3, namely  $V_3 = I_3 = 0$ , in the impedance matrix. Introducing this constraint into the impedance matrix and solving for the input impedance gives

$$Z_{in} = Z_{11} - \frac{Z_{21}^2}{Z_{31}} \tag{3.13}$$

The condition at port two is also fixed by this boundary condition to the complex conjugate of the input impedance. A circuit configuration that displays this adjustment is illustrated in Figure 3.4. If the inphase mode is approximated by a frequency independent short circuit at the terminals of the ferrite then a simple equivalent circuit may be derived for the complex gyrator impedance. The derivation of this result starts by expressing the complex gyrator impedance in equation (3.13) in terms of the impedance eigenvalues. It continues by replacing the impedance eigenvalues with the admittance ones as a preamble to formulating an equivalent circuit consisting of shunt elements. The required result in the vicinity of the center frequency is given solely in terms of the counter rotating admittance eigenvalues

$$Y_{in} = -j\sqrt{3}\left(\frac{y_+ - y_-}{2}\right) + \left(\frac{y_+ + y_-}{2}\right) = G_{in} + jB_{in} \quad (3.14)$$

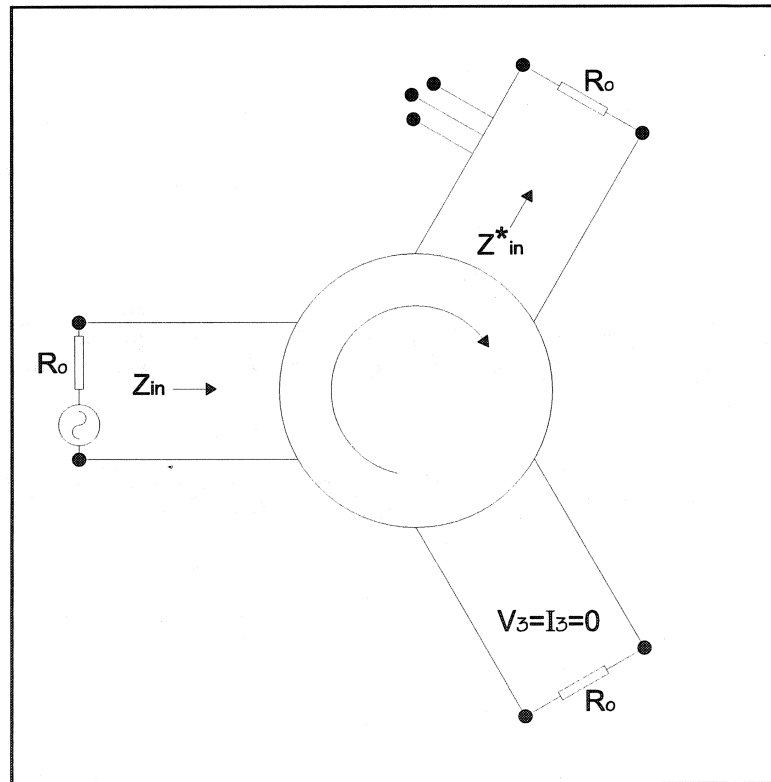


**Figure 3.4: Definition of input admittance**

Recognizing that the admittance eigenvalues of a circulator are purely imaginary the equivalent circuit therefore consists of a conductance in shunt with the counter rotating eigennetworks. Equation (3.14) is often written in terms of the split frequencies of the resonator and the susceptance slope parameter of the demagnetized junction by expressing the admittance eigenvalues in terms of the split frequencies of the gyromagnetic resonator. If the splitting between the counter rotating eigenvalues is small, the complex gyrator conductance may be written in terms of the split frequencies

$$g = \sqrt{3}b' \left( \frac{\omega_+ - \omega_-}{\omega_o} \right) \quad (3.15)$$

where  $b'$  is the susceptance slope parameter of the degenerate eigennetwork

$$b' = \frac{\pi y_1}{4} \quad (3.16)$$

and  $y_1$  is the normalized characteristic admittance of the degenerate eigennetwork. The quality factor is defined as the ratio of the susceptance slope parameter to the conductance in the usual way

$$\frac{b'}{g} = Q = \frac{1}{\sqrt{3} \left( \frac{\omega_+ - \omega_-}{\omega_o} \right)} \quad (3.17)$$

The quality factor is inversely proportional to the split frequencies and this provides one means of evaluating this quantity. The susceptance of a uniform line is related to its susceptance slope parameter in the following way

$$b = 2b' \left( \frac{\omega - \omega_o}{\omega_o} \right) \quad (3.18)$$

This agrees with that found by expanding the input susceptance in a similar fashion as in the case of the gyrator conductance. One means to evaluate the gyrator equation is to resort to an accurate measurement of the scattering parameters and subsequently calculating the eigenvalues. This brute force method however requires that the reference plane of the circulator be accurately known a priori. This method is therefore not directly applicable to the design of SIW circulators since the transition from SIW to



microstrip precludes an accurate measurement of the phase. One straightforward method to determine  $b'$  is to measure the VSWR of the ideal circulator in the vicinity of the center frequency [35]

$$b' = \frac{VSWR - 1}{2\delta\sqrt{VSWR}} \quad (3.19)$$

where

$$\delta = \frac{\omega - \omega_o}{\omega_o} \quad (3.20)$$

One similar method is to resort to the demagnetized junction [36]. Yet another is to resort to the gyrator equation via a separate measurement of the gyrator conductance and junction quality factor. One method of evaluating the gyrator conductance is to again resort to a measurement of the VSWR ( $r$ ) at one port, with the other two ports connected to transmission lines terminated in their characteristic impedance, at the center frequency of the junction. The required result is [36]

$$g = \begin{cases} \sqrt{2r-1} & g > 1 \\ \sqrt{\frac{2-r}{r}} & g \leq 1 \end{cases} \quad (3.21)$$

### 3.4 Impedance Matching

The general impedance matching problem of the junction circulator consists of the addition of a suitable two-port network to each arm of the junction, at a specific reference terminal, to transform the equivalent admittance to the characteristic impedance of the reference line. A matching transformer, suitable at the terminals of the ferrite, consisting of commensurate  $90^\circ$  unit elements (UE's) to obtain a degree- $n$  response was formulated by Helszajn [38] and is illustrated in Figure 3.5 for convenience. In this formulation the shunt resonator is replaced with an equivalent short circuited stub. This load is characterised by the level of its conductance, and its stub's susceptance slope parameter and resonant frequency. An additional parameter to simply its description is its  $Q$ -factor defined as the ratio of the susceptance slope parameter to

conductance. This parameter defines the gain-bandwidth product of the matching network. The matching networks are described by their resonant frequency and characteristic admittance. A degree-2 filter response is obtained with a single matching transformer since the complex load produces an additional transmission pole. Of interest is that the paper demonstrates that a wide range of load impedance levels can be accommodated by varying the minimum voltage standing wave ratio (*VSWR*) in the passband.

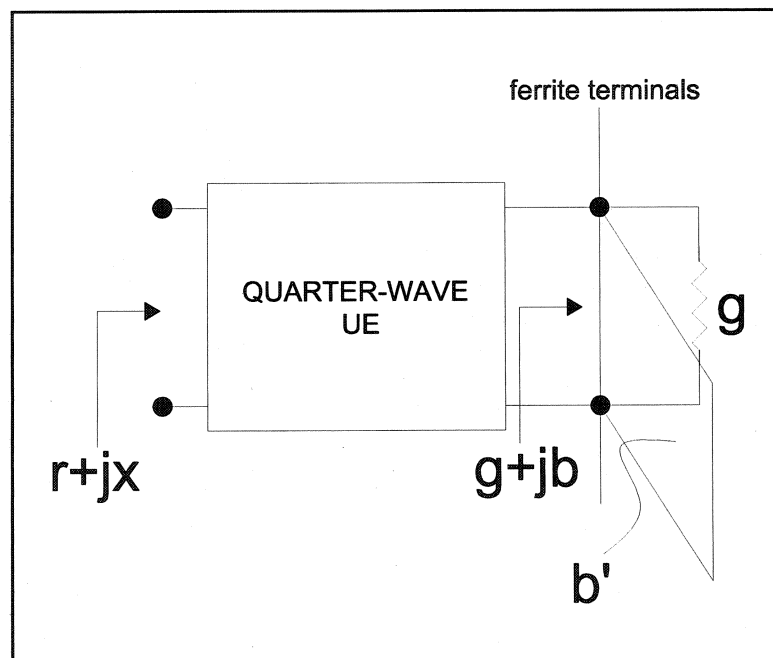


**Figure 3.5: Matching of the junction circulator using  $90^\circ$  UE's**

If the reference terminals are taken at the characteristic planes of the junction then a suitable matching transformer consists of commensurate  $180^\circ$  UE's [39]. The complex load is, in this case, described by the level of its resistance and by the reactance slope parameter and resonant frequency of the series stub in a similar manner to that at the ferrite terminals. The matching transformers are described by their resonant frequencies and characteristic impedance. One difficulty with this arrangement is that the level required of the real part of its load is usually not met in practice. This matching topology however may be used in conjunction with a  $90^\circ$  UE. This configuration is

appropriate in the matching of junction circulators that exhibit network parameters that are not suitable in the design of quarter-wavelength coupled circulators with reasonable specifications. For completeness this matching topology is illustrated in Figure 3.6. This topology also displays a response akin to that of a degree-2 filter section. A non-optimum degree-1 response is realized at the characteristic planes with the  $90^\circ$  UE. The half-wave filter produces the desired degree-2 response at the input terminals of the circulator. Many other matching techniques exist, such as evanescent waveguide sections, however these configurations have not at this time been contemplated in SIW.

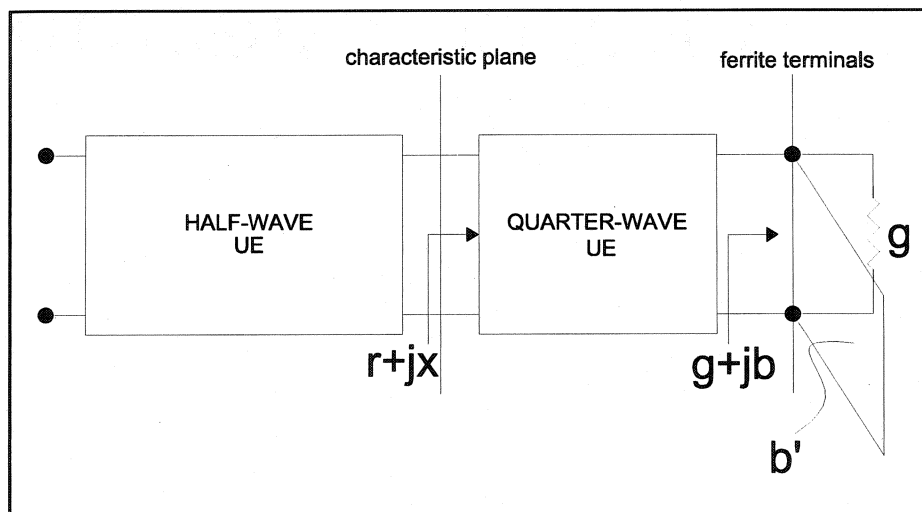


**Figure 3.6: Matching of the junction circulator using  $90^\circ$  and  $180^\circ$  UE's**

## 4 CHAPTER

### PLANAR SIW CIRCULATOR

To date a number of passive components have been realized in substrate integrated waveguide, including transitions, filters, directional couplers and oscillators. However no microwave ferrite devices have been presented. A typical millimeter wave system however often contains non-reciprocal components to isolate the transmitter from the receiver and to protect the power amplifier from antenna mismatches. In addition non-reciprocal components are used extensively in phased array antennas for beam shaping and directing. It is expected that in future millimeter wave systems ferrite devices will be used ubiquitously.

Presently millimeter-wave circulators are available as microstrip drop-in or in standard rectangular waveguide. Waveguide millimeter wave circulators require complex transition structures to interface them with other planar components. Microstrip drop-in circulators, although compatible with other planar circuitry, have typically higher insertion loss than their waveguide counterparts. These configurations are also expensive to manufacture and add considerable cost to a system. The purpose of this chapter is to present a low-cost alternate configuration compatible with other SIW components. The geometry consists of a planar post resonator at the junction of three substrate integrated waveguides. A transition to microstrip is included for measurement purposes. This geometry is presented here for the first time and it is the purpose of this chapter to explore the design of one typical arrangement.

The chapter is divided as follows. It begins with a brief historical review of the present art. It continues by introducing the degree-1 solution and demonstrates that this geometry is indeed suitable to the design of degree-2 circulators with modest specifications. A degree-2 solution is then realized using a single ridge quarter-wavelength matching transformer. A radial SIW coupled one is also included.

#### 4.1 Brief Historical Review

The classic circulator is commercially available in standard rectangular waveguide, transmission line (microstrip, stripline etc...), and in lumped element form. Papers of interest on the stripline geometry include the classic papers by Bosma [32] and Fay [5], and in the lumped element geometry that of Konishi [42]. In waveguide some early papers of note includes Chait's and the classic paper by Davies [43], [44]. Although these geometries have served the commercial industry well over the past 50 years, the proliferation of millimetre wave frequencies and the progression towards higher integration of active and passive components has led to the development of technologies that are more suitable to millimetre wave systems. A high performance Ka-band microstrip circulator using a new ferrite substrate was proposed by Pan and al. [45]. A calibrated insertion loss of less than 0.6 dB was realized over a 17% bandwidth. A Ka-band finline circulator was reported by Goebel and al. [46] and a U-band NRD one by Yoshinaga and al. [47]. A 5% bandwidth with a return loss of 20 dB and an insertion loss of 0.3 dB was reported for the NRD circulator. The purpose of this chapter is to propose and demonstrate a novel millimetre wave planar post SIW circulator that is compatible with other planar active components. The operation of the post waveguide circulator is similar to its stripline counterpart [5]. This resonator supports axial independent electric and magnetic fields with only a z-component of the electric field vector. The modes are thus quasi-TM to the axial direction. Although in a weakly magnetized junction two counter rotating resonant modes may approximately describe the operation of this class of circulators, it is understood that its adjustment is, strictly speaking, an eigenvalue problem [48].

#### 4.2 Degree-1 SIW Planar Post Circulator

A directly coupled SIW planar post circulator consists of a post resonator at the junction of three SIW branches. This resonator is particularly suited to integration in SIW since it supports a quasi-TM, to the axial direction, field pattern that will not radiate

through the discrete synthetic via sidewall of the SIW. A feature of this resonator with axially independent fields is that its resonant frequency, neglecting fringing effects, is approximately independent of its thickness. Another feature of this resonator, which makes it particularly attractive in SIW, is that its susceptance slope parameter may be readily adjusted by varying its aspect ratio.

#### 4.2.1 Gyromagnetic resonator

The post resonator at the junction of three SIW branches is equivalent to that of its rectangular waveguide counterpart when the SIW is replaced with its effective width. The theory already available is therefore applicable. A 3-D view of this configuration is illustrated in Figure 4.1. It is usually operated with axially independent modes of the resonator. Its operation relies on two counter rotating circularly polarized wave patterns that produce a magnetic wall at the terminals of the ferrite, akin to that of a  $TM_{110}^m$  mode, and an in-phase one that places an electric wall there, akin to that of a  $TM_{010}^e$  mode. A circulator is obtained by properly adjusting the splitting between the counter rotating modes when the inphase eigenvalue may be idealized by a short circuit boundary condition. Its resonant frequency is closely related to that of the demagnetized junction and this is the approach used in this work to determine the initial ferrite radius ( $R_f$ ). The radius of the ferrite resonator corresponding to a particular resonant frequency depends on the constituent parameters of the resonator and the details of the SIW. The SIW is described by its  $a$  and  $b$  dimensions, its via hole diameter and separation and by its dielectric constant. In this work the narrow dimension is  $b=0.508$  mm and its aspect ratio is  $b/a=0.07$ . The substrate dielectric constant is  $\epsilon_d=2.33$ . The spacing between via holes is  $p=1.524$  mm and the diameter of the via holes is  $\phi=0.8$  mm. The ferrite material is a lithium one with a saturation magnetization  $\mu_o M_o=0.4800$  T. Its relative dielectric constant is  $\epsilon_f=14.1$ . The design frequency is taken in the middle of the K-band, in particular 22 GHz. The normalized saturation magnetization is  $p=0.61$ . The corresponding demagnetized permeability is  $\mu_d=0.86$ . The radius of the ferrite resonator

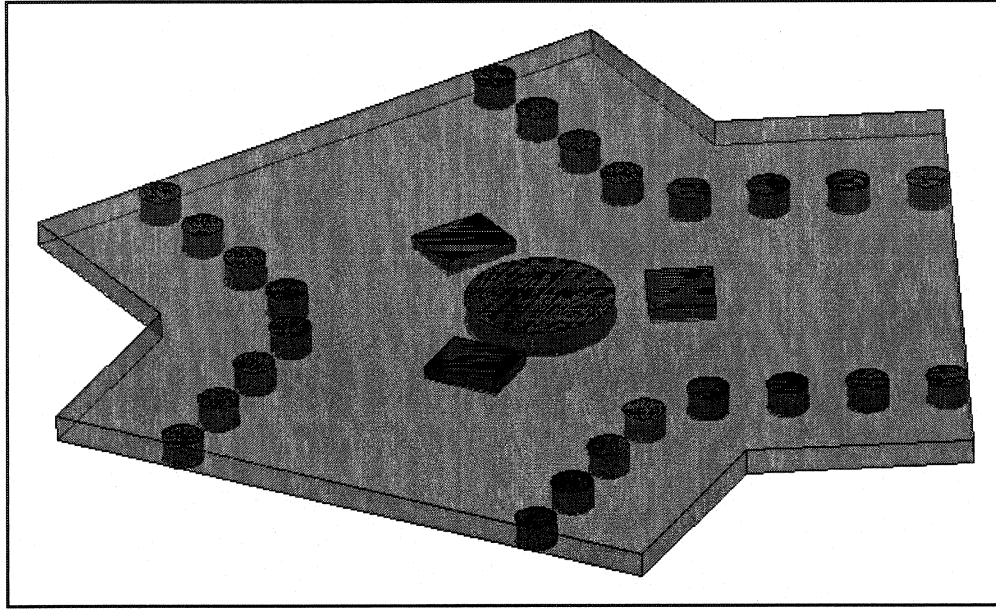


**Figure 4.1: SIW planar post circulator**

is obtained through a solution of the following transcendental equation

$$\sqrt{\frac{\epsilon_f}{\mu_d}} J'_n(k_o \sqrt{\epsilon_f \mu_d} R) K_n(k_o \sqrt{\epsilon_d} R) - \sqrt{\epsilon_d} K'_n(k_o \sqrt{\epsilon_d} R) J_n(k_o \sqrt{\epsilon_f \mu_d} R) = 0 \quad (4.1)$$

where  $\epsilon_f$  is the permittivity of the ferrite,  $\mu_d$  is its demagnetized permeability,  $\epsilon_d$  is the dielectric constant of the surrounding medium,  $k_o$  is the free space wave number and  $R_f$  is the radius of the ferrite [48]. The dominant wave number corresponding to these parameters is found to be  $(k_o \sqrt{\epsilon_f \mu_d} R)_{110} = 2.61$ . This gives a theoretical ferrite radius of  $R_f = 1.6$  mm. The choice of such a thin substrate was to ensure that the radian length of the ferrite does not coincide with any integer number of half wavelengths of any hybrid modes [49]. This ensures that these modes do not get excited in the ferrite.

#### 4.2.2 Experimental procedure

In this work a commercial finite element method (Ansoft HFSS) package is used to optimize the design prior to fabrication. However there are two factors that preclude the complete omission of experiment. Since Ansoft HFSS is being used for the first time, at

the Poly-GRAMES Research Center, to characterize non-reciprocal components, its accuracy is not yet known and must be determined. In addition the package available at Poly-GRAMES does not permit a complete characterization of gyromagnetic media. It is assumed that the ferrite is completely saturated and that it is homogeneously biased; two conditions that are seldom met in practice. A circulator is often operated just below saturation for temperature stability and given that the demagnetizing factors are dependent on the radial coordinate, the spatial magnetization is not homogeneous [50], [9]. The procedure employed in this work is therefore to experimentally characterize the complex gyrator circuit across the full range of bias conditions. The experimental setup is illustrated in Figure 4.2. It consists of an electromagnet with a magnetomotive force sufficient to saturate the ferrite. A power supply is used to vary the current through the coils while an ammeter is used to measure it. The electromagnet was calibrated with a gauss-meter. To measure the device while the bias field is being varied, a TRL coaxial calibration kit was developed. This kit, illustrated in Figure 4.3, consists of three standards of coaxial to microstrip transitions. A TRL calibration is used to remove the effects of the coaxial to microstrip discontinuity of the test jig illustrated in Figure 4.4. The results were verified by comparing them to ones obtained with a standard TRL calibration test set.

#### **4.2.3 Mode chart of SIW circulator**

In general a circulator where the inphase eigennetwork may be approximated by a frequency independent short circuit requires two independent variables for its adjustment. The radius of the resonator is one variable and the gyrotropy the other. Although the first circulation condition has been dealt with to some extent in the previous section its experimental evaluation is of some interest. The circulation frequency coincides with the maximum power transfer condition of the demagnetized junction or the maximum isolation of the magnetized one. Although in an ideal circulator these two solutions are degenerate, this is often not the case in practice.



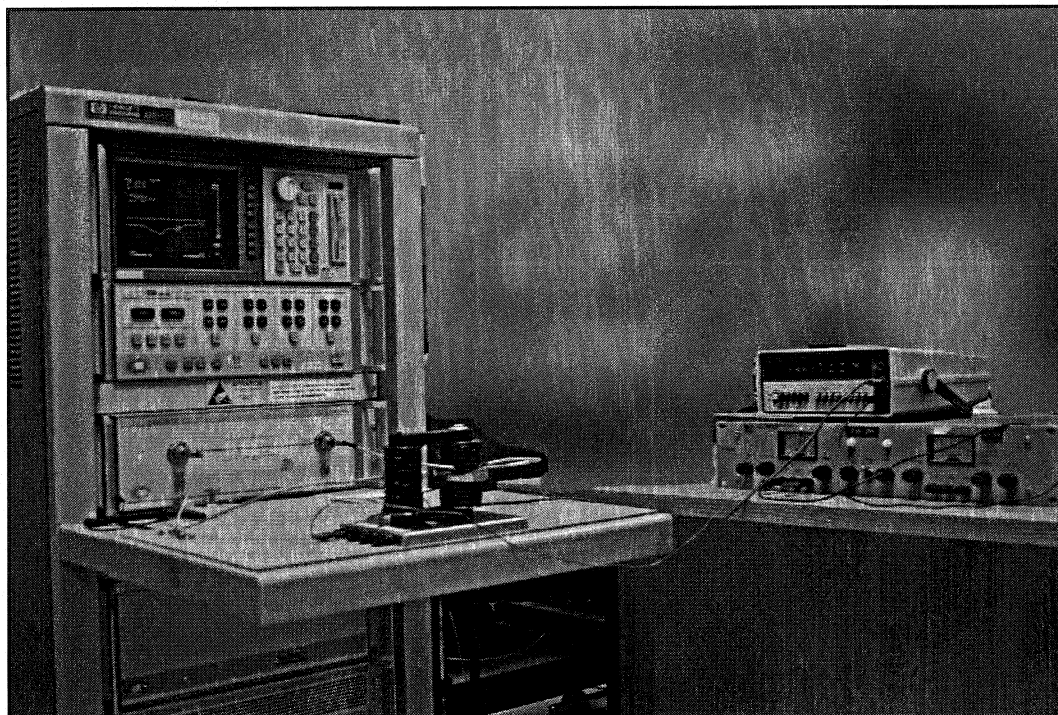


**Figure 4.2: Experimental setup for the characterization of the SIW circulator**

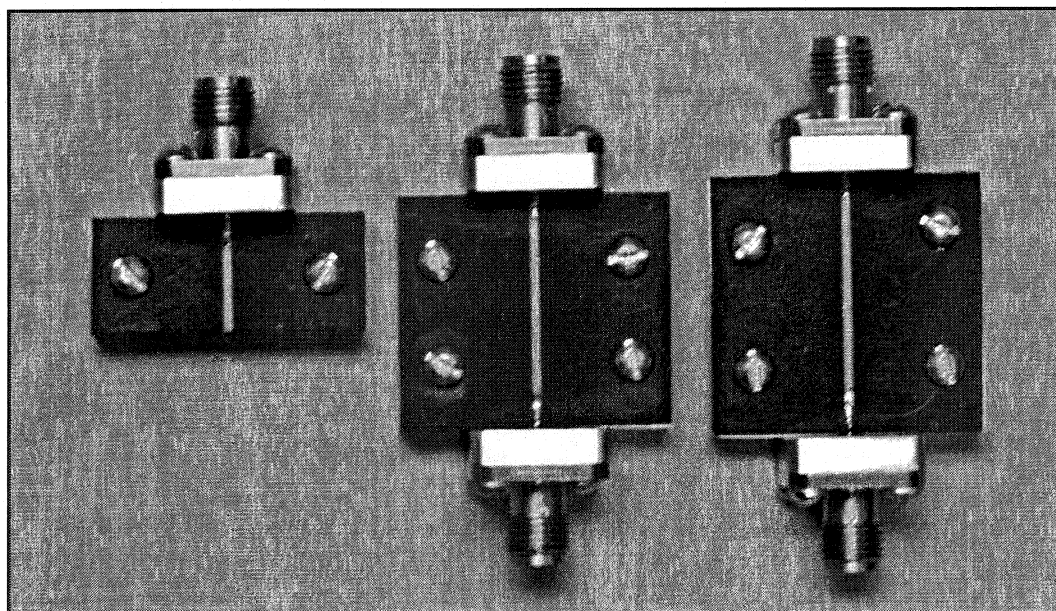


**Figure 4.3: Coaxial TRL calibration kit**

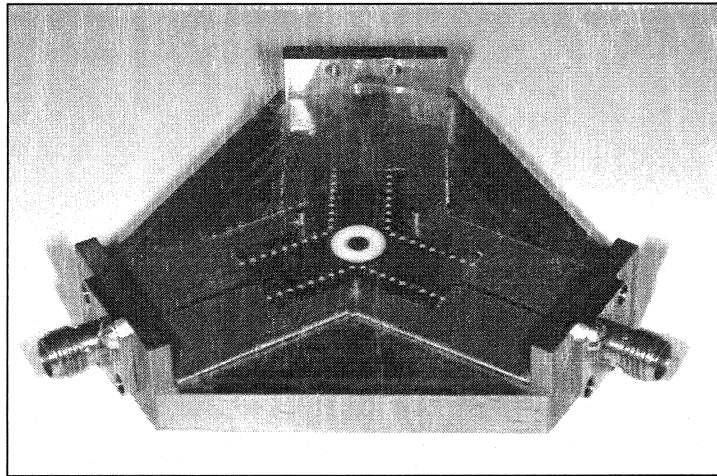


**Figure 4.4: Planar circulator test jig**

As a result the latter method has been employed in this work. A typical response of an ideal junction is illustrated in Figure 4.5. The circulation frequency is quite obvious; it corresponds to the maximum isolation or minimum return loss. The experimental mode chart is separately illustrated in Figure 4.6. The wave number was calculated to be approximately 2.18, in fair agreement with theory. The discrepancy between theory and experiment is in part due to the fact that the SIW's aspect ratio is significantly different from that of air-filled rectangular waveguide.

#### **4.2.4 Complex gyrator circuit**

Although there are many ways of characterizing the junction circulator, the approach used in this work consists of measuring its equivalent 1-port topology across the complete bias conditions of the ferrite. This is done through a measurement of the gyrator conductance and junction quality factor. The universal gyrator equation is then used to obtain the susceptance slope parameter. It must however be understood that in this sort of problem the quality factor and susceptance slope parameter are the independent variables. The quality factor is fixed by the split frequencies of the gyromagnetic resonator while the susceptance slope parameter is separately fixed by its geometry. This approach to characterizing the resonator has been selected because it

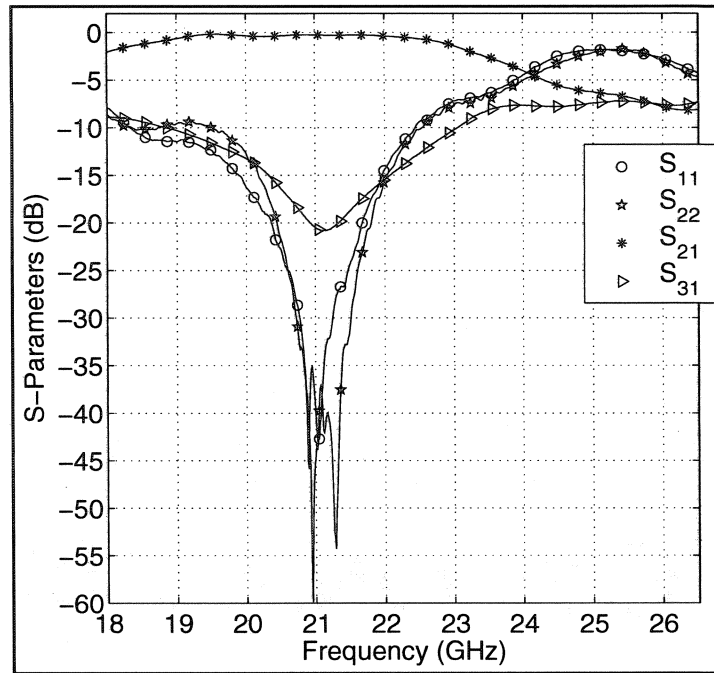


Figure 4.5: Degree-1 SIW planar post circulator experimental results

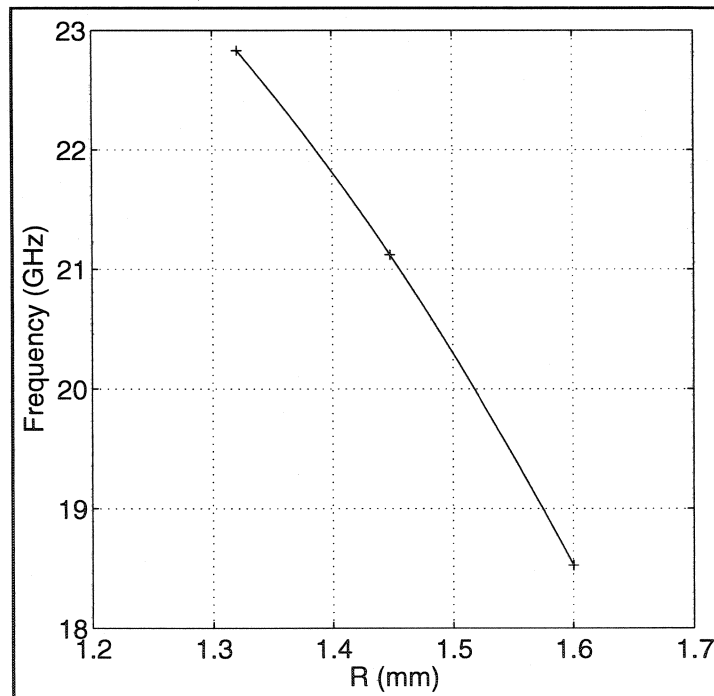


Figure 4.6: Circulation frequency versus ferrite radius

does not require a measurement of any phase parameter, therefore the actual terminals of the junction need not be known a priori. This technique is ideally suited to SIW circulators since the reference planes are in the microstrip, just before the SIW begins. Three different size resonators were characterized in these experiments, one with a radius of 1.32 mm, another with a radius of 1.45 mm and another with a radius of 1.6 mm. The experimental results are illustrated in Figure 4.7-Figure 4.12. The gyrator conductance and split frequencies at saturation have also been extracted from a commercial FEM solver for the  $R_f=1.45$  mm case. These are in fair agreement with experiment. The 1-port circuit displays a gyrator conductance ( $g$ ) of approximately 2, a susceptance slope parameter ( $b'$ ) of approximately 4 and a quality factor ( $Q$ ) of 2. For the 1.32 mm resonator an accurate measurement of the lower split frequency was not possible and it was assumed that the junction was symmetrically split. It will be demonstrated in a later section that these parameters are not compatible with devices of 20 dB return loss [51]. One means to adjust these values is via the resonator thickness. Figure 4.13 illustrates these parameters versus the resonator thickness in a 0.762 mm thick substrate.

### 4.3 Degree-2 Circulator

Two drawbacks prohibit the use of a degree-1 solution in commercial practice. In general degree-1 solutions are narrowband and often there is no guard band to cater for manufacturing tolerance and temperature variations. More importantly degree-1 solutions operate at a bias field that is not compatible with temperature stable devices [50]. These solutions are sensitive to heating effects and ambient temperature variations. The purpose of this section is to demonstrate two degree-2 solutions that are compatible with SIW. One solution resorts to a single ridge SIW transformer to broaden the circulation bandwidth and another to a radial dielectric one.

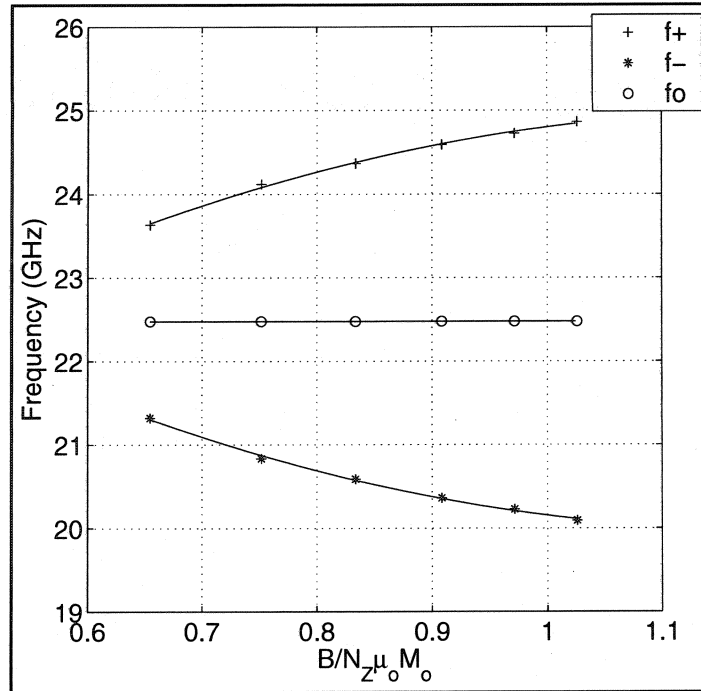


Figure 4.7: Split frequencies versus normalized magnetization ( $R_f=1.32$  mm)

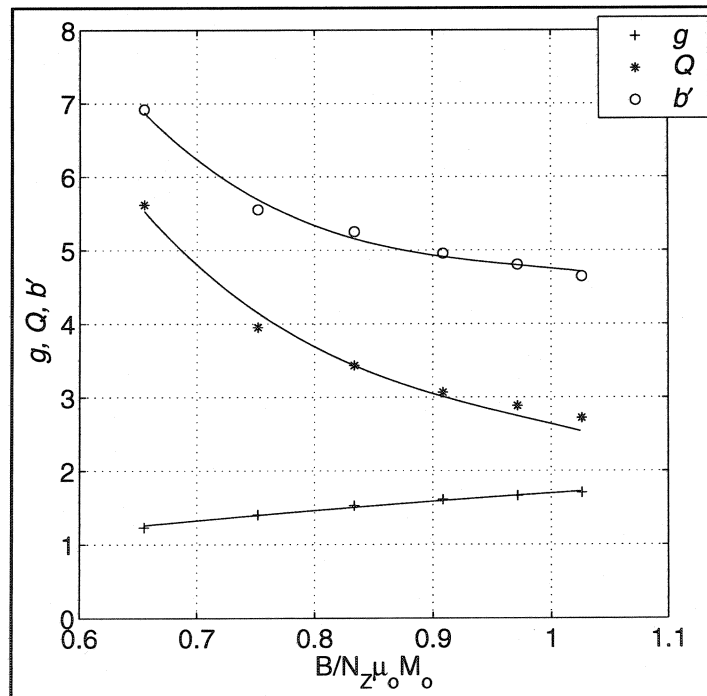


Figure 4.8: Circuit parameters versus normalized magnetization ( $R_f=1.32$  mm)

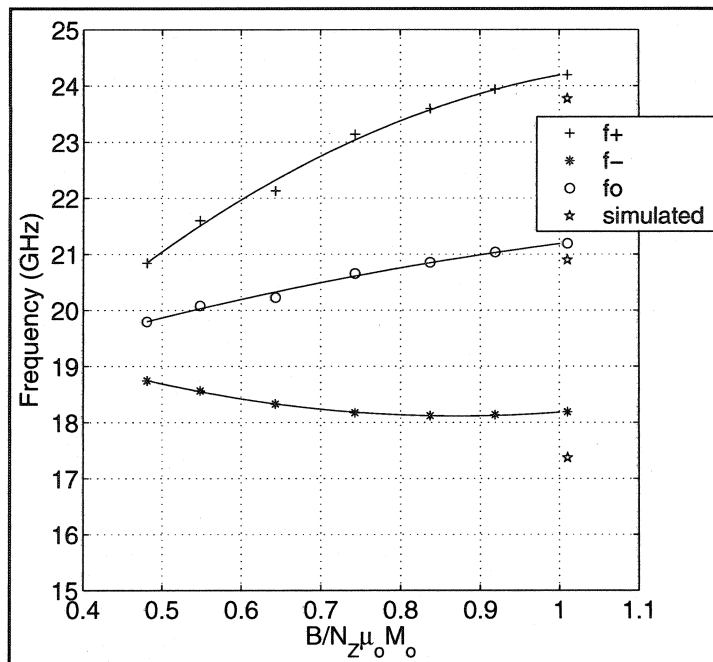


Figure 4.9: Split frequencies versus normalized magnetization ( $R_f=1.45$  mm)

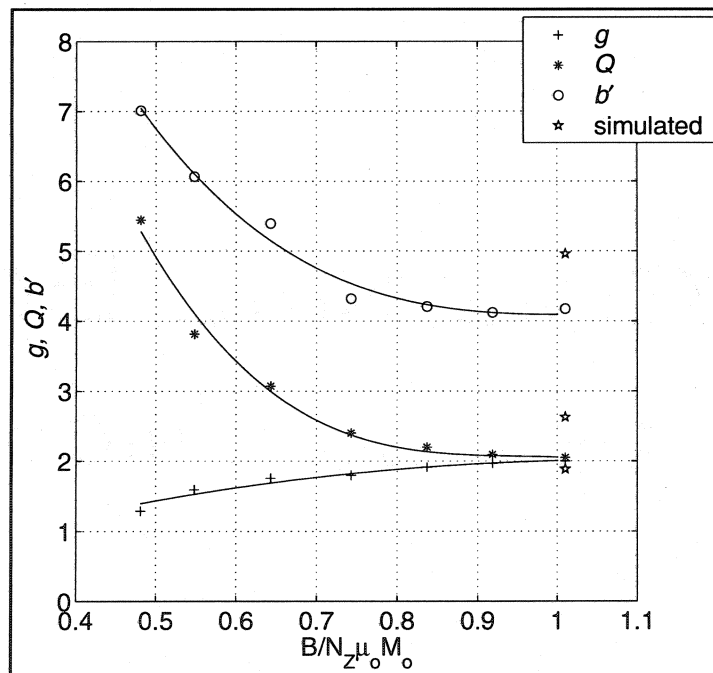


Figure 4.10: Circuit parameters versus normalized magnetization ( $R_f=1.45$  mm)

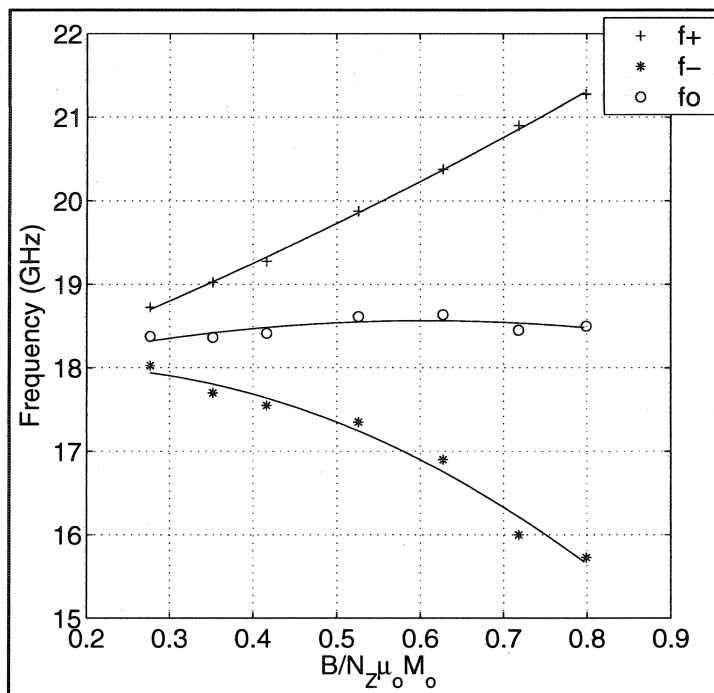


Figure 4.11: Split frequencies versus normalized magnetization ( $R_f=1.6$  mm)

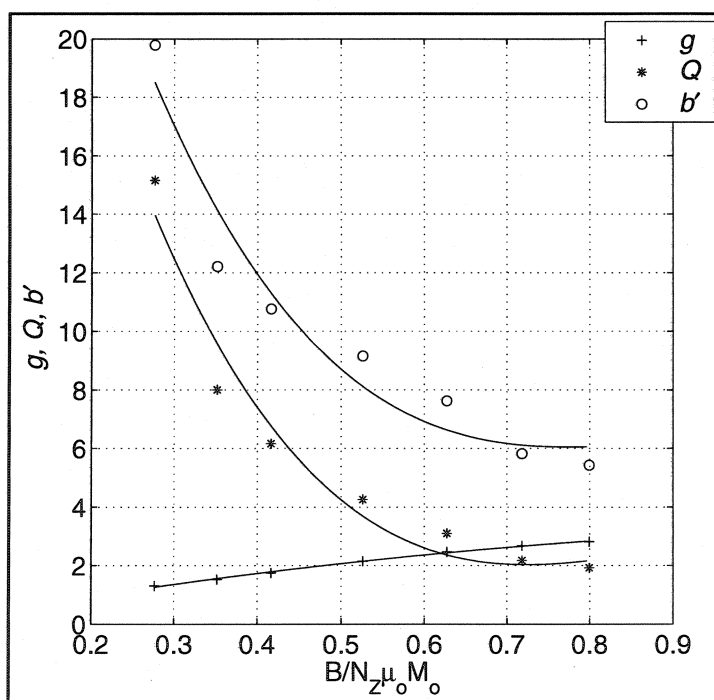
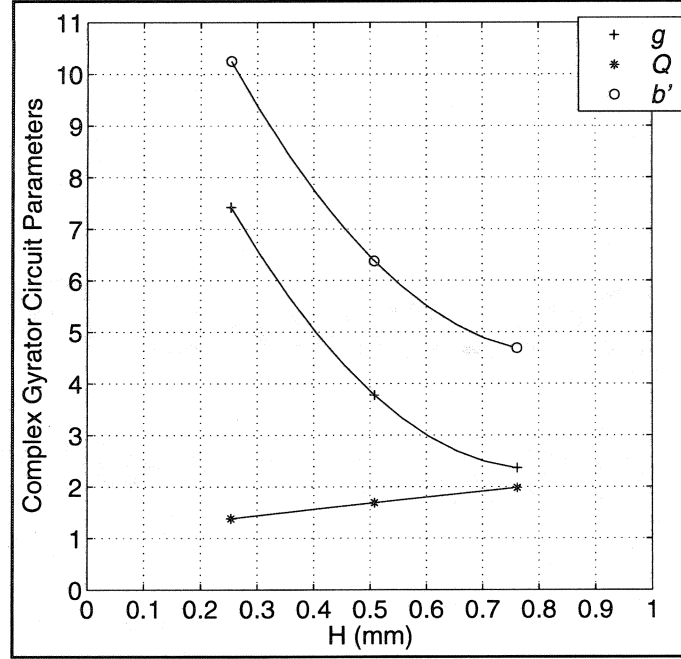


Figure 4.12: Circuit parameters versus normalized magnetization ( $R_f=1.6$  mm)



**Figure 4.13: Circuit parameters versus resonator thickness**

#### 4.3.1 Quarter-wavelength coupled degree-2 solutions

The design of quarter-wave coupled degree-2 devices is completely dealt with in [51], therefore only the practical computations will be summarized here. The network elements are a function of the minimum and maximum VSWR in the pass-band ( $r_{min}$  and  $r_{max}$ ) and the fractional bandwidth ( $w$ ). In normalized quantities, the characteristic admittance of the matching transformer, the susceptance slope parameter and gyration conductance are respectively given by

$$\begin{aligned}
 y_1 &= \frac{n_1}{n_2} \\
 b' &= \frac{\pi n_1 d_o}{4} \\
 g &= n_1^2
 \end{aligned} \tag{4.2}$$

where



$$\begin{aligned}
n_1 &= \sqrt{2\sqrt{(a+1)c} - b + 1} - \sqrt{2\sqrt{ac} - b} \\
n_2 &= \sqrt{a+1} - \sqrt{a} \\
d_0 &= 2\sqrt{c}
\end{aligned} \tag{4.3}$$

and

$$\begin{aligned}
a &= K^2 + \varepsilon^2 \\
b &= 2 \left( \beta \varepsilon^2 - \frac{K^2}{2} \right) \\
c &= \beta^2 \varepsilon^2
\end{aligned} \tag{4.4}$$

These last parameters are given in terms of the network specification of fractional bandwidth ( $w$ ) and minimum and maximum passband VSWR ( $r_{min}$ ,  $r_{max}$ ) as follows

$$\begin{aligned}
\theta_o &= \frac{\pi}{4} (2 - w) \\
\beta &= \tan^2 \theta_o + \frac{\tan \theta_o}{\cos \theta_o} \\
K &= \frac{r_{min} - 1}{2\sqrt{r_{min}}} \\
K^2 + \varepsilon^2 &= \left( \frac{r_{max} - 1}{2\sqrt{r_{max}}} \right)^2
\end{aligned} \tag{4.5}$$

These equations have been implemented in a computer program to relate the circuit parameters to the desired specification. The results of interest to this work are tabulated in Table 4.1. The table illustrates that the experimental values are compatible with degree-2 devices of 30% bandwidth at the 15 dB return loss points.

**Table 4.1: Network parameters of quaterwave coupled degree-2 circulators**

$r_{min}=1.38, r_{max}=1.40$				
$w$	$b'$	$g$	$Q$	$y_I$
0.25	6.417	2.656	2.416	1.928
0.30	3.868	2.030	1.906	1.686
0.35	2.544	1.654	1.537	1.522

### 4.3.2 Single ridge SIW quarter-wavelength coupled circulator

A single ridge quarter-wavelength transformer is suitable in the design of SIW circulators because the ridge may be milled directly into the PCB. In the design of ridge-coupled circulators knowledge of the cutoff space and characteristic impedance of the ridge SIW are necessary for design. One property of ridge waveguide is that the ridge lowers the dominant mode cutoff frequency while maintaining that of the next higher order mode. The bandwidth of the ridge guide is thus considerably enlarged. Another property is that the characteristic impedance may be adjusted by either varying the ridge depth or width. This enables one to cater the ridge characteristic impedance to the network specification.

#### 4.3.2.1 Ridge SIW cutoff space

Design data for ridge waveguides was given by Cohn [52] and Hopfer [53]. The cutoff space, for the even and odd family of  $TE_{m0}$  modes, is obtained respectively from a solution of the following transcendental equations

$$-\cot(\theta_1) + \left( \frac{Y_{02}}{Y_{01}} \right) \tan(\theta_2) + \frac{B}{Y_{01}} = 0 \quad (4.6)$$

and

$$-\cot(\theta_1) - \left( \frac{Y_{02}}{Y_{01}} \right) \cot(\theta_2) + \frac{B}{Y_{01}} = 0 \quad (4.7)$$

where

$$Y_{01} = \frac{k_c}{\omega\mu_o} \frac{1}{b}, \quad Y_{02} = \frac{k_c}{\omega\mu_o} \frac{1}{d} \quad (4.8)$$

are the characteristic impedances of the non-ridged and ridged section respectively and

$$\begin{aligned} \theta_1 &= \pi \left( 1 - \frac{s}{a} \right) \left( \frac{a}{\lambda_c} \right) \\ \theta_2 &= \pi \left( \frac{s}{a} \right) \left( \frac{a}{\lambda_c} \right) \end{aligned} \quad (4.9)$$

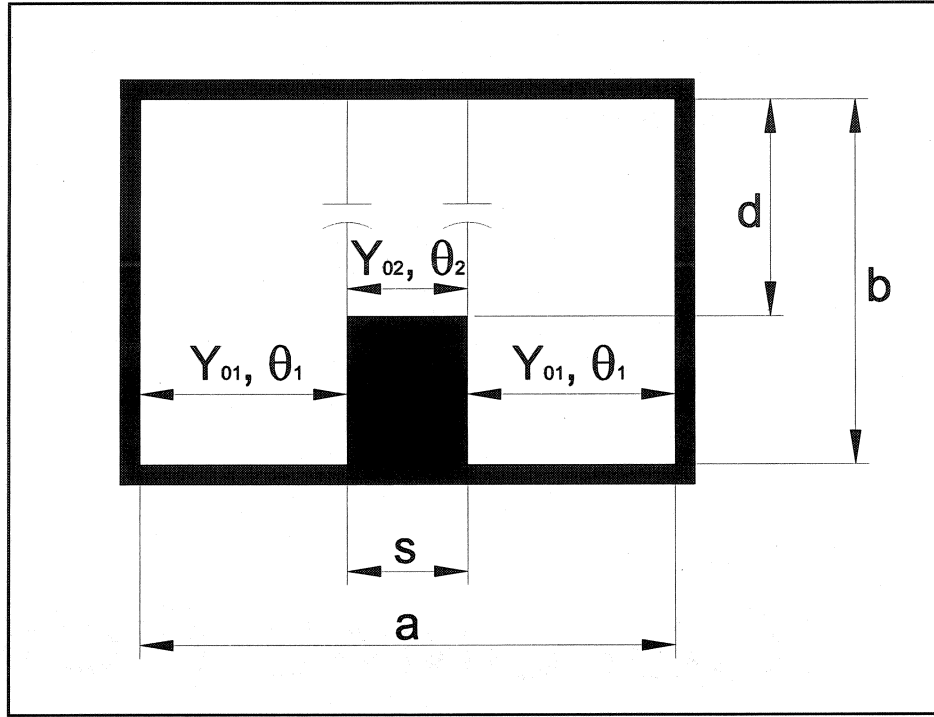


**Figure 4.14: Single ridge SIW**

are the corresponding electrical lengths. These parameters, superimposed on the single ridge geometry, are illustrated in Figure 4.14. The susceptance arises because of the discontinuity on either side of the ridge. According to Marcuvitz [54] it is approximately

$$\frac{B}{Y_{01}} \approx 2R \left( \frac{b}{a} \right) \left( \frac{a}{\lambda_c} \right) \ln \left[ \sin^{-1} \left( \frac{\pi d}{2b} \right) \right] \quad (4.10)$$

where  $R=1$  for a double ridge and 2 for a single ridge. One approximate formula for the cutoff space of the dominant mode, suitable as an initial value in a root finding subroutine, was given by Hoefer [55]

$$\frac{a}{\lambda_c} = \frac{a}{2(a-s)} \left[ \left( 1 + \frac{4}{\pi} \left( 1 + 0.2 \sqrt{\frac{bR}{(a-s)}} \right) \left( \frac{bR}{(a-s)} \right) \ln \left[ \sin^{-1} \left( \frac{\pi d}{2b} \right) \right] + \dots \right)^{\frac{1}{2}} \right. \\ \left. \left( 2.45 + 0.2 \frac{s}{a} \right) \left( \frac{sb}{d(a-s)} \right) \right] \quad (4.11)$$

Equation (4.6) demonstrates that the cutoff space is a function of the ridge aspect ratio ( $d/b$ ) and the waveguide aspect ratio ( $b/a$ ). Although the former quantity is a parameter, the latter one is significantly reduced in SIW. Nevertheless equation (4.6) demonstrates that its effect is second order since the waveguide aspect ratio appears only in the susceptance term. Figure 4.15 illustrates the cutoff space of the fundamental mode as a function of  $s/a$  with  $d/b$  a parameter. Figure 4.16 illustrates that of the first higher order mode. The largest bandwidth is obtained at  $s/a=0.25$  and coupling into the first higher order mode is avoided when  $s/a<0.5$ . In this work the ridge width was always kept below  $0.5a$ . The propagation constant is readily determined from the cutoff space by the usual relationship between the two.

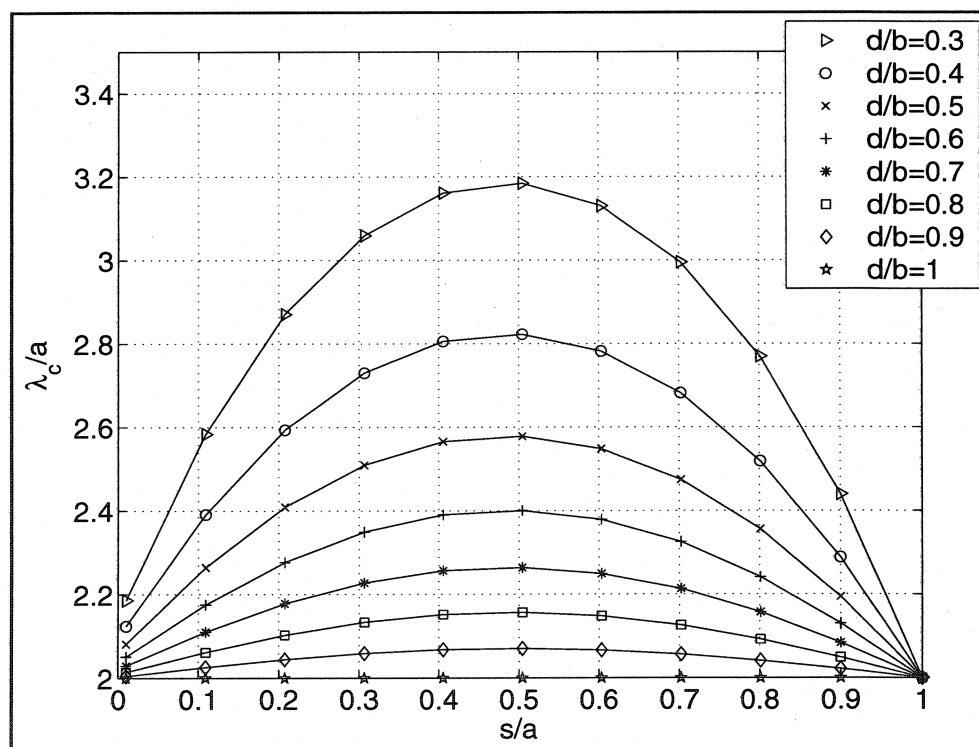
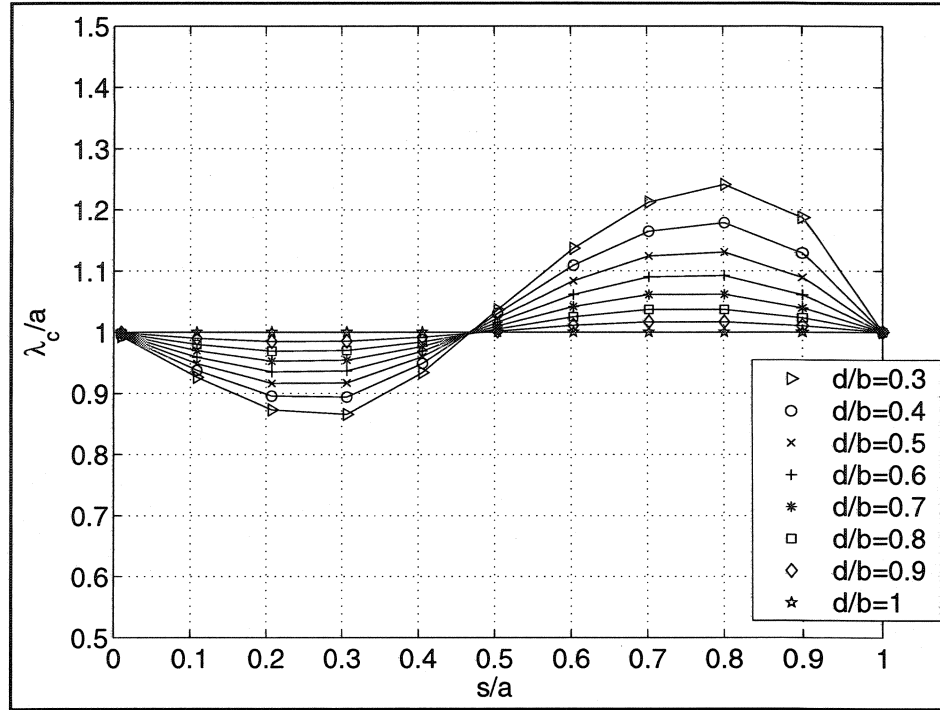


Figure 4.15: Cutoff space of quasi- $TE_{10}$  single ridge SIW mode



**Figure 4.16: Cutoff space of quasi- $TE_{20}$  single ridge SIW mode**

#### 4.3.2.2 Ridge SIW characteristic impedance

The suitability of ridge waveguides as impedance transformers in the design of junction circulators lies in the fact that the characteristic impedance is always lower than that of the corresponding waveguide. Irrespective of its definition, the characteristic impedance is given in terms of that at infinite frequency by

$$Z(\omega) = Z(\infty) \frac{\lambda_g}{\lambda_o} \quad (4.12)$$

Sharma developed a voltage current expression for the characteristic impedance, which includes the effect of the discontinuity [56]

$$Z_{vi}(\infty) = \frac{\pi \eta_o}{\sin(\theta_2) + \left(\frac{d}{b}\right) \left[ \frac{B}{Y_{01}} + \tan\left(\frac{\theta_1}{2}\right) \right] \cos(\theta_2)} \left(\frac{b}{a}\right) \left(\frac{d}{b}\right) \left(\frac{a}{\lambda_c}\right) \quad (4.13)$$

A power voltage definition is also available [53]

$$Z_{PV}(\infty) = \frac{\pi \eta_o \left( \frac{b}{a} \right) \left( \frac{d}{b} \right) \left( \frac{a}{\lambda_c} \right)}{\left( \frac{d}{b} \right) \cos^2(\theta_2) \frac{B}{Y_{01}} + \frac{\theta_2}{2} + \frac{\sin(2\theta_2)}{4} + \left( \frac{d}{b} \right) \left( \frac{\cos(\theta_2)}{\sin(\theta_1)} \right)^2 \left[ \frac{\theta_1}{2} - \sin\left(\frac{2\theta_1}{4}\right) \right]} \quad (4.14)$$

The power voltage definition of characteristic impedance, normalized to that of the reference SIW, is illustrated in Figure 4.17. The figure illustrates that it is indeed possible to realize characteristic impedances that are well below that of the reference SIW. It also illustrates that a small increase in the depth of the ridge has a significant impact on the ridge characteristic impedance. Therefore the sensitivity of the design to the ridge depth must be taken into consideration.

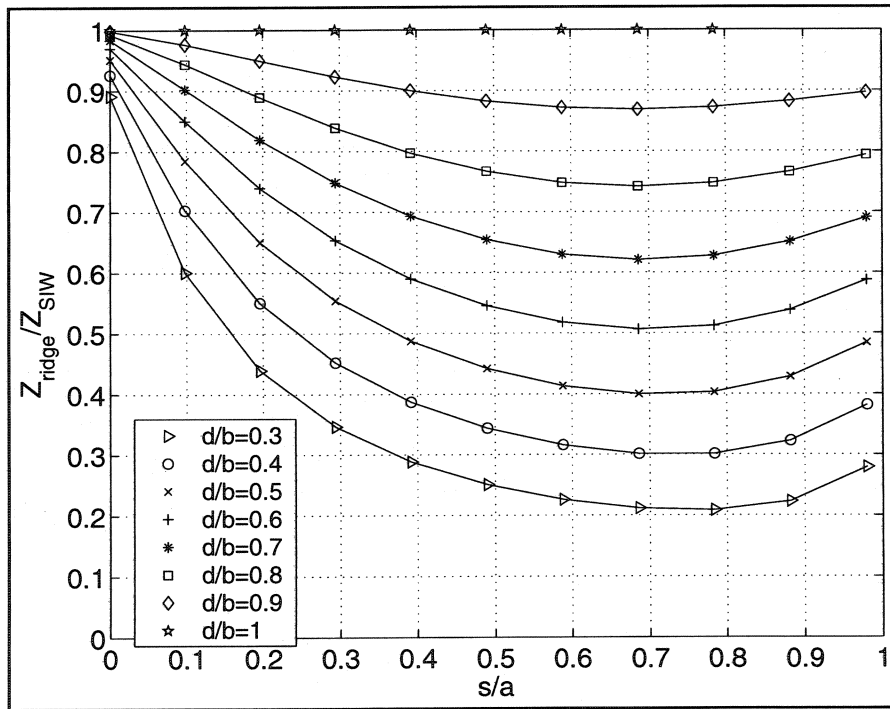


Figure 4.17: PV characteristic impedance versus  $s/a$  for parametric values of  $d/b$

#### 4.3.2.3 Single ridge SIW quarter-wavelength coupled design

One way to match this junction is to employ a quarter-wavelength long transformer at the terminals of the ferrite. One difficulty with such a transformer at the plane of the

resonator is that it will place electric walls there. Another is that the flat vertical face of the transformer adjacent to the ferrite becomes too fragile for handling purposes. In order to avoid these difficulties the transformer has been displaced by  $20^\circ$  (0.635 mm) from the ferrite face. The details of the hybrid transformer produced in this way have been fixed by having recourse to a commercial finite element solver. Initially a magnetized resonator at the junction of three SIW's, with single ridge quarter-wavelength matching sections displaced  $20^\circ$  from the ferrite face, was optimized to obtain a degree-2 response. The transition to microstrip was then included in the simulation and the process repeated. Although, strictly speaking, the theory developed in [51] applies at the terminals of the ferrite, it was nevertheless used to obtain the initial values of the matching transformer's parameters. One means of determining the ridge aspect ratio to satisfy a specific gyrator conductance and *VSWR* specification amounts to solving the following transcendental equation

$$1 - z_r \sqrt{rg} = 0 \quad (4.15)$$

where  $z_r$  is the normalized characteristic impedance of the single ridge transformer represented as a polynomial [57]. The required  $d/b$  ratio for parametric values of  $s/a$  are illustrated in Table 4.2. One appropriate solution is  $s/a=0.2$  and  $d/b=0.451$  with a transformer length of  $L_t=2.57$  mm. The final dimensions after optimization were found to be  $s/a=0.21$ ,  $d/b=0.5$  and  $L_t=1.27$  mm. The transformer length after optimization does not correspond to a quarter-wavelength since its reference plane is not at the ferrite terminals. The simulated results, of the complete circuit, are illustrated in Figure 4.18. The simulated results without the transition are separately illustrated in Figure 4.19 for completeness. The de-embedded insertion loss of the junction is 0.4 dB between 20 and 24 GHz. This insertion loss includes magnetic, dielectric and conductor losses as well as losses due to radiation through the via sidewall. The return loss without the transition is better, however these transitions are needed in the measurement process since a calibration kit directly in the SIW is not currently available.

Table 4.2: Calculation of single ridge SIW geometry

$a=7.266 \text{ mm}, b/a=0.07$		
VSWR=1.4, $g=2$ , $f=22 \text{ GHz}$		
$s/a$	$d/b$	$L \text{ (mm)}$
0.1	0.301	2.55
0.2	0.451	2.57
0.3	0.548	2.59
0.4	0.612	2.61
0.5	0.652	2.63
0.6	0.674	2.65
0.7	0.680	2.67
0.8	0.672	2.70

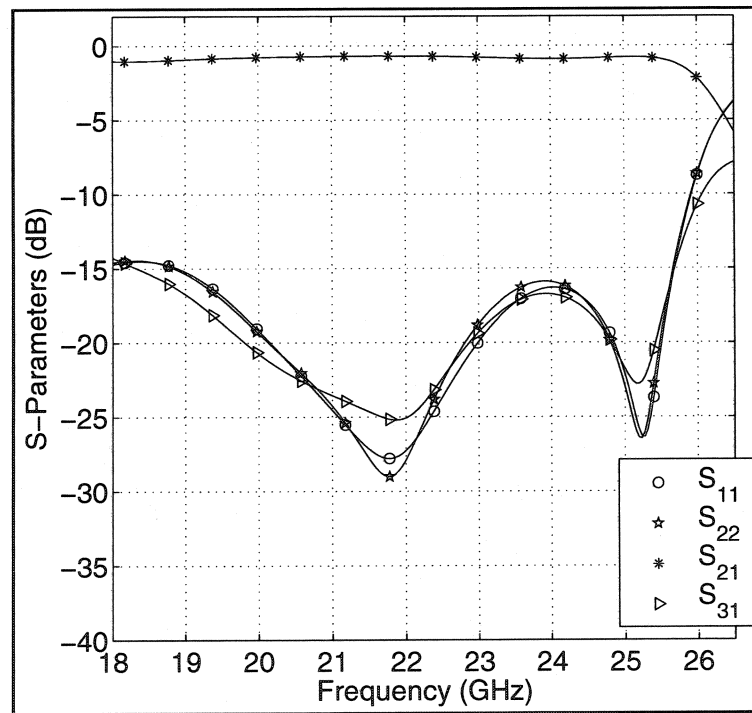
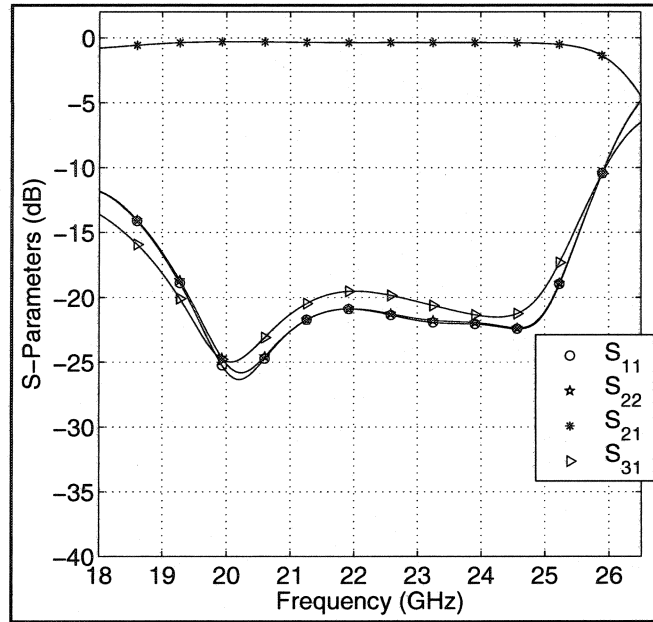


Figure 4.18: Ridge SIW quarter-wavelength coupled circulator simulation results





**Figure 4.19: Ridge SIW quarter-wavelength coupled circulator without transition**

#### 4.3.2.4 Design sensitivity

The critical parameters in this design are the aspect ratio of the ridge ( $d/b$ ), the electric wall boundary condition on the flat face of the ferrite, and the location of the ferrite in the junction. Although the ferrite's dimensions are also important, they have a maker's tolerance of less than 0.01252 mm. The sensitivity of the design to the ridge aspect ratio is simulated by increasing its depth by 0.0254 mm. The effect of the electric wall is simulated by leaving a 0.0254 mm air gap between the flat face of the ferrite and the top ground plane. The sensitivity in misaligning the ferrite is also considered by displacing it by 0.0254 mm from the centre. These simulation results are shown in Figure 4.20 and Figure 4.21. Although the ferrite is insensitive to a misalignment it is considerably affected by changes in the ridge transformer. There is a 3 dB degradation in return loss when the depth of the ridge is increased by 0.025 mm. It is however understood that this may be partially compensated for by adjusting the magnetic field. A small air gap also considerably deteriorates the return and insertion loss. To reduce the simulation time the SIW is replaced with its equivalent waveguide in this analysis.

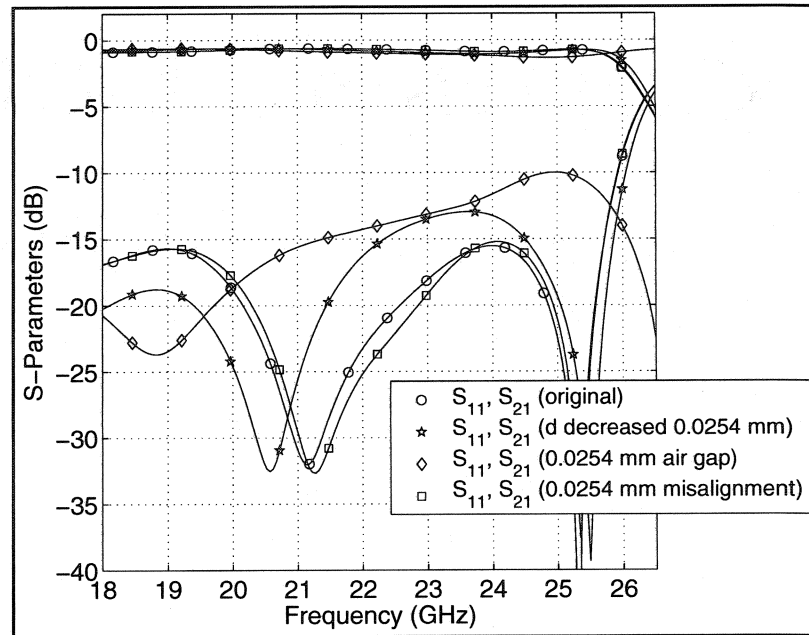


Figure 4.20: Sensitivity of single ridge SIW quarter-wavelength coupled circulator

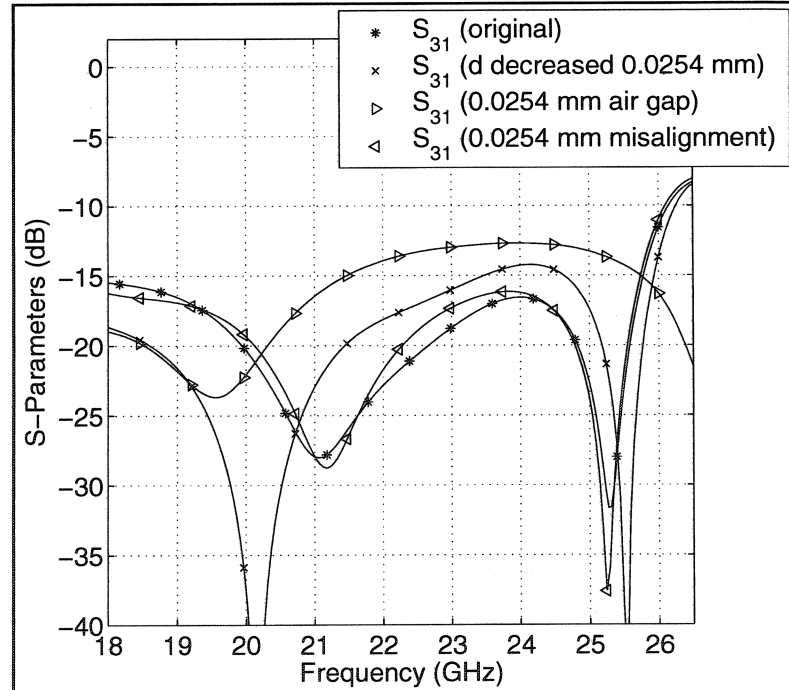


Figure 4.21: Sensitivity of single ridge SIW quarter-wavelength coupled circulator

#### 4.3.2.5 Experimental results

The results are superimposed on the simulated ones in Figure 4.22 and Figure 4.23. An 18% bandwidth at the 15 dB return loss points with an insertion loss better than 1.3 dB was achieved. The de-embedded insertion loss is roughly 0.6 dB, approximately 0.25 dB is attributed to each transition and 0.2 dB is attributed to the microstrip and SIW sections. The discrepancy between theory and experiment is due to the simulator assuming a uniformly saturated ferrite sample, to inaccuracies in adjusting the depth of the ridge, to via holes that are only partially plated, and to an imperfect contact between the top ground plane and ferrite face. In addition differences in the parasitic capacitances between the test jig and actual experimental test set, which are not completely calibrated out by the TRL calibration, may also be a contributing factor.

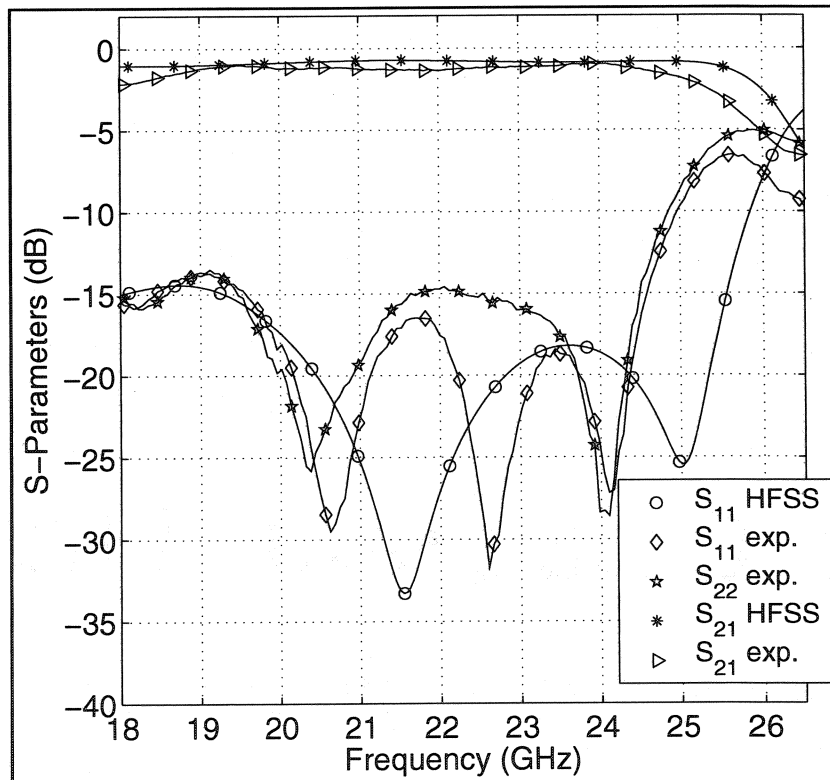
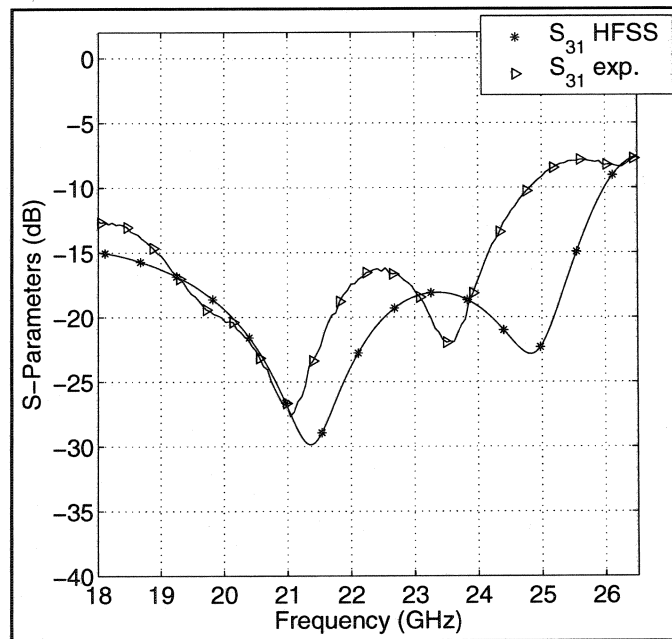


Figure 4.22: Ridge SIW quarter-wavelength coupled circulator results: return loss

To verify the accuracy of the calibration another unit was tested directly with the Wiltron test fixture using permanent magnets. These results are illustrated in Figure 4.24. With the exception of the insertion loss the 2 units have relatively the same scattering parameters. The 1 dB increase in the insertion loss is probably due to partially plated via holes and to air gaps between the top ground plane and the ferrite cover. Small air gaps between these surfaces support large electric fields that increase the insertion loss.



**Figure 4.23: Ridge SIW quarter-wavelength coupled circulator results: isolation**

#### 4.3.3 Radial SIW quarter-wavelength coupled circulator

Another transformer often encountered in the literature is an air-filled radially one. The characteristic impedance of the air filled radial transformer is adjusted by altering its height relative to that of the reference waveguide. This degree of freedom is however not available in SIW. To accommodate a radial transformer a dielectric must therefore be introduced. One drawback of introducing this dielectric is that it alters the boundary conditions at the ferrite face and therefore the circulation frequency and circulator characteristics.

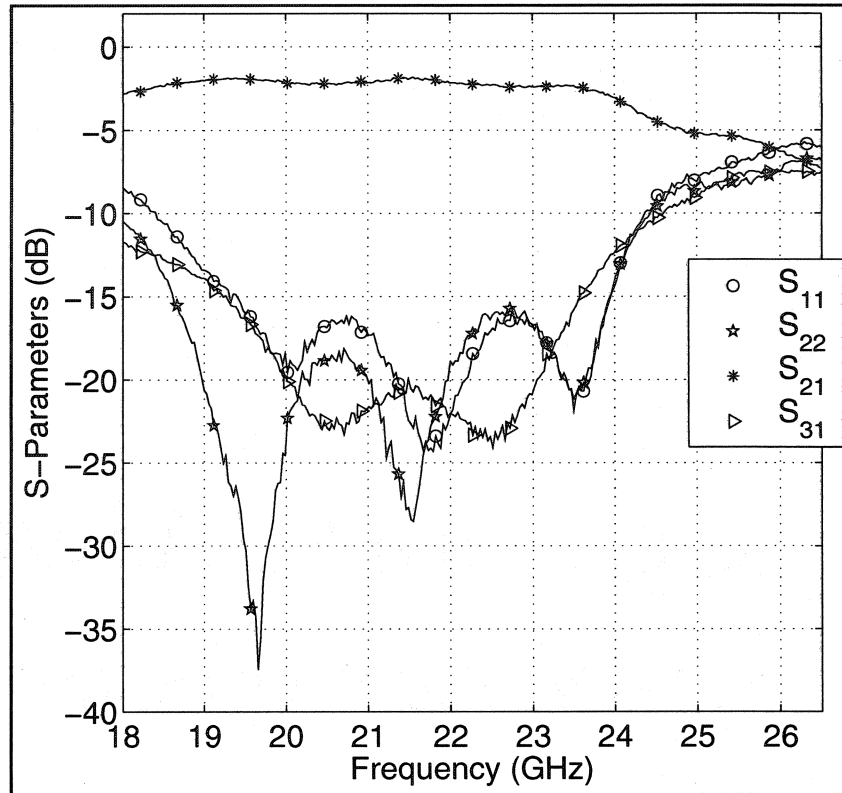


**Figure 4.24: Ridge SIW quarter-wavelength coupled circulator results: Wilttron**

#### 4.3.3.1 Radial SIW quarter-wavelength coupled design

Although it may seem that the circulation frequency may be calculated from equation (4.1), it is unfortunately not the case. Figure 4.25 illustrates the ferrite radius versus the dielectric constant of the environment in which the resonator is embedded. The figure suggests that to obtain the same resonant frequency the ferrite radius should increase as the dielectric constant of the surrounding medium increases. Simulations with HFSS, however, indicate that the ferrite radius should in fact decrease. This may, in part, be understood by recognizing that the circulation frequency corresponds to a vector addition of three eigenvalues and not only the two degenerate ones taken into account by equation (4.1). Also (4.1) assumes that evanescent modes exist outside the ferrite resonator, which implies that energy cannot couple into or out of it. This boundary condition does not correctly model the practical situation. As a result the adjustment of

this design was done empirically with HFSS. One suitable starting point on the geometry of the radial transformer is to consider it as a dielectric filled SIW. The required dielectric constant may be ascertained from a solution of the following equation

$$Z_{TEPV}^{tr} = \frac{Z_{TEPV}^{ref}}{\sqrt{rg}} \quad (4.16)$$

and the length of the transformer is obtained from the SIW guide wavelength. Carrying out this calculation at a design center frequency of 22 GHz gives a dielectric constant of  $\epsilon_{tr} = 4.5$  and an outer transformer radius of  $R_o = 3.1623mm$ .

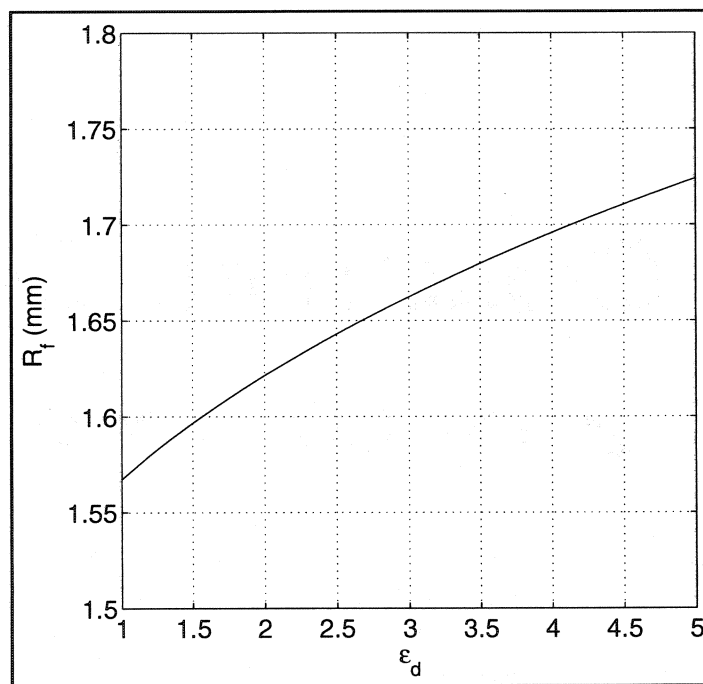


**Figure 4.25: Ferrite radius versus dielectric constant of surrounding medium**

The values arrived at after optimization are  $\epsilon_d = 4.5$ ,  $R_o = 3.683mm$ , and  $R_f = 1.3716mm$ . The simulated results of the complete circuit are illustrated in Figure 4.26. A 21% bandwidth at the 17 dB return loss points with an insertion loss better than 0.9 dB was achieved. It has been observed that decreasing the radius of the ferrite did not proportionally increase the circulation frequency. One means to do so is to reduce the dielectric constant of the radial transformer. One design displays a 14% bandwidth

at the 17 dB return loss points between 20 and 23 GHz with  $R_f = 1.2192\text{mm}$ ,  $R_o = 3.429\text{mm}$  and  $\epsilon_d = 3.5$ . This however does not include the effects of the SIW to microstrip transitions. One problem with this design is that the relative dielectric constant is not a standard one available from ferrite manufacturers.

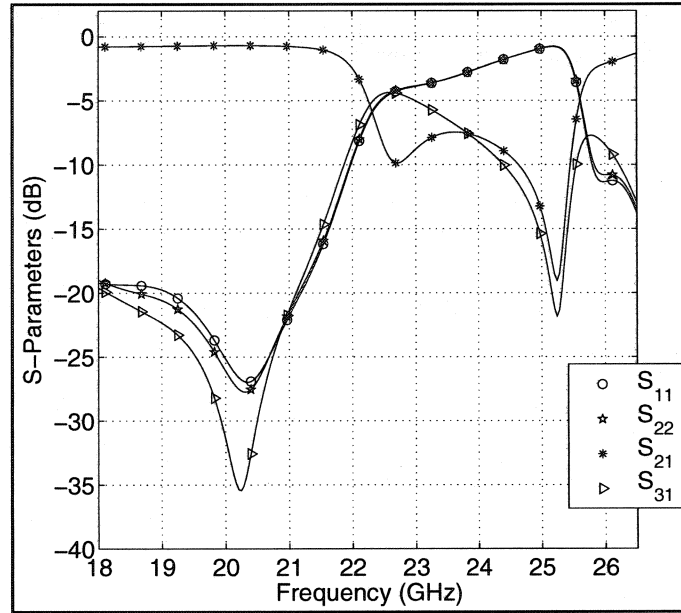


**Figure 4.26: Radial SIW quarter-wavelength coupled circulator simulation results**

#### 4.3.3.2 Design sensitivity

There are fewer factors in this design that are subject to manufacturing tolerances of the lab. The critical parameters in this design are the electric wall boundary condition on the flat face of the ferrite, and the location of the ferrite in the junction. These parameters were simulated in a manner similar to the ridge-coupled circulator. The results are indicated in Figure 4.27 and Figure 4.28. The return loss is significantly affected by the presence of an air-gap and is fairly insensitive to a ferrite misalignment. The ferrite parameters also play a role in the performance of the circulator however these parameters are outside of our control and usually have a tight makers tolerance.

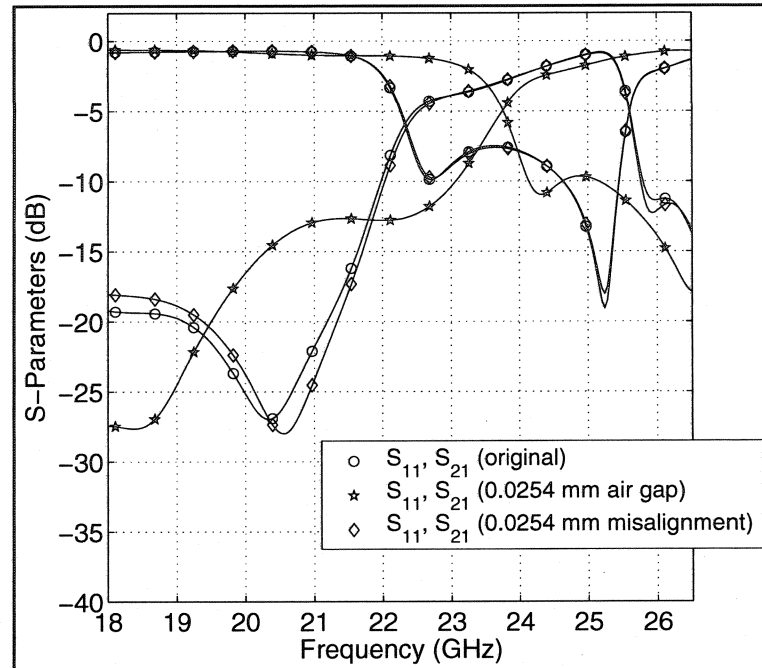


Figure 4.27: Sensitivity of radial SIW quarter-wavelength coupled circulator

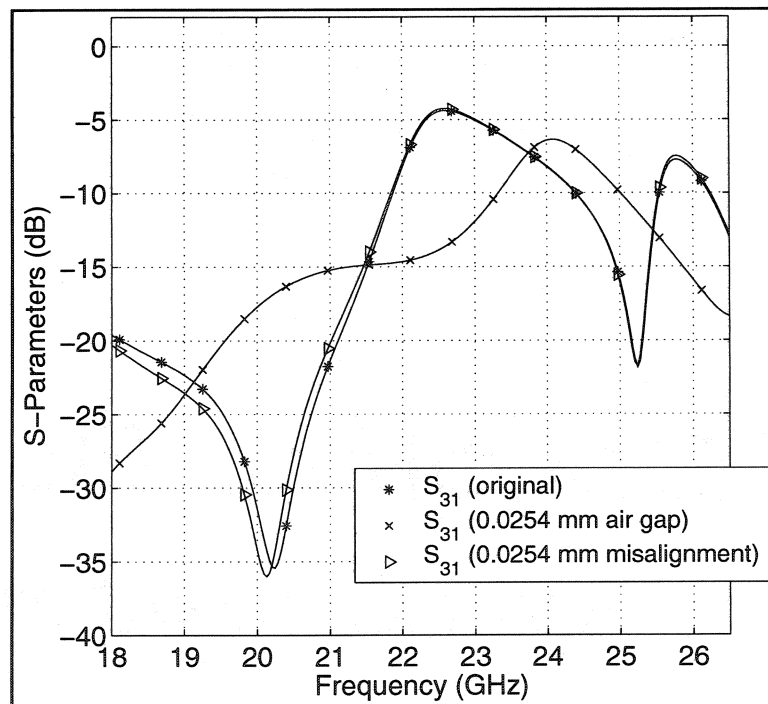
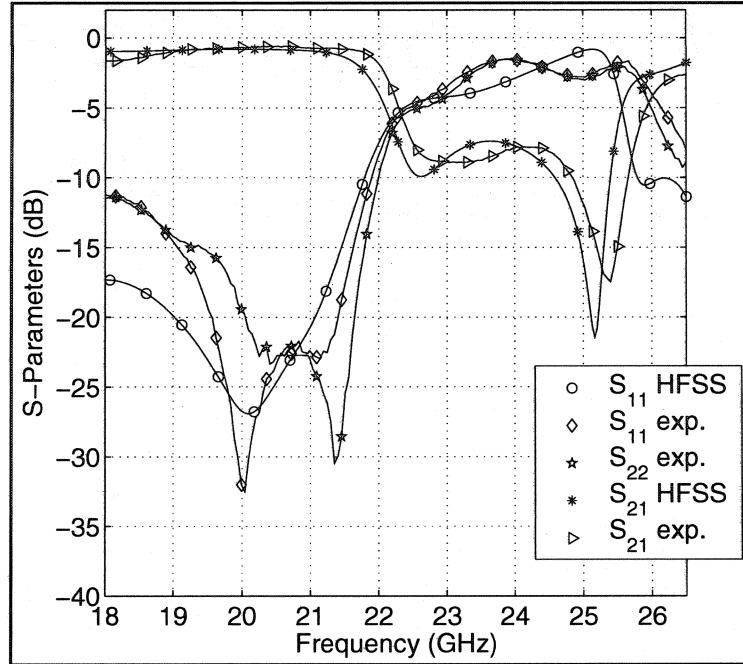


Figure 4.28: Sensitivity of radial SIW quarter-wavelength coupled circulator





**Figure 4.29: Radial SIW coupled circulator experimental results: return loss**

#### 4.3.3.3 Experimental results

The measured results are superimposed on the simulated ones in Figure 4.29 and Figure 4.30. A 10% bandwidth at the 15 dB return loss points, between 19.5 and 21.5 GHz, with an insertion loss better than 0.9 dB is achieved. This corresponds to a de-embedded insertion loss of approximately 0.2 dB. The reasons for the discrepancies between experiment and simulation underlined in the ridge transformer case apply equally in this situation. As in the ridge transformer case, the accuracy of the calibration was verified by testing a unit directly in a Wiltron test fixture with the magnetic bias field applied with permanent magnets. The two units displayed relatively the same scattering parameters. The insertion loss in this case was 1 dB higher at one frequency and 1 dB lower at another. One probable culprit to this discrepancy is the uncertainty in the homogeneity and strength of the applied bias field when permanent magnets are used. Again the uncertainty in the calibration must not be completely dismissed.

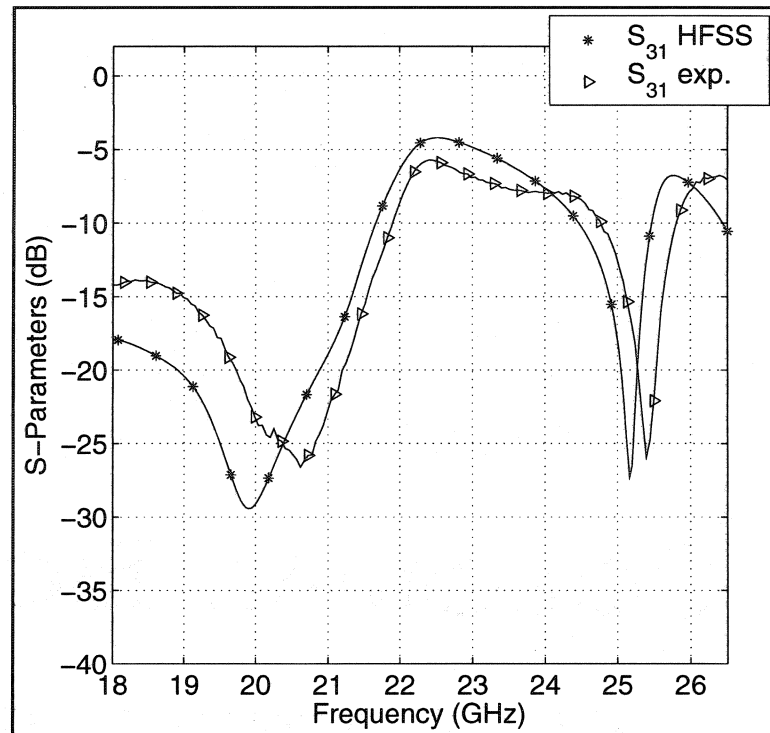


**Figure 4.30: Experimental results of radial SIW coupled circulator: isolation**

## 5 CHAPTER

### TURNSTILE SIW CIRCULATOR

In chapter 4 a SIW degree-2 circulator compatible with thin substrates was proposed and realized. In system applications however it may be advantageous to use a thick substrate as the platform of choice since, as is readily understood, waveguide losses are directly proportional to the narrow wall dimension of the equivalent waveguide. Post resonators with top and bottom electric walls are not suitable with these substrates because of higher order modes, with fields that vary along the axis of the ferrite, intruding into the circulation passband. One arrangement that is compatible with thick dielectric substrates is a re-entrant turnstile junction. Although the turnstile resonator has been extensively studied in the literature, it is applied here, for the first time, in the design of a SIW degree-2 circulator.

The chapter is divided as follows. It begins with a brief historical review. It continues by introducing the degree-1 solution and illustrates an alternative method to extract the complex gyrator circuit parameters. One degree-2 solution is presented which uses a single  $90^\circ$  UE displaced by a half-wavelength from the terminals of the resonator. A second design is presented that uses a non-optimum  $90^\circ$  UE to produce a degree-1 response followed by a  $180^\circ$  UE to obtain the desired degree-2 response.

#### 5.1 Brief Historical Review

Allen provided a qualitative description of the turnstile junction in 1956 [58]. This arrangement consisted of a cylindrical Faraday rotator symmetrically loaded by waveguide ports. Its operation was described in terms of propagating modes of the open gyromagnetic waveguide. A similar arrangement, where the gyromagnetic waveguide was placed inside the junction, was also readily available in the 1950's. A qualitative description of this arrangement was provided by Owen in 1970 where he demonstrated

that this circulator also operated in a turnstile fashion [59]. This description of the circulator operation in terms of propagating modes was later clarified by Owen in 1972 [60]. He demonstrated that circulation occurred at the resonance frequencies of hybrid modes associated with open ferrite resonators with one face short circuited and the other open or both faces open. A design procedure for this re-entrant turnstile circulator based on the propagating theory of operation was published by Denlinger in 1973 [61]. Some more recent publications of interest include those of Helszajn [62], [63].

## **5.2 Turnstile SIW Degree-1 Circulator**

The SIW degree-1 turnstile circulator is in many respects similar to the degree-1 planar post circulator in that they both rely on 30 degree splitting between the resonant modes to satisfy the second circulation condition. However the turnstile SIW degree-1 circulator consists of a partial height ferrite resonator at the junction of three SIW branches. This resonator differs from the post one in that its fields vary along the axis of the ferrite. Its resonant frequency is thus a function of both its radius and its height. Another feature of this resonator is that its susceptance slope parameter is, for all practical purposes, fixed by the filling factor required to satisfy the first circulation condition. One means of adjusting this value to coincide with that required for high quality circulators is to alter the geometry of the resonator. However, as demonstrated in chapter 4, since this quantity is already low, a disk arrangement was retained in developing the turnstile circulator.

### **5.2.1 Gyromagnetic resonator**

The different permutations of this resonator that are encountered in the literature are illustrated in Figure 5.1[62]. They consist of a single half-wavelength long gyromagnetic resonator open circuited at both ends, two coupled quarter-wavelength long ones short circuited at one end and open at the other, and a single quarter-

wavelength long one short circuited at one end and open at the other. Due to the thin profile of the SIW only

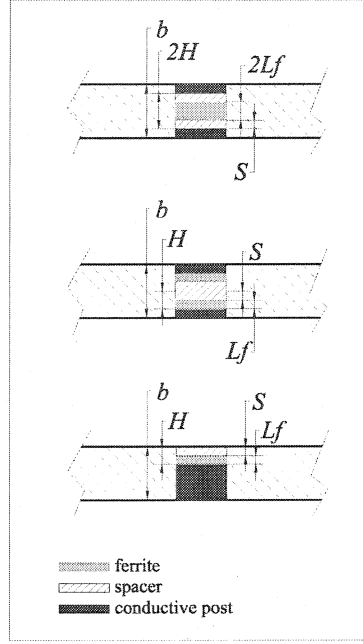


**Figure 5.1: Turnstile resonator configurations**

the single quarter-wavelength long gyromagnetic resonator is appropriate for the design of SIW circulators operating in the K-band. One advantage of this arrangement is that its susceptance slope parameter is twice that of the other configurations [62]. The resonator is described by its length ( $L_f$ ), its radius ( $R_f$ ), the dielectric spacing between the open flat face of the ferrite and waveguide or image wall ( $S$ ) and by its filling factor

$$k = \frac{L_f}{L_f + S} = \frac{L_f}{H} \quad (5.1)$$

The spacing between the open face of the ferrite and waveguide wall has a dielectric constant of  $\epsilon_s$ . Its operation relies on hybrid  $HE_{11\delta}$  modes of the ferrite resonator. The circulation frequency may approximately be calculated by resorting to the resonant frequency of the degenerate modes. The inphase eigennetwork must of course be adjusted to display a short circuit boundary condition at the terminals of the network.

The effect of the SIW wall on the operating frequency is also taken into account via an odd mode transcendental equation. The effect of the surrounding medium is taken into account by using an effective dielectric constant instead of the constitutive one for the gyromagnetic material. This effective dielectric constant is calculated from the exact propagation constant of an open gyromagnetic waveguide. The required transcendental equation is given by

$$\begin{aligned} \epsilon_{eff} \left( \frac{k_o}{\beta_o} \right) \cot \left[ \left( \frac{\beta_o}{k_o} \right) \left( \frac{L_f}{R_f} \right) k_o R_f \right] - \dots \\ \epsilon_s \left( \frac{k_o}{\alpha_o} \right) \coth \left[ \left( \frac{\alpha_o}{k_o} \right) \left( \frac{L_f}{R_f} \right) \left( \frac{1-k}{k} \right) k_o R_f \right] = 0 \end{aligned} \quad (5.2)$$

where  $\epsilon_{eff}$  is the effective permittivity of the ferrite,  $\epsilon_s$  is that of the spacer,  $k_o$  is the free space wave number,  $R_f$  is the radius of the ferrite,  $L_f$  its length and

$$\left( \frac{\beta_o}{k_o} \right)^2 = \epsilon_{eff} - \left( \frac{1.84}{k_o R_f} \right)^2 \quad (5.3)$$

$$\left( \frac{\alpha_o}{k_o} \right)^2 = \left( \frac{1.84}{k_o R_f} \right)^2 - \epsilon_s \quad (5.4)$$

Equation (5.2) is the same as that used for an air filled rectangular waveguide. Although it is tempting to replace the free space wave number with that associated with the dielectric substrate, the effect of the surrounding medium is taken into account in the effective permittivity of the ferrite. The SIW used in the present work has a narrow dimension of  $b=0.15748$  mm, an aspect ratio of  $b/a=0.217$  and a dielectric constant of  $\epsilon_d=2.33$ . The spacing between via holes is  $p=1.524$  mm and the diameter is  $\phi=0.8$  mm. The ferrite material is a lithium one with a saturation magnetization  $\mu_o M_o=0.4618$  T and a relative dielectric constant of  $\epsilon_f=13.92$ . The design frequency was selected as  $f_o=24$  GHz, compatible with some previous work. The normalized saturation magnetization of the ferrite material is  $p=0.54$ . The corresponding demagnetized permeability is  $\mu_d=0.894$ . Figure 5.2 illustrates the required ferrite radius versus the filling factor for two values of the resonator height ( $H$ ), at a design frequency of  $f_o=24$  GHz, using an air

dielectric spacer. Figure 5.3 separately illustrates the results when the dielectric spacer has a relative dielectric constant of  $\epsilon_s=2.33$ . The figures demonstrate that the choice of filling factor and ferrite radius is not unique, although the filling factor is fixed by that required to satisfy the first circulation condition [64]. They also demonstrate that introducing the dielectric spacer lowers the resonant frequency.

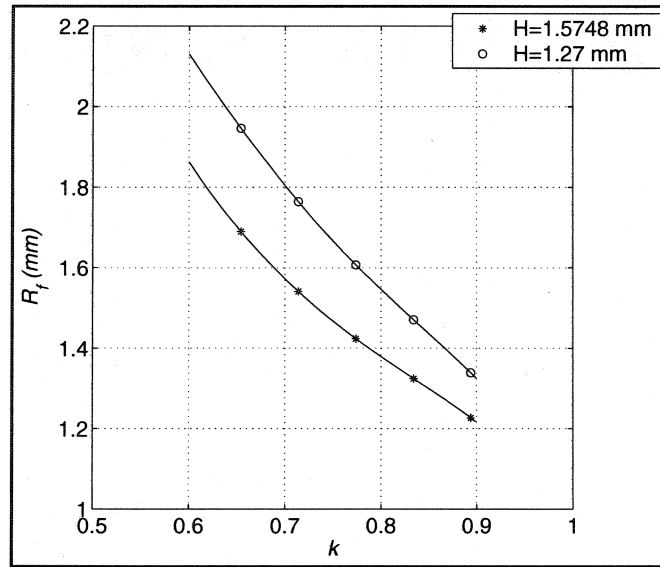


**Figure 5.2: Ferrite radius versus filling factor ( $k$ ) using an air spacer**

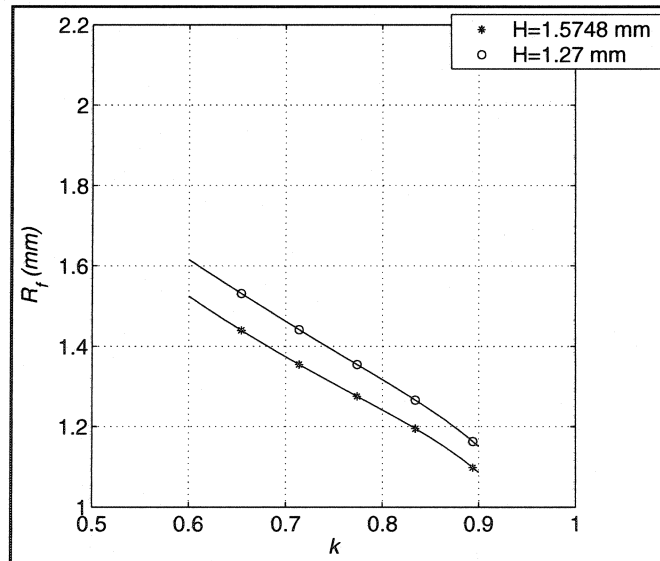


**Figure 5.3: Ferrite radius versus  $k$  using a spacer of dielectric constant  $\epsilon_d=2.33$**

### 5.2.2 Inphase eigennetwork adjustment

Although an analytical formulation of the inphase eigennetwork adjustment is not currently available, it has in the past been associated with a quasi-planar resonator with an electric wall boundary condition. This association may be readily understood by noting that the symmetric modes in the resonator add up in such a way as to produce a virtual electric wall at the terminals of the resonator akin to that of a quasi-planar one supporting the first symmetric mode

$$J_o(k_{eff}R) = 0 \quad (5.5)$$

The effective dielectric constant is that associated with the equivalent capacitance of the configuration

$$\epsilon_{eff} = \frac{\epsilon_f \epsilon_d}{[(1-k)\epsilon_f + k\epsilon_d]} \quad (5.6)$$

Although this semi-empirical formulation does not accurately fix the filling factor it nevertheless provides the required starting point. The filling factor is then adjusted by studying the eigenvalues of the corresponding resonator. This was done in this work with a FEM solver. Figure 5.4 illustrates one ill adjusted arrangement. Since the inphase eigenvalue is relatively frequency independent the adjustment starts by selecting the frequency to where the inphase eigenvalue displays a short circuit boundary condition. In the arrangement considered here the counter rotating ones display an inductive susceptance at this frequency. This is adjusted by decreasing the filling factor to increase the resonant frequency of the counter rotating eigennetworks. One must of course ensure that the frequency where the adjusted eigenvalue diagram satisfies the first circulation condition coincides with the desired circulation frequency. Figure 5.5 illustrates the adjusted eigenvalue diagram. It is understood that this adjustment is a compromise between the required filling factor, and the susceptance slope parameter and loaded-Q factor of the complex gyrator circuit.



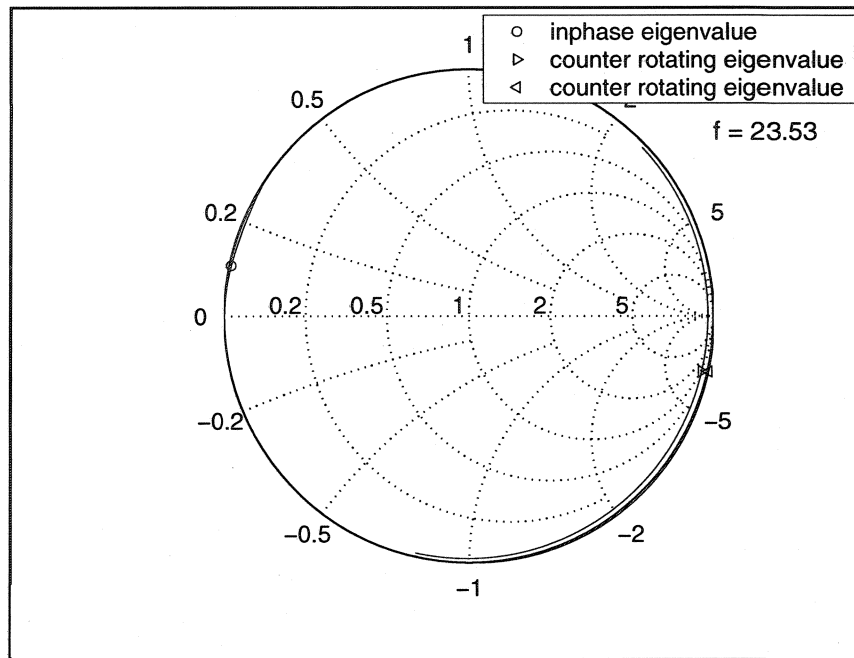


**Figure 5.4: Eigennetwork adjustment of turnstile resonator: ill adjusted diagram**

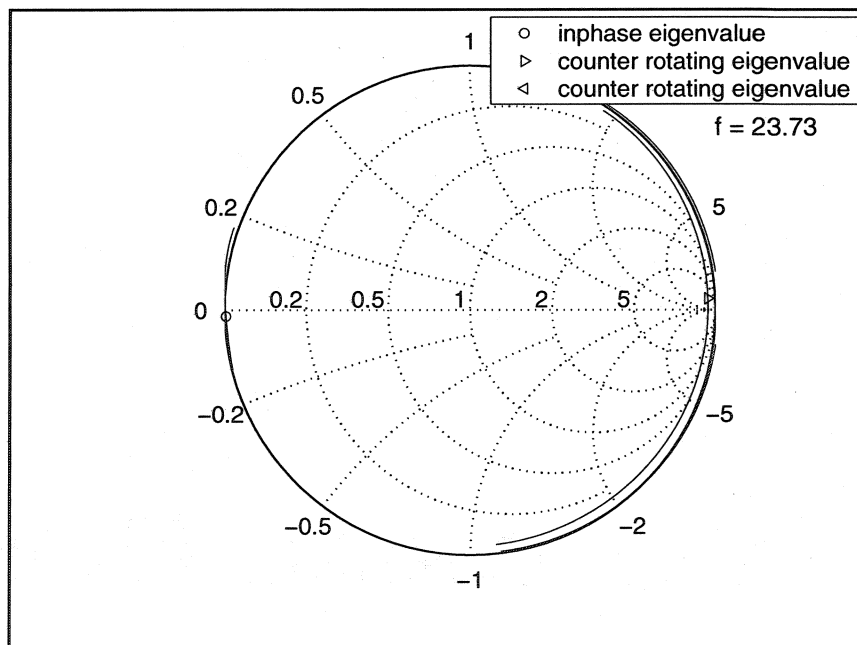


**Figure 5.5: Eigennetwork adjustment of turnstile resonator: adjusted diagram**

### 5.2.3 Complex gyrator circuit

Once the inphase and degenerate eigenvalues are commensurate and the inphase eigenvalue may be represented by a short circuit boundary condition the second circulation condition is met by removing the degeneracy between the counter rotating ones. The complex gyrator circuit exhibited by the junction is then similar to that exhibited by the planar solution. As will be illustrated the susceptance slope parameter displayed by this turnstile arrangement is very low. The loaded  $Q$ -factor being primarily determined by the gyrotropy is on the order of the susceptance slope parameter. This implies that the gyrator conductance is in the vicinity of 1. Unfortunately this complicates the experimental evaluation of the complex gyrator circuit. It also implies that it is theoretically possible to obtain a degree-1 solution without the use of matching networks. These solutions are unfortunately restricted to bandwidths much less than 10% and are not investigated here, although this bandwidth may be sufficient for most millimetre-wave applications [65]. One means of extracting the susceptance slope parameter is by resorting to the demagnetized junction, however, this method does not embody the gyrator conductance or the quality factor. One other method of obtaining these parameters is to resort to an eigenvalue diagram. In this method the circulation frequency is chosen as that where the counter rotating eigennetworks display conjugate reactances and the split frequencies coincide with the frequency where these same eigennetworks display open circuits. The values obtained in this way for a resonator with a ferrite radius of  $R_f=1.397$  mm and a thickness of  $L_f=1.27$  mm using an air spacer are  $g=1.57$ ,  $Q=2.7$  and  $b'=4.25$ . Although these values are not compatible with an optimum degree-2 specification, they are compatible with a non-optimum one of approximately a 10% bandwidth at the 20dB return loss points [65].

## 5.3 Experimental Procedure

A degree-3 air-filled rectangular waveguide to SIW transition is used in this work to characterize the turnstile SIW circulator. Its measured response was previously shown

in chapter 2. A TRL waveguide calibration kit is used to remove the discontinuity of the coaxial to waveguide transition of the test jig illustrated in Figure 5.6; however that of the ridge stepped impedance transformer is retained. The experimental setup is in keeping with that used for the planar solution. The normalized bias field is modified to take into account the new demagnetizing factors associated with a cylindrical geometry instead of a planar one.

#### 5.4 Degree-2 Circulator

It was previously shown that the turnstile resonator displays a low value of susceptance slope parameter. Therefore a degree-1 circulator operating at a temperature stable bias point may be realizable, however, as was pointed out these solutions exhibit bandwidths much less than 10%. In order to exploit the maximum bandwidth of SIW circulators only degree-2 solutions are investigated in this work. The purpose of this section is to demonstrate two degree-2 solutions that are compatible with thick SIW substrates. One design uses a  $90^\circ$  UE displaced a half-wavelength from the ferrite face and one design uses a  $90^\circ$  followed by a  $180^\circ$  UE to produce the desired degree-2 response.

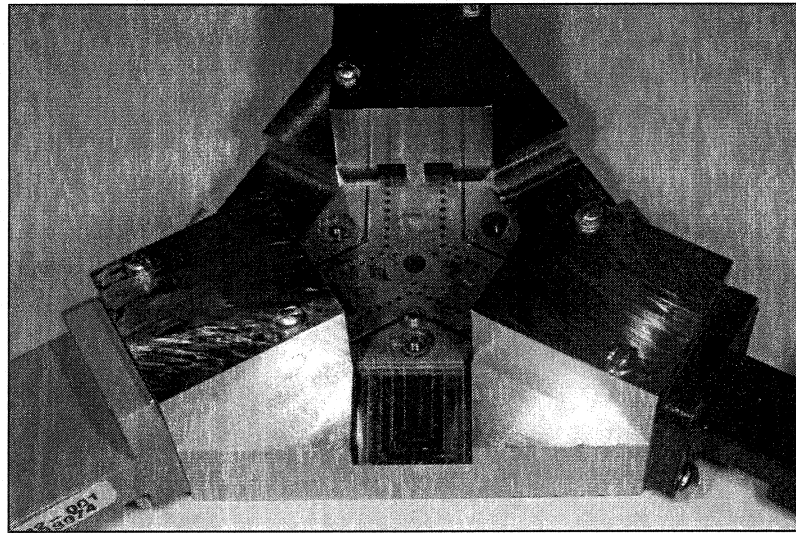


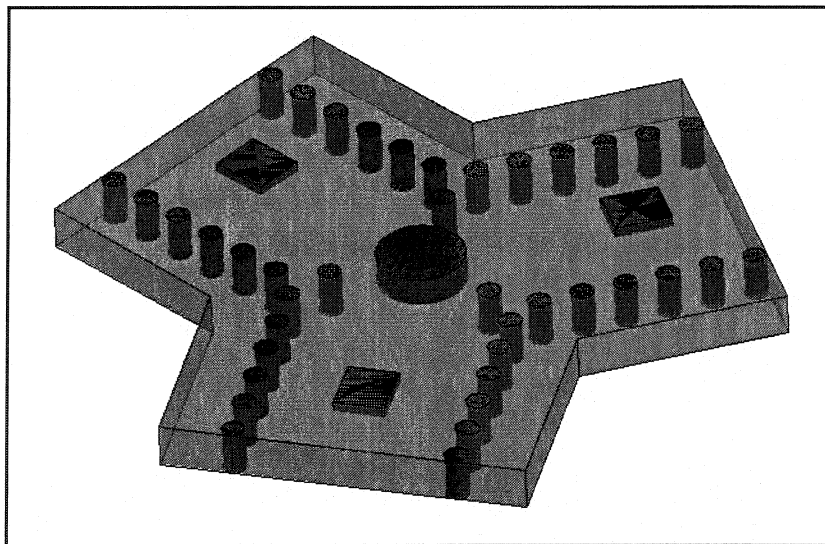
**Figure 5.6: Turnstile circulator test jig**

### 5.4.1 Topology using a $90^\circ$ unit element

The design of quarter-wavelength coupled circulators has been completely dealt with in chapter 4. One difference between the present implementation and the one normally encountered is that the quarter-wavelength transformer is displaced a half-wavelength from the ferrite reference planes. Although this design is not compact the terminal planes were displaced so as not to alter the boundary conditions imposed on the ferrite face. The network formulation previously described is however completely valid at these new reference planes.

#### 5.4.1.1 Design of topology using a $90^\circ$ unit element

As illustrated in Figure 5.3 the choice of resonator filling factor and shape for a particular resonant frequency is not unique, although the filling factor is bracketed between 0.6-0.9 to satisfy the first circulation condition. In this work the distance between the short-circuited face of the ferrite and waveguide wall ( $H$ ) was kept equal to the  $b$  dimension of the waveguide to simplify the fabrication of the circulator. That is the ferrite was not mounted on a conductive post. The dielectric spacer was embodied in the substrate material by milling a pocket directly in the substrate to receive the ferrite.

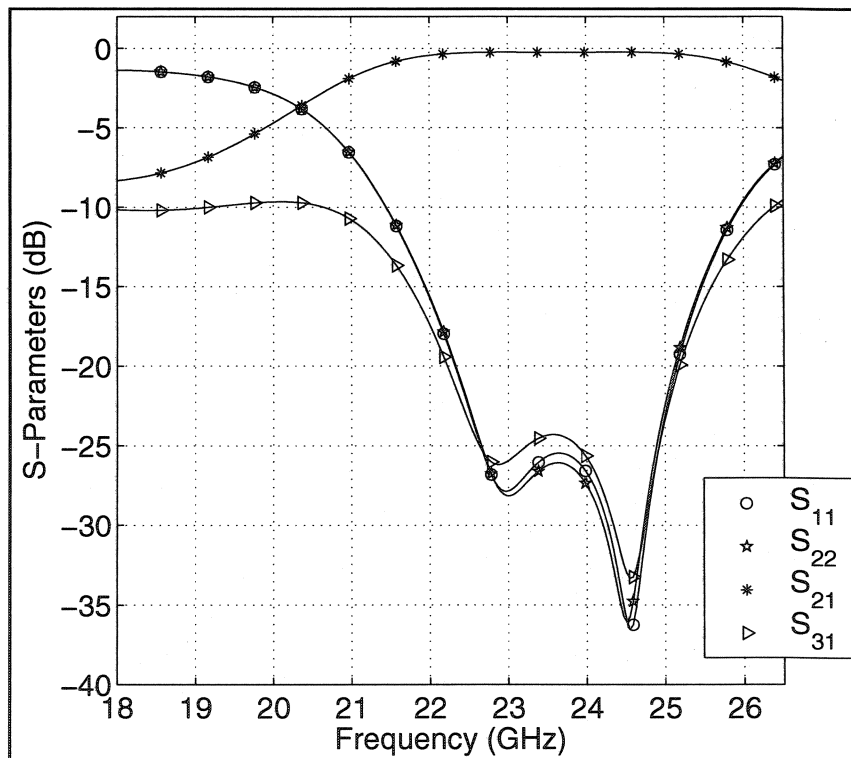


**Figure 5.7: Turnstile SIW circulator**

Although this is somewhat more complicated than simply drilling a through hole and using an air spacer this arrangement ensures that there are no gaps between the flat face of the ferrite and waveguide wall. It also ensures an accurate adjustment of the spacer thickness. A 3-D view of the geometry in question is illustrated in Figure 5.7. The filling factor was fixed at  $k=0.645$  corresponding to a ferrite thickness of  $L_f=1.016$  mm. The theoretically calculated ferrite radius is  $R_f=1.4577$  mm. The corresponding complex gyrator circuit parameters were found to be  $g=1.33$ ,  $b'=3.79$  and  $Q=2.84$ . Although these values are not compatible with optimum degree-2 specifications, they are compatible with non-optimum ones of approximately 10% bandwidth at the 20dB return loss points [65]. The required  $d/b$  ratio, for parametric values of  $s/a$ , was calculated as per chapter 4. The results are illustrated in Table 5.1. One solution is  $s/a=0.25$ ,  $d/b=0.814$  and  $L_r=2.418$  mm. The effect of the radial waveguide was neglected in calculating the ferrite reference plane displacement. This was initially placed at a half-wavelength from the ferrite face to  $Loc=6.35$  mm, with reference to the ferrite center. The final dimensions after optimization were found to be  $s/a=0.245$ ,  $d/b=0.726$ ,  $L_r=2.286$  mm and  $Loc=6.604$  mm. The final dimensions are in fair agreement with the theoretically calculated ones. Once an optimized design was obtained the continuous waveguide was replaced with an equivalent array of metallic via holes and the process repeated. To fine tune the center frequency 3 via holes were symmetrically placed in the junction to effectively narrow the waveguide opening to an equivalent width of  $a_j=5.08$  mm and length of  $L_j=2.54$  mm, with reference to the center of the ferrite, as illustrated in Figure 5.7. The final dimensions did not differ significantly and are given for completeness;  $R_f=1.524$  mm,  $L_f=1.016$  mm,  $Loc=6.604$  mm,  $s/a=0.245$ ,  $d/b=0.774$  and  $L_r=2.032$  mm. The discrepancy between the two sets of dimensions is due to the fact that the metallic via holes do not exactly model the junction details. The simulated results of the final circuit are illustrated in Figure 5.8. A 12% bandwidth at the 20dB return loss points with less than 0.4 dB insertion loss has been achieved. The transition to rectangular waveguide has not been included in this simulation.

Table 5.1: Calculation of single ridge geometry

$a=7.266 \text{ mm}, b/a=0.2167$		
VSWR=1.0, $g=1.33$ , $f=24 \text{ GHz}$		
$s/a$	$d/b$	$L_t \text{ (mm)}$
0.1	0.692	2.404
0.2	0.787	2.414
0.3	0.840	2.422
0.4	0.870	2.428
0.5	0.887	2.434
0.6	0.896	2.440
0.7	0.897	2.446

Figure 5.8: Turnstile SIW circulator using a  $90^\circ$  UE simulation results

#### 5.4.1.2 Design sensitivity

Once again HFSS is used to simulate the sensitivity of the design to manufacturing tolerance. The sensitivity of the design to the ridge aspect ratio is simulated by increasing its depth by 0.0254 mm. The effect of the electric wall is simulated by leaving a 0.0254 mm air gap between the flat face of the ferrite and the ground plane. An error on the filling factor is quantified by reducing the dielectric spacer thickness by 0.0254 mm. These simulation results are shown in Figure 5.9 and Figure 5.10. As expected the turnstile circulator is not very sensitive to the ridge aspect ratio. The midband return loss increased from 28 dB to 24 dB, however, the 20dB bandwidth was not significantly affected. A small air gap considerably deteriorates the return loss. An increase in the return loss from 28dB to 21dB and an increase of 0.06 dB in the insertion loss were observed. The circulation frequency also increased from 23.5 GHz to 24 GHz. A change in the thickness of the dielectric spacer did not affect the response. To reduce the simulation time the SIW was replaced with its equivalent dimension in this sensitivity analysis.

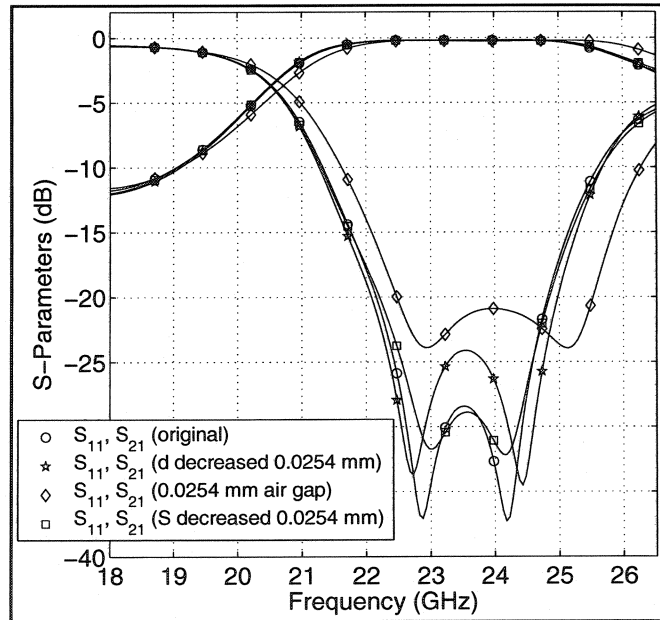
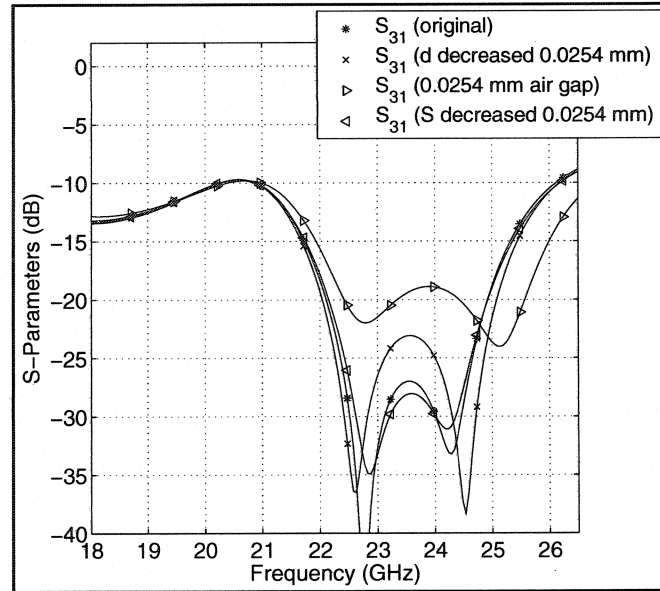


Figure 5.9: Turnstile circulator using a 90° UE sensitivity analysis: return loss



**Figure 5.10: Turnstile SIW circulator using a 90° UE sensitivity analysis: isolation**

#### 5.4.1.3 Experimental results

To verify the simulation a prototype was manufactured and tested and the results are illustrated in Figure 5.11 and Figure 5.12. The simulated ones are superimposed for comparison. An 8% bandwidth at the 15 dB return loss points with a de-embedded insertion loss better than 0.5 dB was measured. The de-embedded insertion loss consisted of a section of curved SIW connecting ports 1 and 2 of the SIW to rectangular waveguide housing. This therefore also removes the insertion loss of the circulator due to the loss in the SIW. This loss is expected to be on the order of 0.1 dB.

#### 5.4.2 Topology using a 90° and 180° unit element

One other topology that may be employed in the matching of junction circulators is a 180° UE [67]. Although this topology requires that the gyrator conductance be unity at the terminals of the ferrite and those of the 180° UE, this requirement may be overcome by forcing the gyrator conductance to unity at the latter terminals with the use of a suitable 90° UE.



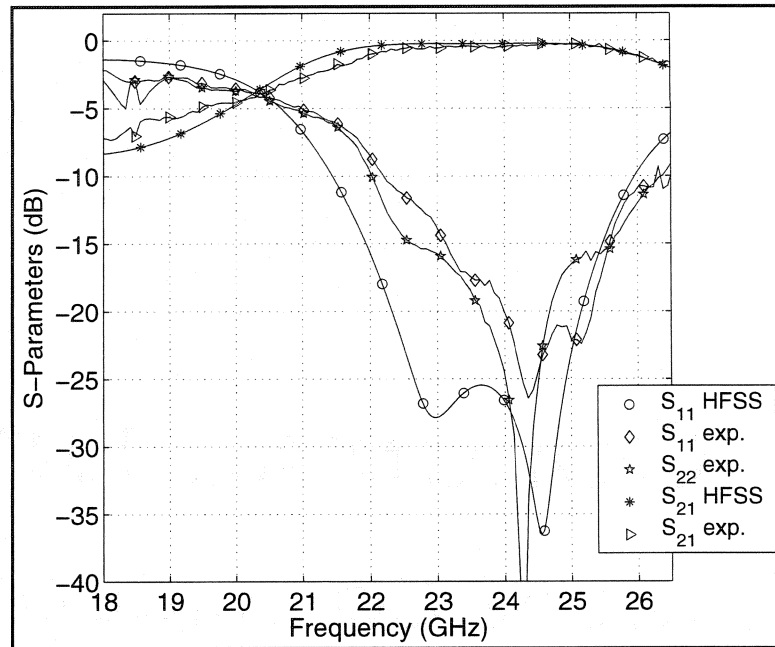


**Figure 5.11: Turnstile circulator using a 90° UE experimental results: return loss**

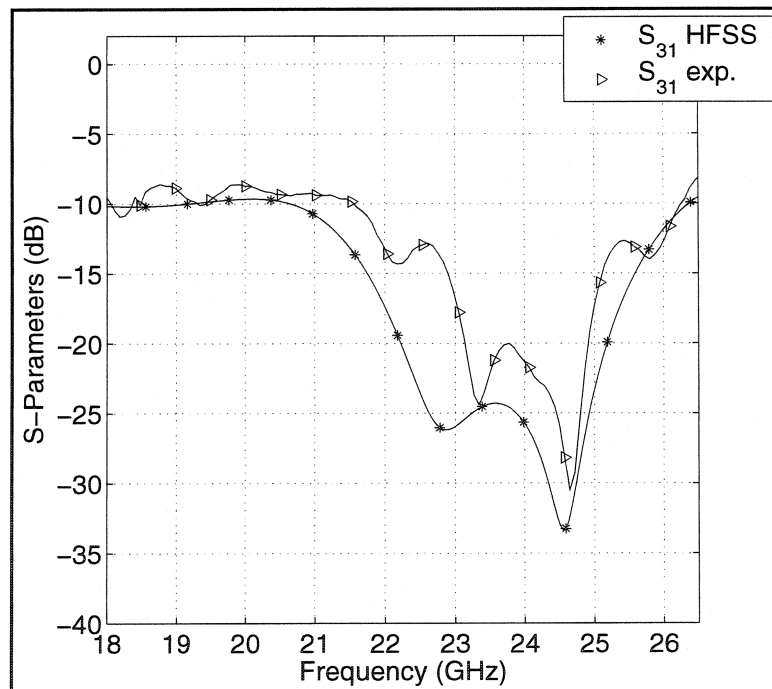


**Figure 5.12: Turnstile circulator using a 90° UE experimental results: isolation**

#### 5.4.2.1 Design of topology using a 90° and a 180° unit element

For diversity the resonator employed in this work consists of a quarter-wavelength gyromagnetic resonator loaded by a cutoff section of air filled waveguide. The initial dimensions of the resonator were calculated as per Figure 5.2. The distance between the short circuited face of the ferrite and waveguide wall was kept equal to the  $b$  dimension of the SIW. The filling factor was fixed at  $k=0.806$  corresponding to a ferrite length of  $L_f=1.27$  mm. The theoretical ferrite radius was found to be  $R_f=1.3726$  mm. The optimized one is  $R_f=1.397$  mm. The corresponding complex gyrator circuit parameters were found to be  $g=1.57$ ,  $b'=4.25$  and  $Q=2.7$ . These values are similar to the ones encountered in the previous section. Although this resonator could also be broad banded by a suitable 90° UE, the topology utilized in this section consists of a 90° UE followed by a 180° one. A schematic diagram of the overall circuit was previously given in chapter 3. Strictly speaking, the reference plane of the 90° UE is at the terminals of the ferrite; however, it was necessary to displace it in this work to avoid altering the boundary conditions at the ferrite terminal planes. This displacement was optimized with HFSS to  $Loc_{90}=2.794$  mm, with reference to the ferrite center. The hybrid transformer produced in this way is fixed with a FEM solver. A 180° UE is then introduced to give the desired degree-2 filter response. Its details are also fixed with the help of a FEM solver. The circuit is first optimized with an equivalent waveguide replacing the metallic via holes. The result at the input and output terminals of the 180° UE are superimposed in Figure 5.13 for comparison. The bandwidth where the return loss is less than 20dB has been increased from approximately 7% to 12%. The optimization was subsequently repeated with the SIW. A 3-D view of the circuit is illustrated in Figure 5.14. As illustrated a second array of metallic via holes was used to narrow the junction from an equivalent width of  $a=7.266$  mm to one of  $a_j=5.08$  mm [66]. To simplify the construction of the circuit the ridge depth of the 90° UE and that of the 180° UE were kept the same. The impedance of the 90° UE is fixed by  $d/b=0.677$  and  $s/a_j=0.4$  where  $a_j$  is the broad dimension of the equivalent narrowed waveguide.

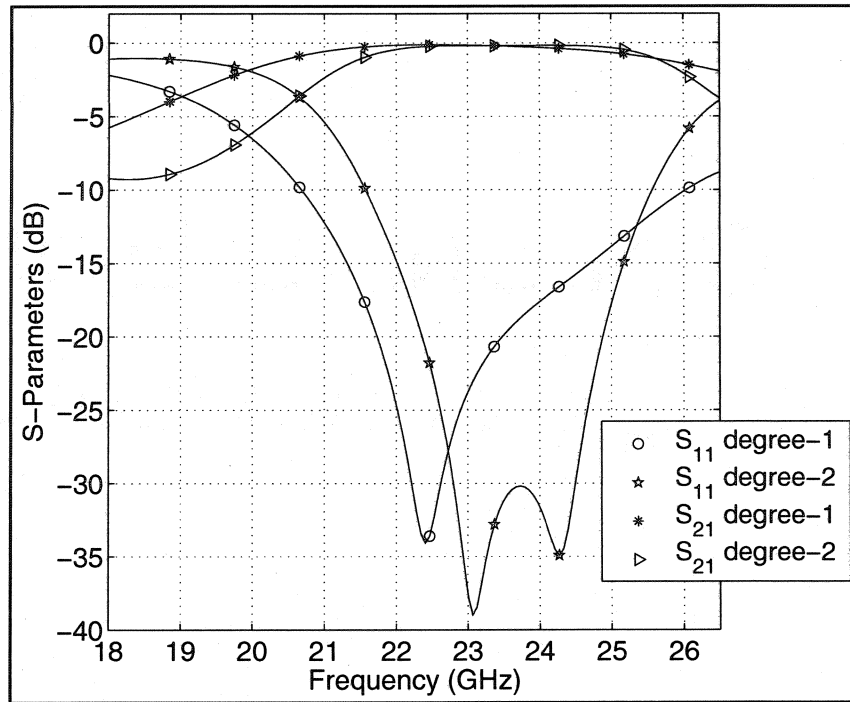


Figure 5.13: Frequency response at input and output terminals of 180° UE

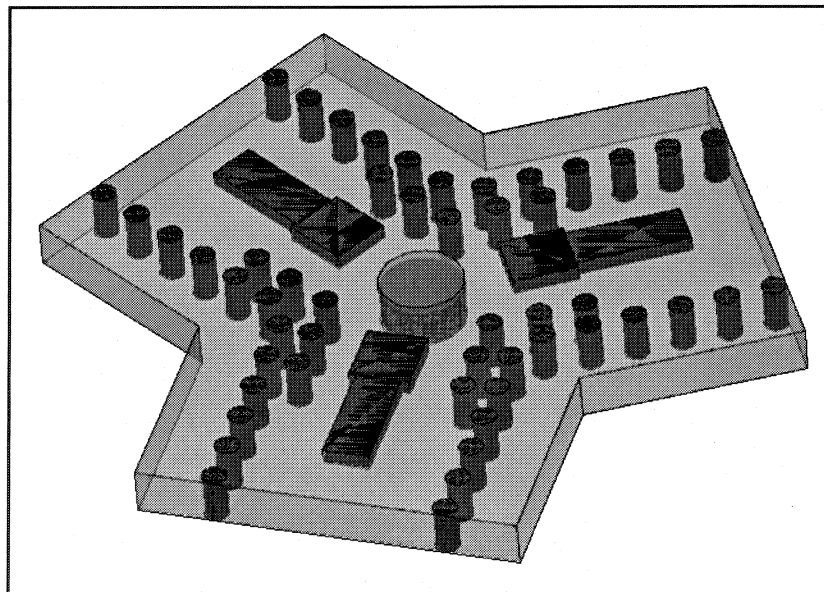
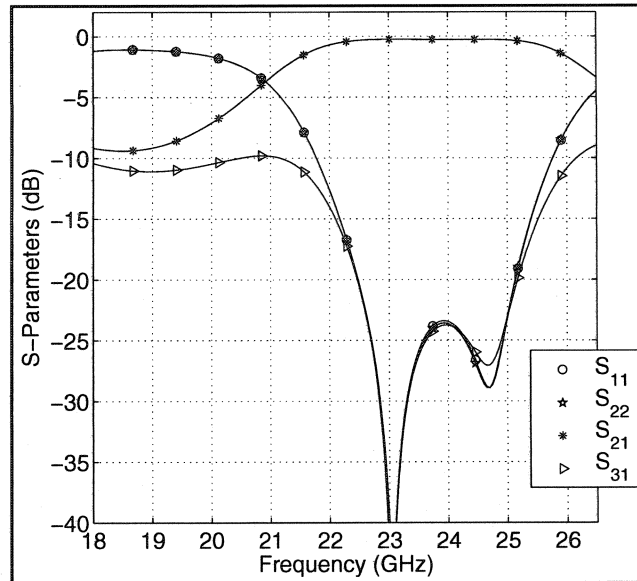


Figure 5.14: Turnstile SIW circulator using a 90° followed by a 180° one



**Figure 5.15: Turnstile SIW circulator simulation results**

Its length is  $L_{90}=2.159$  mm. The details of the 180 UE are  $d/b=0.677$ ,  $s/a=0.210$  and  $L_{180}=3.81$  mm. The simulated results of the final circuit are illustrated in Figure 5.15. The transition to rectangular waveguide has been excluded from the simulation. An 11% bandwidth between 22.5 GHz and 25 GHz with a return loss greater than 20dB and an insertion loss less than 0.4 dB was obtained.

#### 5.4.2.2 Design sensitivity

A sensitivity analysis on a similar geometry was carried out in the previous section, however, no simulation was carried out on the effect of a junction via hole that is not plated. This is demonstrated here for completion. The result is illustrated in Figure 5.16. As expected a significant change in the characteristics is obtained. It is of note that since a non-symmetrical perturbation was carried out on the junction, the corresponding results are also not symmetrical. The port that is affected is that which faces the via hole that has not been plated. For instance an unplated via hole between port-2 and port-3 has a significant affect on the return loss at port-1 and thus the isolation between ports-2 and 3.

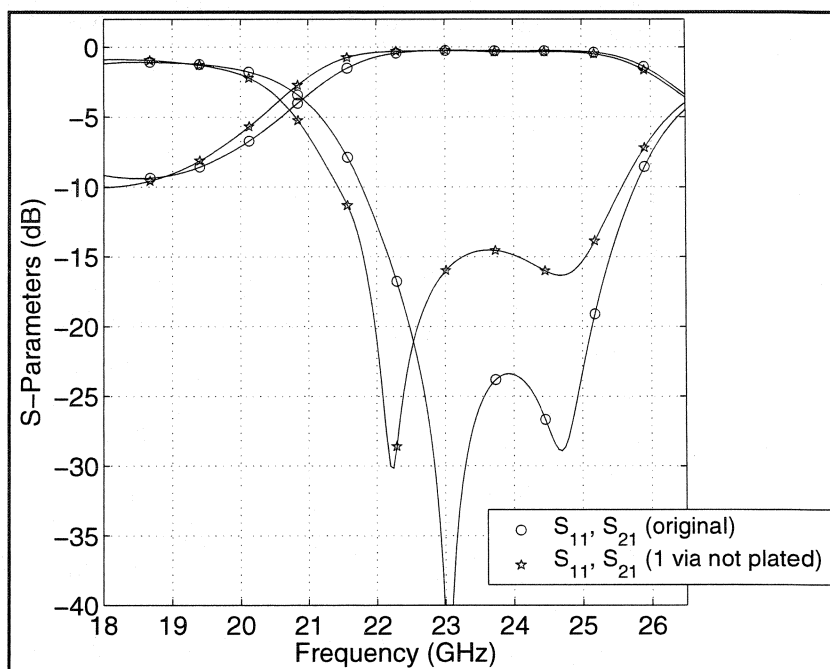


**Figure 5.16: Turnstile SIW circulator sensitivity analysis**

### 5.4.2.3 Experimental results

A prototype was manufactured and tested. The results are illustrated in Figure 5.17 and Figure 5.18. The simulated ones are superimposed for comparison. A 12% bandwidth at the 15 dB return loss points, between 23 GHz and 26 GHz, with a de-embedded insertion loss better than 0.3 dB is obtained. One source of error in de-embedding the insertion loss may be attributed to the curved section of SIW between port-1 and port-2 of the SIW to rectangular waveguide housing. A higher than normal loss associated with this section will decrease the insertion loss that is attributed to the circulator. For convenience a summary of the experimental results obtained for all the SIW circulators is tabulated in Table 5.2.

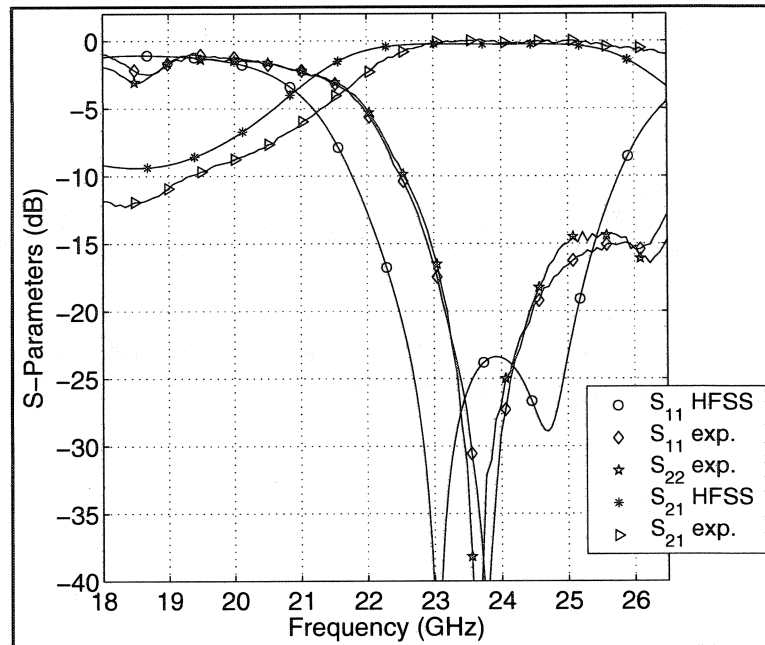


Figure 5.17: Turnstile circulator using a 90° and a 180° UE results: return loss

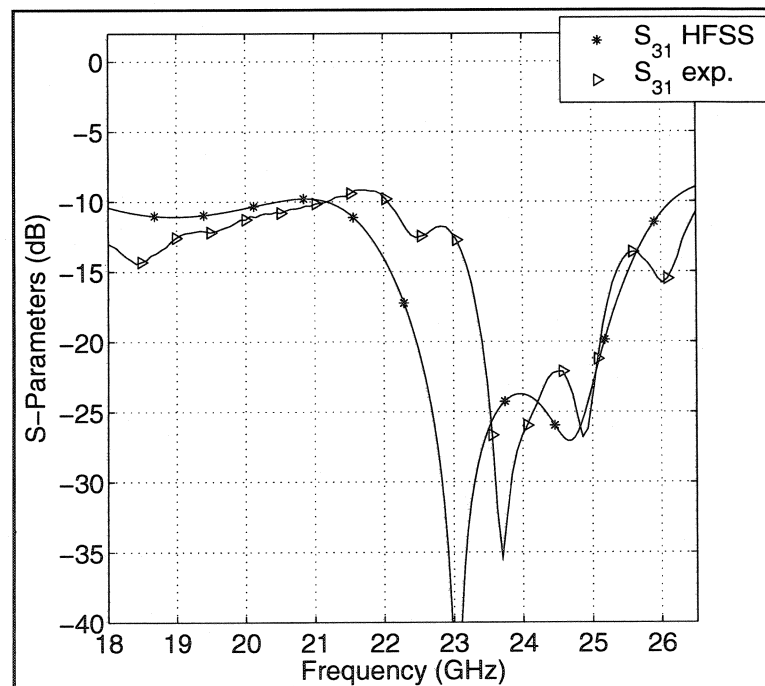


Figure 5.18: Turnstile circulator using a 90° and a 180° UE results: isolation

**Table 5.2: Summary of SIW circulators experimental results**

<b>CIRCULATOR</b>	<b>RL (dB)</b>	<b>I (dB)</b>	<b>IL (dB)</b>	<b>BW (%)</b>
<b>Planar: 90° radial UE</b>	15	15	0.2	10
<b>Planar: 90° ridge UE</b>	15	15	0.6	18
<b>Planar: 90° ridge UE</b>	15	15	0.5	8
<b>Planar: 90° and 180° ridge UE's</b>	15	15	0.3	12

## CONCLUSION AND FUTURE WORK

“Study of Substrate Integrated Waveguide Circulators For Millimeter Wave Applications” reviewed the fundamental principles behind the design of waveguide circulators. To characterize these circuits, a number of integrated transitions from SIW to other classical transmission mediums were studied. This included a transition from SIW to microstrip, co-planar waveguide and rectangular waveguide. Although the SIW to microstrip transition produced the best results, it is not suitable for thick substrates. An improved broad-band co-planar waveguide transition was studied for this purpose; however, it did not possess a bandwidth sufficient to characterize a circulator. A transition from SIW to rectangular waveguide was therefore selected to characterize a circulator embedded in a thick substrate material.

A brief review of the basic principles of junction circulators was also presented. A method of determining the equivalent circuit was underlined and the necessary steps in the adjustment of the junction circulator was demonstrated. These principles were applied to the design of novel waveguide circulators suitable for millimeter wave integration. This waveguide circulator consists of a gyromagnetic resonator at the junction of three SIW branches.

For thin substrate materials it was suggested that a post resonator with top and bottom electric walls was suitable. The junction was characterized through a measurement of the complex gyrator circuit elements as a function of the applied bias field. A method of improving the network parameters was suggested; however, it was not applied to improve the performance of the circulator. A degree-2 junction was realized using offset ridge transformers. It was demonstrated that such a transformer was sensitive to the depth of the ridge and that a tight tolerance on the order of 0.0254 mm was required. Nevertheless acceptable results were obtained.

In thick dielectric substrates higher order modes of the post resonator fall within the passband of the circulator. As a result, a re-entrant turnstile junction was deemed more suitable. This circulator was characterized solely with HFSS by extracting the



eigenvalues of the scattering matrix. It was demonstrated that such junctions are compatible with non-optimum specifications that display a filter response of order-1. A quarter-wavelength coupled circulator, which used the substrate material as the dielectric spacer between the top ground plane and ferrite face, was designed. A method of obtaining a degree-2 response was also demonstrated using both  $90^\circ$  and  $180^\circ$  UE's. Both these circulators produced satisfactory results.

This thesis has contributed significantly to millimetre circulators and millimetre wave integrated circuits. A novel, completely planar, SIW circulator was presented here for the first time. A prototype was manufactured and tested and excellent performance was obtained. It was also demonstrated that network parameters suitable for high performance circulators may be obtained by altering the thickness of the ferrite cylinder.

An improved grounded co-planar waveguide to SIW transition has been proposed. It consists of embedding a suitable  $\lambda_g/2$  UE, directly in the broad wall of the SIW, to produce a wideband degree-2 response. This transition is only slightly longer than the conventional one. A theoretical formulation awaits a solution. In addition a rectangular waveguide to SIW transition was also realized using a stepped impedance transformer. This transition was used to characterize the turnstile SIW circulators.

One other contribution was a re-entrant turnstile SIW circulator, proposed as a suitable solution in thick dielectric substrates. A prototype was manufactured and tested and satisfactory results were obtained. Because of the low gyrator conductance, measuring the gyrator circuit element values by conventional techniques was not feasible since an unambiguous split frequency determination was not possible. A method to extract the gyrator circuit parameters from first principles, using a finite element package was proposed. The split frequencies were taken as the frequency where the counter-rotating eigennetworks displayed open circuits and the center frequency was taken as the frequency where these same eigennetworks display conjugate reactances. The experimental values were in fair agreement with the theoretically calculated ones.

A number of problems became apparent during the development of these circulators. Initially via holes were manually placed and soldered to the ground planes of the PCB. Although this method produces an excellent contact between the ground planes it prevents a proper grounding of the ferrite face. An alternative process where the vias are electrolytically plated alleviates this problem however it becomes difficult to obtain a good contact between the ground planes. One other step that may help improve the results is to position the ferrite in its place before the substrate is re-plated. This will improve the contact to the ferrite faces. In this work the ferrite was sandwiched between two plates that were lined with sponge and copper tape. The sponge enabled the copper tape to mould the junction particularities. This method was sufficient for the present purposes.

Another problem was encountered during the milling of the ridge transformer. In the post resonator case the accuracy of the milling depth is crucial. Presently a milling depth with a precision of  $\pm 0.127$  mm is possible. This problem was alleviated by continuously adjusting the milling depth until satisfactory results were obtained.

One other difficulty encountered during this thesis was the inability of accurately determining the scattering parameters at a desired reference location. One solution to this problem is to design a SIW calibration kit. Knowing the exact terminals of the junction will enable one to experimentally optimize the design. This will also facilitate the measurement of the insertion loss.

In chapter 4 a method of improving the network parameters of post SIW circulators was suggested. It consisted of varying the thickness of the gyromagnetic resonator until the optimum network parameters are obtained. In a future project the thickness of the substrate material may be increased while reducing that of the gyromagnetic resonator until the desired specification is satisfied. This would also reduce the sensitivity of the response to the depth of the ridge, at the expense of increased resonator complexity.

In chapter 5 a compromise was made on the required filling factor to simplify the construction and assembly of the circulator. However it is recalled that ideally a circulator displays a frequency independent short circuit boundary condition at the

terminal planes of the ferrite. One method of improving the results would be to adjust the resonator geometry such that a short circuit is presented at the ferrite terminal planes.

This hybrid integration technique is gaining in popularity and it is expected that future millimetre wave systems will exploit the advantages of SIW. This includes low cost integration of high performance waveguide filters, diplexers and antennas with planar active components. Complete subsystems are envisioned with circuits on either side of a PCB, providing a compact low cost mass producible millimetre wave system. The SIW circulator may provide the isolation between the transmit and the receive filter or maybe used to protect the embedded microwave source from antenna mismatches. A SIW ferrite phase shifter will eventually lead into low cost phased array antennas. One arrangement of a ferrite phase shifter may be to simply glue a ferrite slab directly on a narrow milled section on the broad wall of the SIW. This arrangement avoids the need to have to cut through the PCB to insert the ferrite slab. Once glued in place the device may be electrolytically plated. Although the SIW circulator in this work was realized with a Rogers RT-Duroid high frequency laminate, these same concepts can be extended to other planar transmission mediums such as Low Temperature Co-fired Ceramic (LTCC).

LTCC is a multi-layer ceramic packaging technology that is capable of embedding resistors, capacitors and inductors. Each layer supports a conductive trace as well as interconnection vias to other layers. SIW transmission lines embedded in the LTCC is therefore possible. Experimental ferrite layers are currently available thereby enabling non-reciprocal components to be an integral part of the system. This thesis therefore pioneers further research in the integration of non-reciprocal components. Further research in this area will eventually lead to SIW LTCC circulators that will not require any manual intervention. The realization of a SIW LTCC phase shifter will eventually lead to a completely integrated phased array antenna. The magnetic bias field may also be incorporated into the LTCC material by designing an electromagnet from the ferrite material and metal traces. This high degree of integration will reduce the cost of millimetre wave systems considerably.

On a more fundamental note, an orderly study of the effect of the surrounding medium on the resonance frequencies of the circulator and the network parameters of the complex gyrator circuit, would serve a useful purpose in the design of SIW circulators embedded in substrates with high values of dielectric constants. This might consist of a rigorous electromagnetic solution or simply experimentally characterising a number of SIW circulators with increasing values of dielectric constant.

## REFERENCES

- [1] POZAR, D. M. 1993. *Microwave engineering*. 2<sup>nd</sup> ed. United States : Addison-Wesley. 726p.
- [2] HELSZAJN, J. 1969. *Principles of microwave ferrite engineering*. 1<sup>st</sup> ed. United Kingdom : Wiley-Interscience.
- [3] SOKOLOV, J. 1964. «Below resonance operation of the strip line Y-circulator». *IEEE Transactions on Microwave Theory and Techniques*: Sept. 1964. 12:5. P. 568-569.
- [4] RIBLET, G. P. 1978. «The extent of the similarity between below resonance and above resonance operation of standard circular junctions». *IEEE MTT-S International Microwave Symposium Digest*: June 1978. 78:1. P. 323-325.
- [5] FAY, C. E., COMSTOCK, R. L. 1965. «Operation of the ferrite junction circulator». *IEEE Transactions on Microwave Theory and Techniques*: Jan. 1965. 13:1. P. 15-27.
- [6] HELSZAJN, J., TSOUNIS, B. 1995. «Temperature stability of quality factor of junction circulators». *IEE Proceedings on Microwaves, Antennas and Propagation*: Feb. 1995. 142:1. P. 67-70.
- [7] GREEN, J. J., SANDY, F. 1974. «Microwave characterization of partially magnetized ferrites». *IEEE Transactions on Microwave Theory and Techniques*: June 1974. 22:6. P. 641-645.
- [8] IGARASHI, M., NAITO, Y. 1977. «Tensor permeability of partially magnetized ferrites». *IEEE Transactions on Magnetics*: Sept. 1977. 13:5. P. 1664-1668.
- [9] SCHLOEMANN, E. 1971. «Behaviour of ferrites in the microwave frequency range». *J. Physique*: Feb. 1971. 32. P. C1-443-451.

- [10] ROVEDA, R., BORGHESE, C. CATTARIN, G. 1972. «Dissipative parameters in ferrites and insertion losses in waveguide Y-circulators below resonance». *IEEE Transactions on Microwave Theory and Techniques*: Feb. 1972. 20:2. P. 89-96.
- [11] GREEN, J. J., SANDY, F. 1974. «A catalog of low power loss parameters and high power thresholds for partially magnetized ferrites». *IEEE Transactions on Microwave Theory and Techniques*: June 1974. 22:6. P. 645-651.
- [12] TISCHER, F. J. 1979. «Transmission media for millimeter-wave integrated circuits». *IEEE MTT-S International Microwave Symposium Digest*: April 1979. 79:1. P. 203-207.
- [13] YONEYAMA, T., NISHIDA, S. 1981. «Nonradiative Dielectric Waveguide for Millimeter-Wave Integrated Circuits». *IEEE Transactions on Microwave Theory and Techniques*: Nov. 1981. 29:11. P. 1188-1192.
- [14] DAS, B. N., PRASAD, K. V. S. V. R., RAO, K. V. S. 1986. «Excitation of waveguide by stripline and microstrip-line-fed slots». *IEEE Transactions on Microwave Theory and Techniques*: March 1986. 34:3. P. 321-327.
- [15] GRABHERR, W., HUDER, B., MENZEL, W. 1994. «Microstrip to waveguide transition compatible with mm-wave integrated circuits». *IEEE Transactions on Microwave Theory and Techniques*: Sept. 1994. 42:9. P. 1842-1843.
- [16] PONCHAK, G. E., SIMONS, R. N. 1990. «New rectangular waveguide to coplanar waveguide transition». *IEEE MTT-S International Microwave Symposium Digest*: May 1990. 1. P. 491-492.
- [17] YAMA, H. July 1992. JP Patent, Application no. H4-220881.
- [18] HIROWAKA, J., ANDO, M. 1998. «Single layer feed waveguide consisting of posts for TEM wave excitations in parallel plates» *IEEE Transactions on Antennas and Propagation*: May 1998. 46:5. P. 625-630.

- [19] UCHIMURA, H., TAKENOSHITA, T., FUJII, M. 1998. «Development of a “Laminated Waveguide”». *IEEE Transactions on Microwave Theory and Techniques*: Dec. 1998. 46:12. P. 2438-2443.
- [20] JAIN, N., KINAYMAN, N. 2001. «A novel microstrip mode to waveguide mode transformer and its applications». *IEEE MTT-S International Microwave Symposium Digest*: 20-25 May 2001. 2. P. 623-626.
- [21] DESLANDES, D., WU, K. 2001. «Integrated microstrip and rectangular waveguide in planar form». *IEEE Microwave and Wireless Components Letters*: Feb. 2001. 11:2. P. 68-70.
- [22] DESLANDES, D., WU, K. 2001. «Integrated transition of coplanar to rectangular waveguides». *IEEE MTT-S International Microwave Symposium Digest*: May 2001. 2. P. 619-622.
- [23] HUANG, Y., WU, Ke-Li. 2003. «A broad-band LTCC integrated transition of laminated waveguide to air-filled waveguide for millimeter-wave applications» *IEEE Transactions on Microwave Theory and Techniques*: May 2003. 51:5. P. 1613-1617.
- [24] CASSIVI, Y., DESLANDES, D., WU, K. 2002. «Substrate integrated waveguide directional couplers». *2002 Asia-Pacific Microwave Conference Proceedings (APMC'02)*: 19-22 Nov. 2002, Kyoto, Japan. 3. P. 1409-1412.
- [25] DESLANDES, D., WU, K. 2003. «Single-substrate integration technique of planar circuits and waveguide filters» *IEEE Transactions on Microwave Theory and Techniques*: Feb. 2003. 51:2. P. 593-596.
- [26] CASSIVI, Y., WU, K. 2003. «Low cost microwave oscillator using substrate integrated waveguide cavity» *IEEE Microwave and Wireless Components Letters*: Feb. 2003. 13:2. P. 48-50.

- [27] CHE, W., YUNG, E. Kai-Nig, WU, K. 2003. «Millimeter-wave ferrite phase shifter in substrate integrated waveguide (SIW)». *2003 IEEE Antennas and Propagation Society International Symposium Digest*: June 2003. 4. P. 887-890.
- [28] CASSIVI, Y., PERREGRINI, L., ARCIONI, P., BRESSAN, M., WU, K., CONCIAURO, G. 2002. «Dispersion characteristics of substrate integrated rectangular waveguide» *IEEE Microwave and Wireless Components Letters*: Sept. 2002. 12:9. P. 333-335.
- [29] ANSOFT CORPORATION. 2003. Ansoft HFSS. Version 9.1. [Software]. Pittsburgh.
- [30] AULD, B. A. 1959. «The synthesis of symmetrical waveguide circulators». *IRE Transactions on Microwave Theory and Techniques*: April 1959. 7:2. P. 238-246.
- [31] HAGELIN, S. 1966. «A flow graph analysis of 3-and 4-port junction circulators». *IEEE Transactions on Microwave Theory and Techniques*: May 1966. 14:5. P. 243-249.
- [32] BOSMA, H. 1964. «On stripline Y-circulation at UHF». *IEEE Transactions on Microwave Theory and Techniques*: Jan. 1964. 12:1. P. 61-72.
- [33] ANDERSON, L. K. 1967. «An analysis of broadband circulators with external tuning elements» *IEEE Transactions on Microwave Theory and Techniques*: Jan. 1967. 15:1. P. 42-47.
- [34] SIMON, J. W. 1965. «Broadband strip-transmission line Y-junction circulators». *IEEE Transactions on Microwave Theory and Techniques*: May 1965. 13:3. P. 335-345.
- [35] HELSZAJN, J. 1973. «Microwave measurement techniques for below resonance junction circulators». *IEEE Transactions on Microwave Theory and Techniques*: May 1973. 21:5. P. 347-351.



- [36] HELSZAJN, J. 1994. «Experimental evaluation of junction circulators: a review». *IEE Proceedings on Microwaves, Antennas and Propagation*: Oct. 1994. 141:5. P. 351-358.
- [37] HELSZAJN, J. 2000. «1-port topology of the degree-1 and -2 terminated circulator». *IEE Proceedings on Microwaves, Antennas and Propagation*: Dec. 2000. 147:6. P. 437-443.
- [38] HELSZAJN, J. 1972. «Synthesis of quarter-wave coupled circulators with chebyshev characteristics». *IEEE Transactions on Microwave Theory and Techniques*: Nov. 1972. 20:11. pp. 764-769.
- [39] LEVY, R., HELSZAJN, J. 1993. «Synthesis of series stub-R complex gyrator circuits using halfwave long impedance transformers» *IEE Proceedings on Microwaves, Antennas and Propagation*: Dec. 1993. 140:6. P. 426-432.
- [40] HELSZAJN, J., TSOUNIS, B., CAPLIN, M. 2002. «WR75 junction circulator using 90° and 180° ridge UEs». *IEE Proceedings on Microwaves, Antennas and Propagation*: April 2002. 149:2. P. 129-137.
- [41] HELSZAJN, J. 1970. *Waveguide junction circulators: theory and practice*. 1<sup>st</sup> ed. England : John Wiley & Sons Ltd. 543p.
- [42] KONISHI, Y. 1965. «Lumped element Y circulator,” *IEEE Transactions on Microwave Theory and Techniques*: Nov. 1965. 13:6. P. 852-864.
- [43] CHAIT, H. N., CURRY, T. R. 1959. «Y-circulator». *J. Appl. Phys.*: 1959. 30. P. 152.
- [44] DAVIES, J. B. 1962. «An analysis of the m-port symmetrical H-plane waveguide junction with central ferrite post». *IRE Transactions on Microwave Theory and Techniques*: Nov. 1962. 10:6. P. 596-604.

- [45] PAN, J. J., SHIH, M., RILEY, L. 1990. «High performance millimetre-wave microstrip circulator for deep space communications». *IEEE MTT-S International Microwave Symposium Digest*: 8-10 May 1990. 3. P. 1015-1017.
- [46] GOEBEL, U., SCHIEBLICH, C. 1982. «Broadband fin-line circulators». *IEEE MTT-S International Microwave Symposium Digest*: June 1982. 82:1. P. 249-251.
- [47] YOSHINAGA, H., YONEYAMA, T. 1998. «Design and fabrication of a nonradiative dielectric waveguide circulator». *IEEE Transactions on Microwave Theory and Techniques*: Nov. 1998. 36:11. P. 1526-1529.
- [48] HELSZAJN, J., SHARP, J. 2003. «Post dielectric resonator at the junction of three rectangular waveguides: calculations and measurements». *IEE Proceedings on Microwaves, Antennas and Propagation*: April 2003. 150:2. P. 90-96.
- [49] CASTILLO, J. B. Jr., DAVIS, L.E. 1971. «Identification of spurious modes in circulators» *IEEE Transactions on Microwave Theory and Techniques*: Jan. 1971. 19:1. P. 112-113.
- [50] TOKUMITSU, Y., KASAHARA, T., KONIZO, H. 1976. «A new temperature stabilized waveguide circulator» *IEEE MTT-S International Microwave Symposium Digest*: June 1976. 76:1. P. 260-262.
- [51] LEVY, R., HELSZAJN, J. 1982. «Specific equations for one and two section quarter-wave matching networks for stub-resistor loads». *IEEE Transactions on Microwave Theory and Techniques*: Jan. 1982. 30:1. P. 55-63.
- [52] COHN, S. B. 1947. «Properties of ridged waveguide». *IRE Proceedings*: Aug. 1947. 35. P. 783-788.
- [53] HOPFER, S. 1955. «The design of ridged waveguides». *IEEE Transactions on Microwave Theory and Techniques*: Oct. 1955. 3:5. P. 20-29.

- [54] MARCUVITZ, N. 1951. Waveguide handbook : M.I.T. RAD Lab Series. New York: McGraw-Hill.
- [55] HOEFER, W. J. R., BURTON, M. N. 1982. «Closed-form expressions for the parameters of finned and ridged waveguides». *IEEE Transactions on Microwave Theory and Techniques*: Dec. 1982. 30:12. P. 2190-2194.
- [56] SHARMA, A. K., HOEFER, W. J. R. 1983. «Empirical expressions for fin-line design». *IEEE Transactions on Microwave Theory and Techniques*: April 1983. 31:4. P. 350-356.
- [57] HELSZAJN, J. 2000. *Ridge waveguide and passive microwave components*. Cornwall England : IEE Electromagnetic Waves Series. 327p.
- [58] ALLEN, P. J. 1956. «The turnstile circulator». *IEEE Transactions on Microwave Theory and Techniques*: Oct. 1956. 4:4. P. 223-227.
- [59] OWEN, B., BARNES, C. E. 1970. «The compact turnstile circulator». *IEEE Transactions on Microwave Theory and Techniques*: Dec. 1970. 18:12. P. 1096-1100.
- [60] OWEN, B. 1972. «The identification of modal resonances in ferrite loaded waveguide Y-junction and their adjustment for circulation» *Bell Systems Tech. J.*: March 1972. 8.
- [61] DENLINGER, E. J. 1974. «Design of partial height ferrite waveguide circulators». *IEEE Transactions on Microwave Theory and Techniques*: Aug. 1974. 22:8. P. 810-813.
- [62] HELSZAJN, J., TAN, F. C. 1975. «Design data for radial-waveguide circulators using partial-height ferrite resonators». *IEEE Transactions on Microwave Theory and Techniques*: March 1975. 23:3. P. 288-298.
- [63] HELSZAJN, J., SHARP J. 1983. «Resonant frequencies, Q-factor, and susceptance slope parameter of waveguide circulators using weakly magnetized open

resonators». *IEEE Transactions on Microwave Theory and Techniques*: June 1983. 31:6. P. 434-441.

[64] HELSZAJN, J., SHARP J. 1985. «Adjustment of in-phase mode in circulators using turnstile junctions». *IEEE Transactions on Microwave Theory and Techniques*: April 1985. 33:4. P. 339-343.

[65] HELSZAJN, J. 1998. «Non-optimum frequency response of UE coupled STUB-R load». *Microwave Engineering Europe*: Oct. 1998. P. 339-343.

[66] HO DONG, K., IOURI, K., NIKOLAI, V. 1998. «The new approach to designing W-band Y-junction circulator with small insertion loss». *IEEE MTT-S International Microwave Symposium Digest*: 7-12 June 1998. 2. P. 637-639.

[67] AKAIWA, Y. 1974. «Bandwidth enlargement of a millimetre-wave Y circulator with half-wavelength line resonators». *IEEE Transactions on Microwave Theory and Techniques*: Dec. 1974. 22:12. P. 1283-1286.